Instituto Tecnológico y de Estudios Superiores de Monterrey

Campus Monterrey

School of Engineering and Sciences

Technological development of Alginate/Gelatin composite hydrogel fabricated by microextrusion based printing for tissue regeneration

A thesis presented by

Rodrigo Alejandro Urruela Barrios

Submitted to the
School of Engineering and Sciences
in partial fulfillment of the requirements for the degree of

Master of Science

In

Manufacturing Systems

Monterrey Nuevo León, May 14th, 2018

Instituto Tecnológico y de Estudios Superiores de Monterrey

Campus Monterrey

School of Engineering and Sciences

The committee members, hereby, certify that have read the thesis presented by Rodrigo Alejandro Urruela Barrios and that it is fully adequate in scope and quality as a partial requirement for the degree of Master of Science in Manufacturing Systems

Dr. Wendy de Lourdes Ortega Lara
Tecnológico de Monterrey
School of Engineering and Sciences
Principal Advisor

Dr. Alejandro Alvarez Guerra
Tecnológico de Monterrey
School of Engineering and Sciences
Co-advisor

Dr. Elisa Virginia Vázquez Lepe
Tecnológico de Monterrey
Committee Member

Dr. Erika García López
Tecnológico de Monterrey
Committee Member

Tecnológico de Monterrey
14 MAY 2018
Dirección Nacional de Posgrado
Dr. Rubén Morales Menéndez

Dr. Rubén Morales Menéndez
Associate Dean of Graduate Studies
School of Engineering and Sciences

Monterrey Nuevo León, May 14th, 2018

Declaration of Authorship

I, Rodrigo Alejandro Urruela Barrios, declare that this thesis titled, "Technological development of Alginate/Gelatin composite hydrogel fabricated by microextrusion based printing for tissue regeneration" and the work presented in it are my own. I confirm that:

- This work was done wholly or mainly while in candidature for a research degree at this University.
- Where any part of this thesis has previously been submitted for a degree or any other qualification at this University or any other institution, this has been clearly stated.
- Where I have consulted the published work of others, this is always clearly attributed.
- Where I have quoted from the work of others, the source is always given. With the exception of such quotations, this thesis is entirely my own work.
- I have acknowledged all main sources of help.
- Where the thesis is based on work done by myself jointly with others, I have made clear exactly what was done by others and in what I have contributed myself.

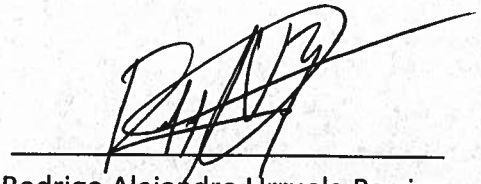

Rodrigo Alejandro Urruela Barrios
Monterrey Nuevo León, May 14th, 2018

Dedication

To Patty and JR. Thanks for all your unconditional confidence, love, support, patience, and encouragement. You were my main motivation and inspiration.

A Patty y JR. Gracias por su confianza incondicional, amor, apoyo, paciencia y aliento. Ustedes fueron mi motivación principal e inspiración.

Acknowledgements

This thesis becomes a reality with the kind support and help of many individuals. I would like to express my deepest gratitude to all of them.

First, I would like to thank my thesis advisors, Dr. Wendy Ortega and Dr. Alejandro Alvarez of the School of Engineering and Sciences at Tecnologico de Monterrey. The door to Dr. Ortega's office was always open whenever I ran into trouble or had the simplest question. She allowed this project to be my own work, but also steered me in the right direction whenever she thought I needed it. The guidance and motivation of Dr. Alejandro Alvarez were exceptional, our meetings were enlightening and inspirational. He gave me a once-in-a-life-time opportunity, I took it, and I will always be grateful to him. I wish to acknowledge the valuable advice I received from my thesis committee, Dr. Elisa Vazquez and Dr. Erika García. Thanks!

I would also like to thank Professor Allan Myerson of the Chemical Engineering Department at the Massachusetts Institute of Technology for allowing me to continue my research as a visiting student at his lab and providing me guidance during that time. I am also thankful to all the members of the Myerson group, without their passion for research and helpful insights, my visit to MIT would have not been as valuable.

I would like to acknowledge Tecnológico de Monterrey for giving me the opportunity of doing my postgraduate studies in its innovation-driven environment, that allowed me to grow as a person; and CONACyT, this project would have been impossible without their support. My sincere thanks go to all my colleagues and professors from the Masters program for their support and knowledge. Special thanks go to Erick Ramírez and the 3D Factory MX team, that help me turned many of my ideas into a reality; and to my friends from the Masters program and from my visiting exchange, whose continuous encouragement, sleepless nights, and support made these last two years extraordinary.

Finally, my deepest gratitude goes to my family that supported me always. Thank you! Last, but not least, I would like to thank God, that always led the way.

Technological development of Alginate/Gelatin composite hydrogel fabricated by microextrusion based printing for tissue regeneration

by

Rodrigo Alejandro Urruela Barrios

Abstract

Alginate hydrogels have shown an enormous potential for tissue engineering due to its non-toxicity, biocompatibility, and structural similarity to extracellular matrices. To produce these hydrogels, different manufacturing techniques can be used, including microextrusion 3D printing. Current efforts for hydrogels in tissue engineering are centered on improving bioactivity and mechanical properties by the incorporation of a second biopolymer or bioceramics; and loading these materials with pharmaceutical drugs to promote a better healing process. In this work, the study of the synthesis process of alginate/gelatin hydrogels reinforced with TiO_2 and beta-tricalcium phosphate (β-TCP) and loaded with ibuprofen, its extrusion in a modified 3D Printer, and its material characterization were proposed. The hydrogel systems were successfully micro-extruded by tuning the concentration of the pre-crosslinking agent up to 0.20 w/v% and a rheological profile was obtained. FT-IR, XRD, and TGA were used to perform a physicochemical characterization and prove the growth of ibuprofen crystals inside the porous material. For the drug loading, stable microemulsions were obtained with polyvinyl alcohol (PVA) as emulsifier and various solvents, including dichloromethane. The pores of the crosslinked printed structures were measured using SEM and resulted in an average pore size from 160 µm to 40 µm, depending on the material composition, all with adequate porosity for tissue engineering. Furthermore, the hydrogels reinforced with TiO_2 and β-TCP showed enhanced mechanical properties up to 65 MPa of elastic modulus. Controllable drug loading was achieved up to 35 w/w% of the dry hydrogel with more than 50% of the loaded ibuprofen dissolving in less than one hour. Additionally, while the hydrogel was microextruded in the 3D printer, it was found that as more layers of the design were deposited in the built platform, there was an increase of the line width of the bottom layers due to its viscous deformation. Shrinkage of the design when the hydrogel is crosslinked and later freeze-dried was also measured and found to be up to 27% from the printed design. Overall, the approach taken enables to synthesize a printable composite alginate solution, loaded with an API, with adequate physical properties for tissue regeneration.

Table of Contents

List of Figures

List of Tables

1. Chapter 1 – Introduction

Every year, millions of patients suffer the loss or failure of an organ or tissue as a result of accidents or disease. Over 8 million surgical procedures are performed to treat these patients in the U.S. each year, and the overall cost of these problems to the U.S. economy is estimated to exceed $400 billion per year. The increasing demand of patients waiting for an organ or tissue donation outnumbers the number of donors by more than five times [1]. In dentistry, advanced carious lesions can irreversibly damage the dental pulp by propagating a sustained inflammatory response throughout the tissue, and oral and craniofacial bone defects are caused by chronic infections such as periodontal diseases, congenital defects, syndromes, cancer or trauma [2]. To address these problems of tissue or organ lost and lack of sufficient donors, tissue engineering and regenerative medicine propose regeneration strategies to mimic the 3D native tissue and all the biological structures, while the functions are maintained. Bone augmentation and regeneration can be performed using bone grafts and other technologies as guided bone regeneration and guided tissue regeneration. The materials used in tissue engineering have evolved in the last 70 years, going from metals to synthetic polymers, biodegradable polymers, and later to more advanced and engineered composite materials [3]. This is one of the reasons of the importance of more in-depth studies for engineered materials like the one presented in this work.

1.1 Background

One of the most appealing materials to develop tissue engineering technologies and to create biologically compatible scaffolds for bone and tissue regeneration is the hydrogel, which is revolutionizing the fields of material sciences and biomedical engineering. Due to their many unique characteristics, hydrogels have been researched vigorously in the last 30 years for tissue engineering applications with drug delivery capabilities. Some of these characteristics include biocompatibility and non-toxicity, flexible methods of synthesis allowing desirable physical characteristics, degradability, and a wide range of possible constituents [4]. For drug release capabilities many challenges are being addressed in today's investigations, including controlled

release kinetics of the drugs from the porous hydrogels and increasing the types of drugs that can be released using the same material [5]. Regarding tissue engineering, some investigations are intensely focused on the mechanical properties of the hydrogel while maintaining its biocompatibility with the body, mimicking the extracellular matrix (ECM) with adequate pore size to promote cell proliferation, and controlling the degradation rate to match the regeneration process of the cells [6]–[8]. Furthermore, combining the structural properties for tissue constructions and a controlled drug and protein delivery system of hydrogels has been the focus in regenerative medicine in the last years [9].

Basically, hydrogels are 3D networks of polymer chains that have been used extensively for different biological applications and many of their fabrications methods are still studied today. These manufacturing methods include additive manufacturing and 3D bioprinting. These techniques have disrupted manufacturing strategies and traditional design allowing structures that seem impossible using standard methods [10].

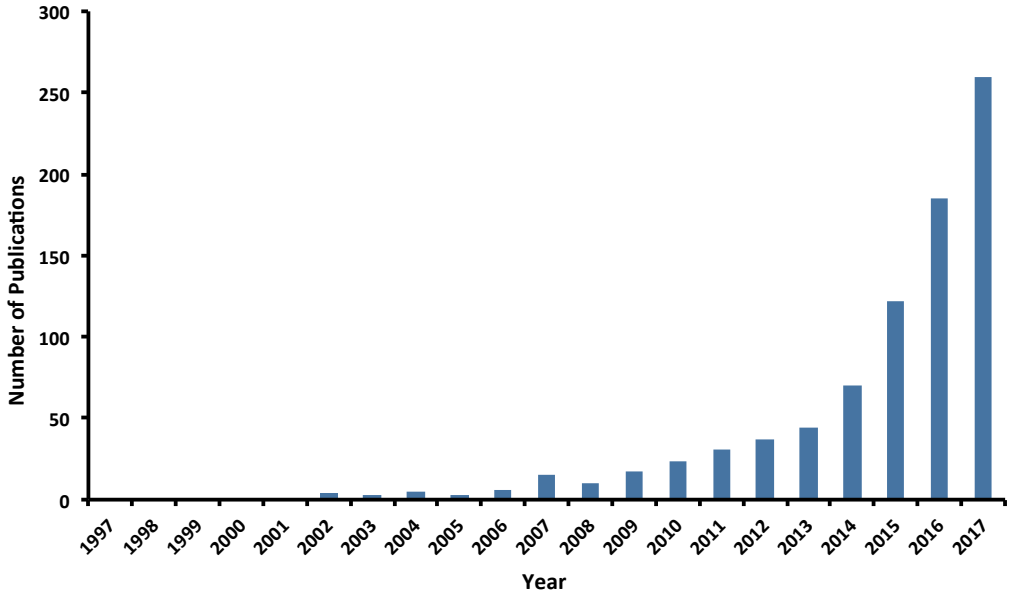

Figure 1. Number of publications of **TOPIC**: (hydrogels) AND **TOPIC**: (print*) obtained from the citation report tool of Web of Science

The combination of hydrogel science and the additive manufacturing techniques creates new possibilities in the biomedical engineering fields. Even though this research field is relatively

young, great advances have been made in the last few years and more resources are being spent to know more about the different possibilities in the field. In Figure 1, it can be observed how the number of publications including the topics of hydrogel and printing has increased in the last decade.

Hydrogels can be synthesized from a wide range of constituents. Natural biopolymers hydrogels, including the polysaccharides-base hydrogels, have high water content, functionality properties, high biocompatibility, and are relatively cheap and nontoxic. For this reason, these types of hydrogels are of great interest for tissue engineering and drug delivery. Another important quality of these materials is that they are renewable and abundant in nature, unlike other of the synthetic polymers used in the fabrication of hydrogels. Some of the biopolymers that had been used for hydrogel production include alginate, gelatin, chitosan, hyaluronic acid, polyethylene glycol diacrylate (PEGDA), etc. Two highly researched biopolymers are alginate and gelatin for the applications of tissue engineering and drug delivery.

Alginate is a polysaccharide derived from brown seaweed with a fast gelation rate. This fast gelation is possible due to its crosslinking properties in ionic solutions of calcium, such as calcium chloride and calcium sulfate [11]. Gelatin is a protein obtained by the hydrolysis of collagen and it has good biocompatibility and high-water absorbing ability. Alginate hydrogel has poor mechanical properties by its own, but its synthesis adding a second biopolymer, the addition of bioceramic particles, and chemical functionalization to change its morphology are used to improve its stability in printability [12]. Calcium phosphates are also added to the hydrogel to promote bioactivity for tissue regeneration. Some of the major challenges that still need to be addressed include the fabrication of these hydrogels with desired mechanical properties [4] and a desired macro-porous design. The use of additive manufacturing to fabricate them is one step closer to overcome those challenges.

1.2 Motivation

To need to address the great demand for tissues and organs leads to the study of materials that can regenerate and mimic their functions. The hydrogels present a great opportunity to address this demand. Hydrogels used in specific applications like periodontal tissue and bone

regeneration need specialized and in-depth studies of characterization and fundamental understating of the chemistry behind them. These polymer matrixes need to be multifunctional to comply with all the requirements needed to perform the job. Additionally, manufacturing methods must be studied to produce these materials. For example, it is possible to modulate the rheological and physicochemical properties of the hydrogel inks made of natural polysaccharides by varying the cross-linking agents and exploiting their thixotropic behavior to use in additive manufacturing [13]. The properties of the ink are important for the printing feasibility and to maintaining the structure of the printed design after the extrusion in the built platform.

Nevertheless, there are still many challenges to be addressed when using a biopolymer for tissue engineering while maintaining the desired mechanical strength, porosity, and printability. Furthermore, performance of the scaffold is enhanced when active pharmaceutical ingredients (API), or drugs, are released from it while the tissue is regenerating, and a controllable and stable method to load the hydrogels is needed. For this reason, a study of the processability of different composite alginate/gelatin hydrogel reinforced with nanoparticles, calcium phosphate, and loaded with API for tissue and bone regeneration to be manufactured by additive manufacturing (3D printing) is proposed.

1.3 Aims and Objectives

The main objective is to synthesize a robust biopolymer hydrogel scaffold manufactured by 3D microextrusion for bone and tissue regeneration, specifically for odontology applications, that possesses the following characteristics: appropriate mechanical properties and pore size for cell proliferation, bioactivity, and with drug delivery capabilities. To do this, various specific objectives are listed:

- Synthesize alginate/gelatin pre-crosslinked ink with adequate viscoelasticity behavior to be used in a modified and affordable 3D printer to obtained well-structured 3D designs.
- Characterize the crosslinked hydrogel for mechanical properties, structure, thermal properties, and bioactivity of the hydrogel and enhanced them by the addition of nanoparticles and bioceramics to its polymer matrix.

- Synthesize a composite hydrogel with the capability to release an active pharmaceutical ingredient crystallized inside its porous structure.
- Screening of the printing parameters in the modified 3D printer to ensure the materials correct manufacture.

To accomplish the specific objectives, various actions need to be executed. The adequate percentage of pre-crosslinking agent added to the alginate/gelatin ink for its microextrusion will be determined. The ink will be characterized with a rheometer to obtain its viscoelastic behavior. Furthermore, the printed composite alginate/gelatin hydrogel reinforced with nanoparticles and bioceramics will be measured using FTIR spectroscopy, X-ray diffraction, electron and optical microscopy, thermo gravimetric analysis, and the universal machine. A model API, anti-inflammatory ibuprofen, will be crystallized inside the porous structure of the hydrogel and obtain its release kinetics curves. Finally, assess the material printability in a modified 3D printer modified for gels and obtain the optimal printing parameters.

Overall, determine if the natural biopolymer hydrogel studied is suitable for 3D printing technology as a hydrogel ink and incentive further study of these inks in the field of regenerative medicine and drug delivery systems. The composite alginate/gelatin hydrogels reinforced with TiO_2 and β-TCP and drug delivery capabilities process investigated in this project as scaffolding matrices are shown in Figure 2.

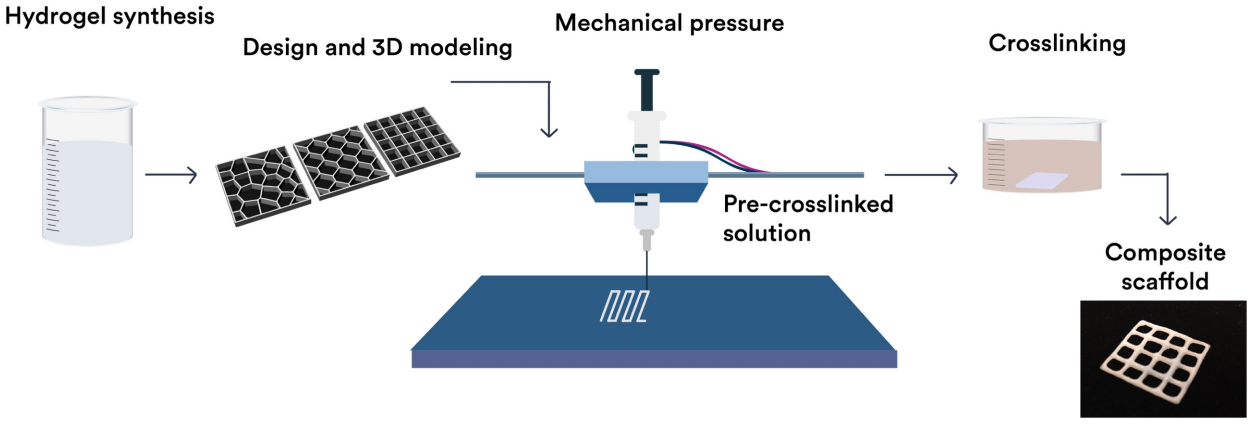

Figure 2. Schematic overview of the approach followed in this research project outlining the process to fabricate the alginate/gelatin composite hydrogel by 3d microextrusion manufacturing

The thesis is organized in the following manner, after the “Literature Review” chapter (Chapter 2), in Chapter 3 the “Materials and Methods” are presented. This chapter includes the synthesis method of the alginate/gelatin composite hydrogel reinforced with bioceramics, nanoparticles and drug delivery capabilities, its characterization methods, and finally its design and manufacturing method. In the Chapter 4, the results of all the characterizations of the material are discussed and the best parameters of for the manufacturing process for this material are presented. Finally, in Chapter 5, the conclusions of the work are included and a scope of future work.

2. Chapter 2 – Literature Review

The loss of tissue due to trauma, disease, or congenital abnormalities is a major health problem worldwide. Over 8 million surgical procedures are performed to the patients with this problem each year just in the United States [1]. There are various actual solutions to solve this problem, which are evolving every day. Materials used in tissue engineering have evolved from metals, to synthetic polymers, and now to natural and degradable polymers that have mayor interaction with the body, like hydrogels [14]. Several types of biopolymer hydrogels have been used in tissue engineering with drug delivery capabilities. This search determines where the research is focused today. In Table 1, it can be identified the number of publications made searching for the combination of keywords.

Table 1. Number of publications based on the combination of different keywords. Search done in Web of Science on March 2018

Keywords				No. Ref. Found
Hydrogel	Drug delivery	-	-	9,941
	Tissue Engineering	-	-	5,963
	Drug delivery	Tissue engineering	-	1,256
			Alginate	174
			Chitosan	234
			Collagen	120
			Gelatin	148
			Poly Vinyl Alcohol	46
	Print*	-	Alginate	173
		Tissue engineering		107
		Drug delivery		14
		-	Chitosan	43
		Tissue engineering		20
		Drug delivery		9
		-	Gelatin	125
		Tissue engineering		85
		Drug delivery		9
		Tissue engineering	Calcium phosphate	17
		Tissue engineering	Bioceramics	0

As the research in hydrogels for different applications in drug delivery systems and tissue engineering advances, more complex and specialized materials are synthesized. Composite hydrogels with different combination of polymers, micro and nanoparticles, micro-emulsions,

bioceramics, and crystals are used to enhance and control its properties. Also, many fabrication techniques have been developed to produce these hydrogels, from basic techniques such as molding, to more innovative techniques such as bioplotting or electrospinning. Each of the different manufacturing techniques used to produce the hydrogels will depend on the final application, just like the materials used to synthesize them will depend on the desired technical features as well as the type of the interaction desired with the human body.

A review of different hydrogels used for tissue engineering and drug delivery will be presented with a more in-depth review of alginate and gelatin, the two biopolymers used in this work and how nanoparticles and bioceramics are being used to enhance the properties of the material. Applications and methods to load active pharmaceutical ingredients in the structure of hydrogels are also reviewed, its different applications, and the work done already in the field. Finally, a review of the different manufacturing techniques for additive manufacturing of hydrogels in tissue engineering will be presented with an emphasis in microextrusion, the technique used in this work.

2.1 Hydrogels

Hydrogels are three-dimensional networks of crosslinked hydrophilic polymer that can maintain their structure while holding substantial amounts of water. Given that hydrogels can be formulated in a large variety of physical forms like films, micro particles, spheres, and scaffolds, the unique properties of these materials have drawn a lot of attention in the medical and pharmaceutical fields, especially in the drug delivery systems, tissue engineering, and regenerative medicine. The structure of the hydrogels can be manipulated to control its crosslinking density, porosity, and swelling properties depending on its environment; these manipulations permit the loading of drugs in the polymeric matrix and a controlled release afterward [4], [15]. Another important characteristic of the hydrogels is their biocompatibility due its high water content and physiochemical similarity to cellular tissues. The hydrogels are relatively deformable and can change their shape according to the surface to which they are applied [5].

Hydrogels can be prepared from synthetic or natural polymers. These two types of hydrogels

differentiate mainly in their properties such as mechanical strength, degradability, and biocompatibility, for which they are chosen depending on the intended application. Recently, covalently cross-linked hybrid hydrogels consisting of natural and synthetic polymers have been designed by the introduction of functional groups in both categories [15]. Other researchers have investigated different composites including two different biopolymers [16], a natural biopolymer with microemulsions [17], crystals [18], or bioceramics [19]. Another classification of the hydrogels is the smart hydrogels, which present the ability to undergo reversible sol–gel phase transition in response to the external physical or chemical stimuli such as temperature, pH, ionic concentration, and light [20]. This last classification is also under extensive study given the potential for specific target drug delivery and cell differentiation in tissue engineering.

Table 2. Polysaccharides and proteins used in literature for tissue engineering and drug delivery. Adapted from [10]

Molecule class	Polymer	Common gel transition method	Limitations	Properties
Protein	Collagen	Physical en chemical crosslinking	Immunogenic	Collagenase proteolysis
	Gelatin	Physical or chemical gel formation	Retention of water	Biocompatibility and cell adhesion
	Fibrin	Self-assembling	Thrombogenicity	Excellent cell-adhesion
Polysaccharides	**Alginate**	Ionotropic gel formation	Low cell adhesion	Hydrolysis chelation degradability
	Chitosan	Chemical gel formation	High viscosity	Antibacterial and antifungal
	Agarose	Gel formation below 36 °C	No biocompatibility	Ether functionality
	Dextran	Ionotropic gel formation	Immunogenic	Aqueous two-phase microsphere formation
	Methylcellulose	Methylation-dependent gel formation	Non-degradable	Natural biocompatibility

There are different studies in the initial phases for hydrogels with specific applications in the fields of tissue engineering or drug delivery. One study includes the investigation and experimental work on a hydrogel to fight tuberculosis by targeting the drug delivery in the lungs

of the human body [21]. In tissue engineering, thermo-responsive hydrogels also have been studied. In this case, hyaluronic acid hydrogels were synthesized to study the chondrogenesis in human mesenchymal stem cells [22]. More recently, hydrogels with added bone cements such as calcium phosphate have also been studied with success for bone regeneration. This not only promotes bioactivity of the material, but also enhances one of the most important mechanisms of bone tissue regeneration, that is nucleation of calcium phosphates [23].

One type of natural polymer used vigorously in the investigation of hydrogels is the polysaccharides. They are considered useful due to their ionic groups, which enables an easy functionalization and modification of their chemical properties [13], and depending on their application, their biodegradability. Some of the most studied polysaccharides in drug delivery systems and tissue engineering are alginates, chitosan, collagen, hyaluronic acid, and gelatin. In Table 2 these polysaccharides are summarized with some of its unique properties. Alginate and gelatin are synthesized into the composite hydrogel in this work.

2.1.1 ALGINATE

Alginate gels have been extensively studied due to their biocompatibility, low toxicity, and their former use in the food industry. Alginates are naturally derived linear copolymers of 1,4-linked ß-D-mannuronic acid and a-L- guluronic acid residues that in presence of divalent cations form crosslinked structures. This polysaccharide can be isolated from brown algae. These hydrogels are soft, dissipative materials, that are being mainly studied for biomedical and pharmaceutical applications [24]. In Figure 3 the graphic molecule of the alginate is presented with its two different copolymers.

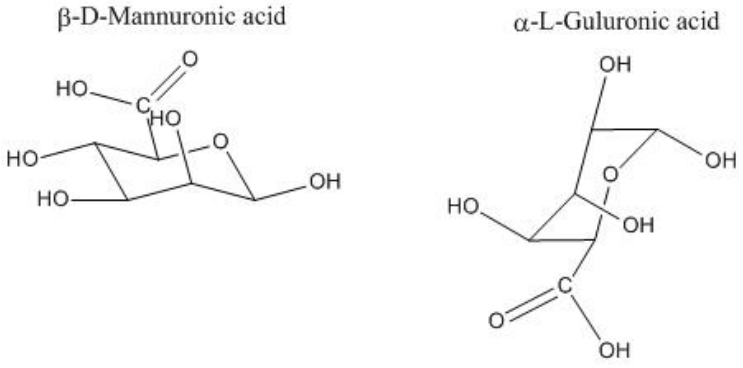

Figure 3. Structural monomers of alginic acid

The most recent studies on alginate gels investigate their properties and the possibility to enhance them, given that by its own, this biopolymer may present deficient performance in mechanical properties and degradation rate, among others. The alginate gels are made by crosslinking an alginate salt with a metal cation. Alginate hydrogels cross-linked with Iron (III) cations have successfully been used for cell culturing due to their cell adhesion and photo-degradation [25]. Other studies, targeting the improvement of mechanical properties and permeability, were feasible by crosslinking an alginate salt with calcium and thiol-groups simultaneously [26]. The method of pre-crosslinking, or in other words partially crosslink the monomers of the polymer, has also been used to increase the viscosity of alginate and "customize" it for the intended application. Although discussed later in this work, certain viscosity is needed to achieve printability for additive manufacturing, one of the applications intended for alginate in this research. Therefore, pre-crosslinking is used with an cation, Ca^{+2}, and its concentration is optimized for extrusion.

The gelling conditions and the type of crosslinker can affect the mechanical properties and porosity. The gelation temperature can influence gelling time, low temperatures causes reduced diffusion rate and slower crosslinking, which at the same time causes a more ordered structure and enhanced mechanical properties. Alginate gels can be covalently modified to promote cell attachment, given that naturally this material does not promote significant adhesion. One important characteristic of this type of hydrogels is that encapsulation and release of proteins or drugs can significantly enhance their efficacy and targeting. By their own, proteins and API degrade rapidly in the body, which results in unnecessary high doses; localized delivery aided with the hydrogels can ensure concentrated local exposure over a prolonged time without the negative effects of high doses [11]. Alginate has been used in scaffolds for tissue engineering as well, especially scaffolds manufactured by molding or 3D printing. One of the biopolymers alginate is blended with to enhance the properties mentioned above is gelatin, which will be described in the next section.

2.1.2 GELATIN

Gelatin is a hydrocolloidal polypeptide that has found widespread use in food and pharmaceutical industries over the years, where it fulfills various roles as stabilizer, thickener, and texturizer. Gelatin contains mostly protein and is produced by hydrolysis of native collagen. In hydrogels, gelatin is used widely in biomedical applications, mainly because it is a thermo-responsive polymer that undergoes reversible sol-gel transition, which depends not only on temperature but also on concentration of the gelatin solution [27]. The molecule of this biopolymer can be observed in Figure 4. The approach of covalent crosslinking of gelatin with polysaccharides is a very effective way to design gelatin-based biocompatible and biomimetic hydrogels [12]. As it was mentioned in the previous section, one of the blends that have caught the attention for studies in drug delivery and tissue engineering effects is alginate/gelatin to enhance the properties of the synthesized hydrogel.

Using the concept of blending the two polymers for enhancement, Balakrishnan et al. reported biodegradable, injectable hydrogels that can be prepared by self-crosslinking alginate and gelatin in the presence of borax, without using any toxic crosslinking agents which resulted in a cell-attracting adhesive matrix for cartilage formation [28]. On other experimental work done by Zehnder et al., an alginate/gelatin hydrogel adequate for cells is formed at pH of 7.4, which resulted in a defined, biocompatible, and cell-friendly material [29].

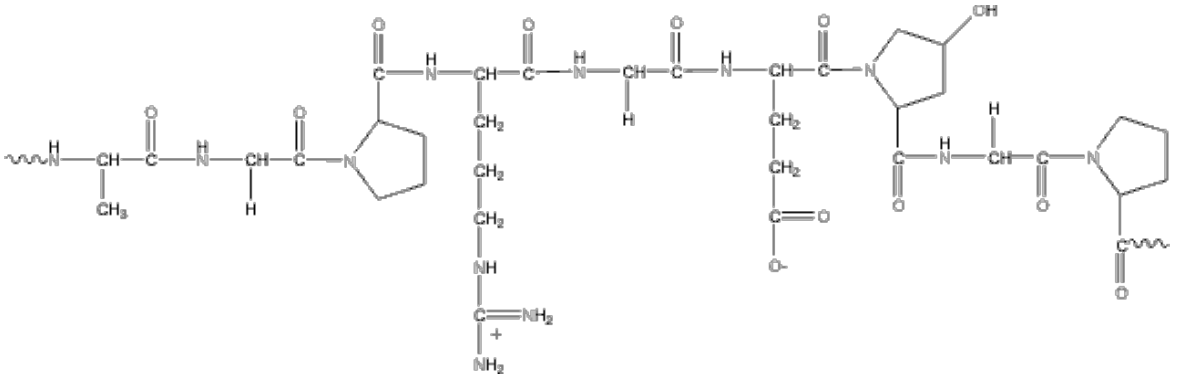

Figure 4. Chemical structure of gelatin composed of different aminoacids

Furthermore, it was found by Rosellini et al. that the blend of these two biopolymers with different weight ratios optimized the properties to use for cardiac tissue engineering [30].

Mechanical properties have also been enhanced when gelatin is blended with alginate as a composite hydrogel [31]. Cell-growth experiments and characterization of hydrogels made of alginate and gelatin are also reported [32], [33]. In this experiments Sarker et al. found this blend to be a promising material for biomedical applications due to the enhancement of fibroblasts adhesion with increased gelatin content.

To further improve some of the properties of the hydrogels, other additives can be added to the blend. The most common of these additives include nanoparticles, crystals, micro-emulsions, and bioceramics. Some of these additives will be further reviews in the next section.

2.1.3 Additives in Hydrogels

As research in the field of hydrogels for tissue engineering and drug delivery advances, more specialized and complex materials are needed to comply with all the functions they were synthesized for, while at the same time, try to keep it as simple as possible. To do that, additives should be chosen carefully. For bone and tissue regeneration, generally, bioceramics such as hydroxyapatite (HA) or other calcium phosphate such as beta-Tricalcium phosphate (β-TCP) are used in composite hydrogels to improve the conditions for cell proliferation, bioactivity, bioresorption, etc. [34], [35]. These studies have shown higher osteoconductivity in the composite alginate hydrogels with the bone cements in vivo studies. Furthermore, the hydrogels also presented improved mechanical properties. In other study, Santana et al. showed that nano-/microfibers of titanium dioxide (TiO_2) also increased cell viability in the long term (after 24 hours) and the combination of this material with alginate and a bioceramic such as calcium phosphate is cytocompatible [36].

One of the properties of the alginate hydrogel is its crosslinked structure that permits to load drugs and proteins. Therefore, another important additive that can be added to the biopolymer hydrogels is the API or drug. Chen et al. synthesized and alginate hydrogel loaded with bovine serum albumin [37]. In that work it was concluded that the release rate, degradation rate, and biocompatibility were ideal for bone defect reparation for a dental clinical application. There are many ways to load the drug inside the pores of the hydrogel. In this work, the one that will be used is crystallization through solvent evaporation of the microemulsions in the pre-crosslinked

hydrogel matrix. Badruddoza et al. have used this method previously, where a hydrophobic API was first dissolved in a solvent, and then through this solvent evaporation, the API nucleated and grew inside the porous structure of the alginate [38]. The crystallization of drugs allows a more stable form of the API and the control of dissolution rates. In the next two sections, the drug release systems of hydrogels as well as its applications in tissue engineering will be reviewed.

2.2 Tissue Engineering

Tissue engineering is a rapidly expanding field involving biomaterials science, cell biology, cell-material interactions and surface characterization. Research in this field aims to restore, preserve, or enhance tissue functions. It also aims to replace diseased or damaged organs, or tissues that are defective or have been lost. One of the key factors of tissue engineering today is the design of biologically active scaffolds with optimal characteristics. Recently, hydrogels have received a considerable interest as leading candidates for engineered tissue scaffolds due to their unique compositional and structural similarities to the natural extracellular matrix, in addition to their desirable framework for cellular proliferation and survival [6]. One of the basic requirements of a scaffold for tissue engineering is cellular proliferation, which is enhanced by the adequate porosity and the correct materials. In many cases, the scaffold's life depends on the material biodegradation. Therefore the rate and extent of biodegradation are critical design considerations for hydrogels in tissue engineering [39], [40].

In dentistry, not only pulp tissue regeneration is needed, but also bone regeneration. Bone tissue engineering is another field wherein hydrogels have been used with success. In particular, interesting results were obtained with the incorporation of inorganic components such as hydroxyapatite, calcium phosphate or titanium dioxide micro- and nanoparticles into the hydrogels [13]. Tissue regeneration can be facilitated using biomimetic materials that create a suitable microenvironment for the recruitment, adhesion, proliferation, and differentiation of cells. This process can be further stimulated by the addition of pharmaceutical drugs that have an influence on cellular function and tissue regeneration. Drugs may refer to small molecule chemicals, peptides, proteins, growth factors, cytokines, and other bioactive molecules used to

support or stimulate cellular activities and new tissue regeneration. Advanced tissue engineering systems often combine two or the three of these integral components: biomaterial matrices, living cells, and bioactive drugs [41]. In this work, biomaterial matrices will be combined with active drugs.

2.3 Drug Release Systems

There has been considerable progress in recent years in addressing the clinical and pharmacological limitations of hydrogels for drug delivery applications. Nevertheless, substantial challenges remain, including the expansion of the types of kinetic release profiles which can be achieved using hydrogels [42]. There are many design variables that can be manipulated to control the desirable kinetics and types of drugs that can be introduced in the matrix. In Table 3, the design criteria and its variables are shown for drug delivery formulations.

The design variables control the porosity of the hydrogels. Their porosity permits loading of drugs into the hydrogel matrix and the drug release at a rate that is dependent on the diffusion coefficient of the API through the gel network and the degradation profile of the biopolymer material. The drug loading into hydrogels may be limited, particularly in the case of hydrophobic drugs; and the large pore sizes of the hydrogels often result in relatively rapid drug release, over a few hours to a few days [5].

There are different mechanisms to describe the drug release systems of hydrogels, including diffusion, swelling, and chemically-controlled mechanism [43]. One approach of designing a successful clinical formulation is to mimic natural systems [44]. This is valid especially in hydrogels for tissue engineering, where it's attempted to replicate the function and complexity of the organs while delivering an API that will be beneficial to the body while the tissue is regenerating. For this reason, polysaccharide-based hydrogels such as alginate and gelatin that have high water content, adjustable chemical and mechanical properties, and an interior network for the loading of drugs, there exists a great potential in biomedical applications [45].

Table 3. Design criteria for drug delivery formulations in hydrogels. Adapted from [43].

Criteria	Design Variable
Physical Properties	Polymer and initiator
	Cross-linker
	Functionalization of polymer
	Concentration of degradable and responsive groups
	Mechanical strength
Biological properties	Cytotoxicity
	Capsule formation
Transport properties	Size of drug / protein
	Molecular weight of polymer
	Crosslinking density
	Polymer interaction with drug / protein
	Hydrogel degradation rate

There are distinct types of drugs that can be loaded into the hydrogel matrix. Previously it has been mentioned that there are hydrophilic and hydrophobic drugs. Nevertheless, the type and function of the drug also must be considered. In tissue engineering, especially in dentistry, the most common drugs to be loaded in scaffolds are the antibiotics and anti-inflammatories. Antibiotics are needed to treat bacterial infections when the tissue is implanted and trying to regenerate. On the other hand, implantation of engineered biomaterials might cause local inflammation because of the host's immune response, thus use of anti-inflammatory agents is required. Cardea et al. developed a composite scaffold with ibuprofen with homogeneous drug distribution and controlled release [46]. In other research, Mostafa et al. developed a biopolymer scaffold loaded with ciprofloxacin, an antibiotic [47]. In this work, it was concluded that the drug release enhanced the cell proliferation. Nevertheless, several aspects remain unstudied, for example, drug solubility, amount of loaded drug available for the release, drug diffusion through the polymeric matrix, and degradation and erosion mechanisms of the

polymer. Some of these aspects are addressed in the work done through this research. In this work, an anti-inflammatory and hydrophobic drug will be used, ibuprofen.

To push the field of tissue engineering with drug delivery capabilities into clinical use, the material matrix design, drug delivery, and regenerative cells need further research. Nevertheless, an efficient and cost-effective manufacturing process is needed to fabricate this material into the desired design. Between all the manufacturing techniques, additive manufacturing shows enormous potential. In the next section, the additive manufacturing technique is further reviewed, where the use of hydrogels is already a trend in research.

2.4 Microextrusion-Based 3D printing

One of the techniques of additive manufacturing used to fabricate hydrogel designs is 3D printing or microextrusion-based printing. This technique translates computer-aided design (CAD) virtual 3D models into physical objects with digital slicing, 3D scan, or tomography data. Additive manufacturing builds objects layer by layer without the need for molds or machining and it allows more design freedom because of its ability to form complex shapes and unique geometries with a minimum need for post-processing. Other of the unique properties of this technique is that its designs can be built from specialized and tailored materials with near-zero material waste [48].

In Figure 5 a simple diagram is presented explaining how tissue engineering (and drug delivery capabilities) is made compatible to work with additive manufacturing techniques. 3D printing has now been recognized as a very practical technique to create 3D structures with a micro-scale resolution, and even today that resolution is still improving. In tissue engineering, this manufacturing technique is able to integrate biodegradable polymers to 3D tissue scaffolds [49]. The 3D printers can print various biologics, including cells, tissues, tissue constructs, organ modules and microfluidic devices, useful for basic research and clinical use. Despite the great benefits and flexibility in printing a wide range of polymers and polymer inks, including the design of tissue spheroids, tissue strands, cell pellets, decellularized matrix components, micro-carriers and cell-laden hydrogels, the technology currently faces several limitations and

challenges. Among those challenges there is specialized and expensive machinery, resolution in the micro and nano-scale, and repeatability [50].

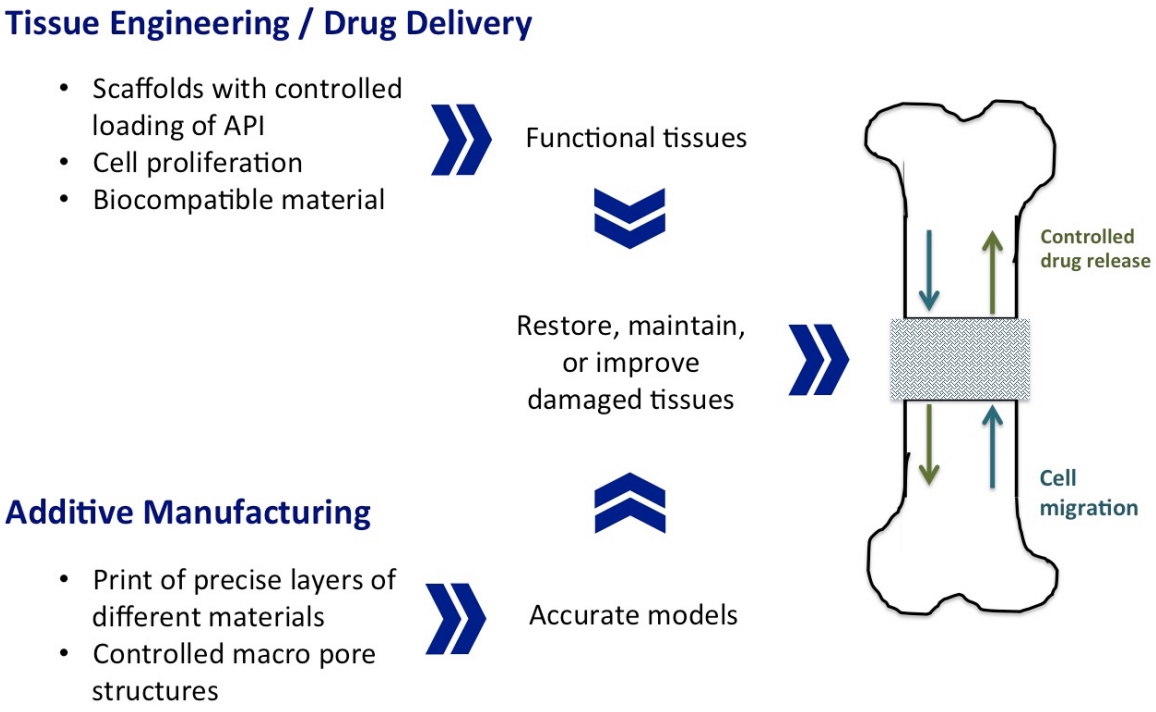

Figure 5. Diagram 'Tissue engineering and Additive manufacturing'

In Table 4, a summary of the types of techniques of additive manufacturing with its classifications is presented. Basically, in this work, the mechanical extrusion (in this work microextrusion) with a plotting system is used. Although the costs of these machines are not addressed in this work, is important to mention that most of the 3D printers for biomedical applications are usually highly specialized for one material alone and very expensive. In the market, bioprinters such as EnvisionTEC 3D Bioplotter, GeSim's Bioscaffolder, RegenHU 3DDiscovery, and Advanced Solutions BioAssemblyBot are available to buy for more than $200,000 USD. In this work a commercial and affordable machine was adapted to print gels. One of the benefits of using open-source printers, like the one used in this work, is the low cost related to it. Availability and reach is high. The RepRap Mendelmax printer, which is the open-source printer used in this research, can be modified and adapted to the researcher needs. In

this case, it was modified to microextrude continuous gel ink that later will be introduced in a chemical cross-linker to form the hydrogel.

Table 4. Process configurations for hydrogel ink materials (Adapted from [50], [51])

<table>
<tr><th>Type of Technique</th><th>Classifications</th><th>Form of material deposition</th></tr>
<tr><td rowspan="5">Mechanical / Pneumatic extrusion</td><td>Bioprinting / printing</td><td rowspan="2">Extrude continuous hydrogel line</td></tr>
<tr><td>Bioplotting / plotting</td></tr>
<tr><td>UV-integrated system</td><td rowspan="3">Continuous droplets deposited to form line</td></tr>
<tr><td>Thermally-controlled nozzle</td></tr>
<tr><td>Multi-chamber single-nozzle</td></tr>
<tr><td>Stereolithography (SLA)</td><td rowspan="2">UV-curing</td><td rowspan="2">Shapes formed through selective curing</td></tr>
<tr><td>Digital light processing (DLP)</td></tr>
</table>

Hydrogels that can be manufactured in microextrusion-based printing can be classified into three main groups depending on its gel transition method: physical, enzymatic, and chemical crosslinking. Each of these hydrogels will use different machines to form the modeled structures. The alginate hydrogels used in this project will use a machine designed for chemical crosslinking. In this type of machines, it is important to precisely control the gel deposition during the printing process, given that the final design will be a three dimensional scaffold or the tissue defect that has to be addressed [52]. Although a diagram of the 3D printer is presented in the coming chapters of this work, it is important to emphasize that some of the parameters that must be controlled for this process of pre-treatment of the gel ink, printing speed, layer height of line, distance of extruder from build platform, volume of extrusion, printing route, and post-treatment, among others.

One of the main advantages of 3D printing for biomedical applications is that it allows the manufacturing of objects having complex geometries and intricate internal structure, which can be designed according to the needs of individual patients [53]. The end goal in printing scaffolds

and tissues is to mimic nature. The design of the scaffold is also an important parameter to consider besides the material of the scaffold. One of the main reasons for this is that there are designs that could promote cell proliferation. Most designs proposed in this work are based in the repetition of unit cells forming regular shapes, such as the grid design or hexagon-shaped pores design. Fantini et al. proposed the use of voronoi lattices not only to mimic the anatomical shape of the defect, but to exploit the computer tools available with the additive manufacturing technique [54]. With this design, the author was able to reproduce the architecture of a bone suitable for tissue engineering.

As it was mentioned before, still many challenges are being faced regarding the ideal properties of the hydrogel matrix used as the main printing material, but the material's potential is one of the main motivations of this research, and as it was observed in Figure 1, its potential growing rapidly.

3. Chapter 3 – Methodology

The study of the alginate/gelatin composite hydrogel will be divided in two general sections. The first one is the synthesis and characterization of the pre-crosslinked hydrogel or ink. This gel-like material is the one that will be extruded to form the designed structure in the built platform of the 3D Printer. The second section is the characterization of the completely crosslinked hydrogel structures. That means that once the pre-crosslinked gel is micro-extruded, the printed design will be crosslinked in a cationic solution and then this material will be characterized. In Figure 6 a chart with the summary of the different techniques that will be used to execute the study of the materials is shown.

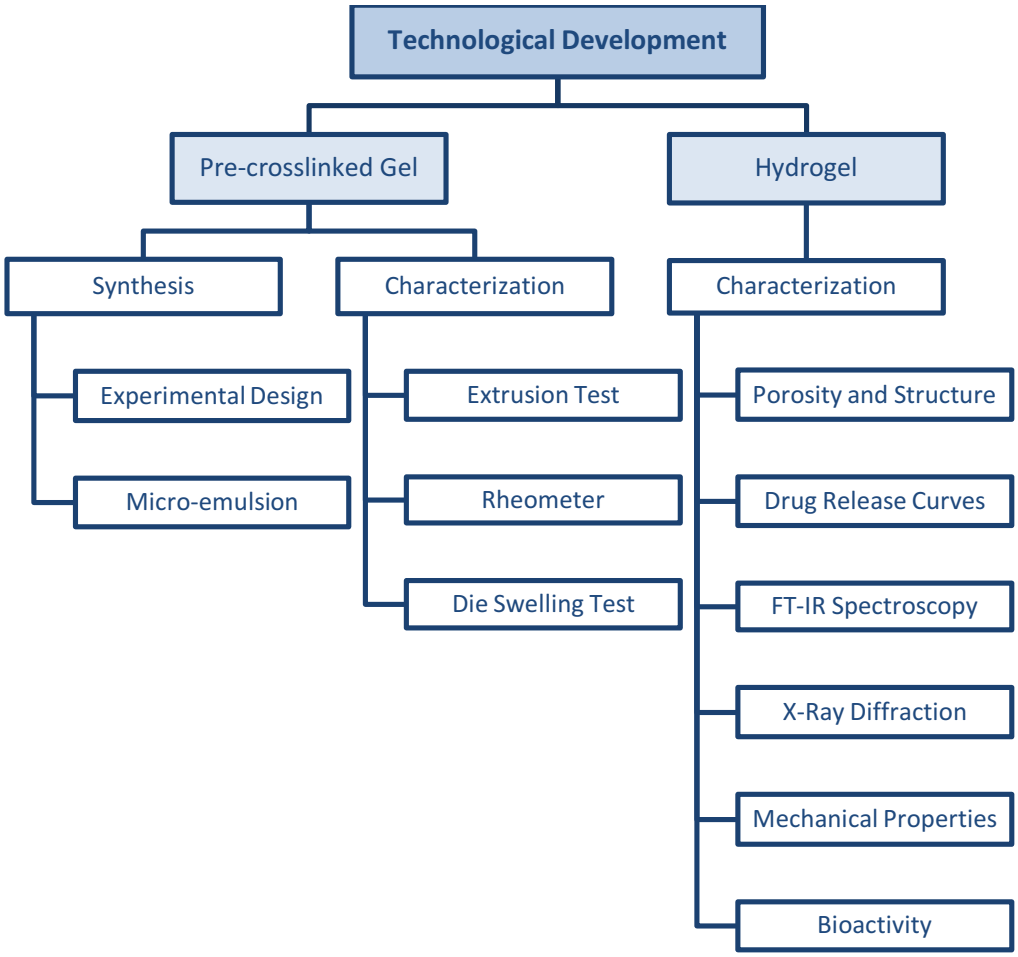

Figure 6. Organizational chart of the techniques followed in the research

A modified 3D printer, described later in detail, will be used to assess the hydrogel pre-crosslinked inks and determine the correct parameters for the manufacturing process.

3.1 Materials and Synthesis Methods

3.1.1 Materials

The following materials were used to synthesize the composite hydrogel and to carry out most of the characterization procedures. Sodium alginate (CAS no. 9005-38-3) a polysaccharide consisting of mannuronic (M) and guluronic (G) acid, and Titanium dioxide (TiO_2) nanopowder (21 nm, CAS no. 12188-41-9), Polyvinyl alcohol (PVA) used as an emulsifier (CAS no. 9002895, M_w 85,000 – 124,000, >99% hydrolyzed), Ibuprofen (IBU) (CAS no. 15687-27-1, >98% pure), Phosphate buffer saline (PBS) tablets, and beta-Tricalcium phosphate (β-TCP) (CAS no. 7758-87-4, >95% pure) were purchased from Sigma Aldrich (Missouri, USA). Gelatin (CAS no. 9000-70-8) and Calcium chloride ($CaCl_2$) (CAS no. 10043-52-4, >96% pure) were obtained from CTR Scientific (Control Técnico y Representaciones Scientific, Monterrey, Mexico). Dichloromethane (DCM) (CAS no. 75-09-2, anhydrous, >99.8% pure) was used as a solvent to dissolve the drug and it was purchased in Desarrollo de Especilidades Químicas (Monterrey, Mexico). Precision tips SNS-D 051/025 for the 3D printer were purchased from Nordson (Inner-0.25 mm) (Nordson Corporation, Ohio, USA).

3.1.2 Pre-crosslinked hydrogel solution preparation

The experimental design followed to synthesize the different systems of the alginate/gelatin composite hydrogel is presented in Table 5. In the first group of the table, from HG-0.0 to HG-0.4, the concentration of the crosslinker in the hydrogel systems was varied. With the first group, the $CaCl_2$ was added to the deionized water first and then the alginate. The solution was stirred at least two hours until all the alginate was dissolved.

For the second group, where the different factors added to the composite hydrogel was studied, the deionized water was used to dissolve first the pre-crosslinking agent, then the bioceramic and the nanoparticles were added. An ultrasonic bath was used to avoid agglomeration of the particles. Finally, both biopolymers were added, and it was stirred for at least two hours.

Finally, for the third group, where a composite hydrogel loaded with a drug was synthesized, first 2.00 w/v% PVA (used as an emulsifying agent) was dissolved in deionized water together with the pre-crosslinker. Once the polymer and $CaCl_2$ were completely dissolved with the aid of a magnetic stirrer, sodium alginate and gelatin were slowly added. The solution was stirred for at least two hours to ensure homogeneity. To avoid agglomeration, as it was done in the second group of hydrogel systems, the TiO_2 nanoparticles (0.1 w/v%) and the β-TCP (1.0 w/v%) were added before the two biopolymers. How to make the emulsion is explained in the following section.

Table 5. Labels used for different samples as a function of their composition

Group	Key	Composition								
		Alginate	Gelatin	TiO_2	β-TCP	Pre $CaCl_2$	PVA	IBU (in solvent)	Solvent	Volume Fraction
1 Pre Cross-linked	HG-0.0	2.00%	-	-	-	0.00%	-	-	-	-
	HG-0.1	2.00%	-	-	-	0.05%	-	-	-	-
	HG-0.2	2.00%	-	-	-	0.10%	-	-	-	-
	HG-0.3	2.00%	-	-	-	0.15%	-	-	-	-
	HG-0.4	2.00%	-	-	-	0.30%	-	-	-	-
2 Factors	HG-1	2.00%	-	-	-	0.20%	-	-	-	-
	HG-2	2.00%	0.50%	-	-	0.20%	-	-	-	-
	HG-3	2.00%	-	0.10%	-	0.20%	-	-	-	-
	HG-4	2.00%	0.50%	0.10%	-	0.20%	-	-	-	-
	HG-5	2.00%	0.50%	-	1.00%	0.20%	-	-	-	-
	HG-6	2.00%	0.50%	0.10%	1.00%	0.20%	-	-	-	-
	HG-7	3.50%	-	-	-	0.20%	-	-	-	-
	HG-8	3.50%	0.88%	-	-	0.20%	-	-	-	-
	HG-9	3.50%	-	0.10%	-	0.20%	-	-	-	-
	HG-10	3.50%	0.88%	0.10%	-	0.20%	-	-	-	-
	HG-11	3.50%	0.88%	-	1.00%	0.20%	-	-	-	-
	HG-12	3.50%	0.88%	0.10%	1.00%	0.20%	-	-	-	-
3 Loaded	HG-A	3.50%	0.88%	-	1.00%	0.20%	2.00%	20.0%	DCM	0.20
	HG-B	3.50%	0.88%	0.10%	1.00%	0.20%	2.00%	20.0%	DCM	0.20

3.1.3 Emulsion-laden pre-crosslinked hydrogel

To prepare the microemulsions in the third group of hydrogel systems, first the dispersed phase (dichloromethane with dissolved ibuprofen) was added to the continuous phase (pre-crosslinked hydrogel solution) with a volume fraction (φ) of the dispersed phase of 20%. The system was mixed using a magnetic stirrer bar for at least three hours and 1000 rpm at room

temperature in a closed system to avoid evaporation of the solvent. The dispersed phase was prepared by bringing ibuprofen in a concentration of 20 w/v% (0.40 of the saturation point) in contact with the organic solvent and mixing it until IBU is completely dissolved. Each of the prepared emulsions was observed under an optical microscope to assure their stabilization, where three different emulsifiers were compared: Sodium dodecyl sulfate, Kolliphor® P118, and PVA. For the rest of the study and characterization, the hydrogels with the PVA as emulsifier where used (HG-A and HG-B).

3.1.4 Crosslinked hydrogel preparation

To crosslink the hydrogels, a 6 w/v% $CaCl_2$ solution was prepared. The pre-crosslinked hydrogels were immersed in the calcium chloride solution for at least 24 hours to ensure complete crosslinking. After crosslinking, the hydrated hydrogels are washed with deionized water at least five times to remove all the excess calcium chloride left in the material.

3.2 Material Characterization

3.2.1 Rheology

Once the different pre-crosslinked hydrogel solutions were ready, they were characterized using a plate rheometer Anton Paar MCR 301 (Anton Paar GmbH, Graz, Austria). A flow curve was obtained for each sample from 0.1 to 100 s^{-1} shear rates to obtain the viscoelastic behavior of the hydrogel solution before complete cross-linking. The test was done for the first group to study the effect of crosslinking degree in the hydrogel's viscosity. Flow curves were also obtained to study the effect of the composition of the hydrogel (Group 2) on viscosity. Finally, the test was also repeated with the third group to study the effect of the microemulsion in the solution. Strain tests were also performed on all the hydrogel systems at a constant angular frequency (10 s^{-1}) to measure the storage (G') and loss modulus (G") of the samples.

3.2.2 Fourier transform infrared spectroscopy (FTIR) and X-Ray diffraction

Functional groups resolution was identified of each hydrogel sample with an infrared spectrometer coupled with Fourier transform Perkin Elmer (Massachusetts, USA) model Spectrum 400 recorded in the wavenumber range of 4,000–400 cm^{-1} at room conditions.

XRD techniques were used to validate the crystallinity of the nanoparticles inside the matrix of the composite hydrogel. XRD was recorded in the 2θ range between 10 and 85 and a step size of 0.026 using a PANalytical Empyrean diffractometer (PANalytical, Almelo, The Netherlands), CuKα radiation, of which the wavelength was λ=1.5406 Å. The applied voltage was 45 kV and the current was 40 mA. Samples were pulverized before measuring. Crystalline components of the samples were identified.

To make sure crystals of ibuprofen were forming inside the porous matrix of the hydrogel (Group 3), an XRD was also recorded in the 2θ range between 10 and 35 and a step size of 0.026 using the PANalytical Empyrean diffractometer. The characteristic peaks of crystalline ibuprofen were identified in that range. Samples were pulverized before measuring them in the equipment and the results were compared with the results of a sample of pure ibuprofen.

3.2.3 Thermogravimetric analysis and differential scanning calorimetry

Thermogravimetric and thermal analysis was carried out with a LINSEIS STA Platinum Series instrument (Linseis, Selbe, Germany). Samples were placed in alumina crucibles. Both samples of Group 3 (HG-A and HG-B) were analyzed for TGA and DSC in the same run. The samples were equilibrated 5 minutes at ambient temperature and then heated to 350 °C with a rate of 5 °C/min. Finally, they were equilibrated again for 5 minutes at 350 °C.

3.2.4 Microscopy, pore size, drug crystal size, and elemental analysis

For the pore size analysis, sphere-shaped hydrogels were synthesized following the crosslinked hydrogel preparation described before. The spheres were first frozen at -80 °C and then lyophilized in a LabConco FreeZone freeze dryer (LabConco, Missouri, USA) for 48 hours at -49 °C, and 0.04 mbar. The resulting dried spheres were sliced carefully using a razor and tweezers, and then the cross-section of the discs was analyzed in EVO MA25 Zeiss Scanning electron microscope (Zeiss, Jena, Germany) with an accelerating voltage of 20 kV and high vacuum. Three images were taken from each disc, ImageJ (National Institutes of Health, North Carolina, USA) processing program was utilized to calculate the average pore size.

In the case of the hydrogel systems in Group 3, the crystals of ibuprofen were also observed and compared to hydrogels of the same compositions without the drug. The crystals were also

measured using ImageJ. Energy dispersive x-ray spectroscopy (EDX, Bruker Analytical Systems, Massachusetts, USA) was done to some of the images, including general elemental analysis of the image taken and point elemental analysis, where just a specific location of the image taken was selected for the analysis.

3.2.5 Mechanical tests

The mechanical tests of the crosslinked hydrogel samples were characterized under the ASTM D638 standard Type V specimens for tensile tests. The pre-crosslinked solutions were poured into the molds and then they were crosslinked with the 6 w/v% $CaCl_2$ solution. The resulting dumbbell shape hydrogel specimens were washed with deionized water and then freeze-dried for later testing in the Instron Universal Machine 3365 (Instron, Massachusetts, USA) at 1 mm/min following the same norm for rigid and semirigid specimens. Four samples of each of the hydrogels were measured and the average elastic modulus was obtained.

3.2.6 Loading measurements and loading percentage

The volume fraction is described as the volume of the dispersed phase, relative to the continuous phase. This method will be used to characterize the amount of drug loaded in the matrix using 20% volume fraction in the solution. For each hydrogel system of Group 3, two batches of hydrogels were prepared following the same cross-linking method making spheres. One was the reference batch carrying no drug and the other the test batch carrying the desired drug concentration (HG-A and HG-B). After the spheres were pat-dried and weighed, both batches are placed in a vacuum oven over 2 days at 60°C. Loading is defined as the difference between the dried test batch carrying the drug and the dried reference batch, divided by the weight of the dried test batch. A material balance of all the “ingredients” used to synthesize the composite material is used to obtain the theoretical loading. It is important to mention that the API loading is measured assuming that all the water was removed.

3.2.7 Bioactivity

To measure the bioactivity of the material, or in other words, the interaction the material has with the human body, the nucleation of calcium phosphate in form of hydroxyapatite is studied. For this, the material is introduced in simulated body fluid (SBF) with a pH of 7.4 and at 36.5 °C.

The SBF was prepared following the methodology of Kokubo et al. [55]. The two composite hydrogels loaded with ibuprofen (HG-A and HG-B) were left in the SBF for 7, 21, and 28 days, and then analyzed using the SEM and energy-dispersive X-ray spectroscopy (EDX). Imaging was used to observe if the particles of β-TCP inside the hydrogel matrix were nucleating into hydroxyapatite in two replicates, and the spectroscopy analysis to confirm the formation of the calcium phosphates.

3.2.8 Drug dissolution profiles

The profiles were done with concentration curves. Aliquots of the solution are transferred into 10 mL cuvettes and introduced inside a UV-spectrophotometer HACH DR 6000 (Hach, Düsseldorf, Germany). The wavelength is set a 221 nm, characteristic of ibuprofen. A calibration curve is made based on known concentrations of ibuprofen in a Phosphate buffer saline solution and the resulting absorbance.

$$\boldsymbol{Abs = m * conc + b} \quad (1)$$

Where Abs is the absorbance in a determined wavelength of the UV-Vis. After the calibration curve is obtained, the drug dissolution profiles are obtained. The in vitro drug dissolution experiments are carried out at 37°C ± 0.1 using a jacketed glass reactor fed by a controlled temperature system. The hydrogel structures are introduced into the PBS solution. Every certain amount of time, a sample is taken out and introduced into the spectrophotometer, where the absorbance value at 221 nm is reported. The sample is returned to the jacketed reactor after the absorbance value is read. When the concentration reaches a constant value, it is assumed that the available drug has been fully dissolved, and the experiment is finished. Three replicates are done for each of the systems tested. With the calibration curve, the concentration released is obtained and compared to the theoretical loaded value.

Fickian, Non-Fickian and Case II diffusion mechanism for the drugs released from the polymer matrix can be calculated from the Equation (2).

$$\frac{\boldsymbol{M_t}}{\boldsymbol{M_\infty}} = \boldsymbol{kt^n} \quad (2)$$

where M_t/M_∞ is the fractional drug release in time t, k is the constant characteristics of the drug-polymer system, in this case the hydrogel-ibuprofen, and n is the diffusion exponent characteristics of the release mechanism. For a Fickian release mechanism, n = 0.5, for Case II diffusion n = 1.0, and for Non-Fickian diffusion, n = 0.5 - 1.0 [56]. Values of n and k of HG-A and HG-B are presented in the results section.

Furthermore, the diffusion coefficients D_E and D_L were calculated using approximations of the equations obtained when solving Fick's second law of diffusion under initial and boundary conditions equivalent to those of those of testing in this work [57]:

$$\frac{M_t}{M_\infty} \cong 4\left(\frac{D_E t}{\pi \delta^2}\right)^{0.5} \quad (3)$$

$$\frac{M_t}{M_\infty} = 1 - \frac{8}{\pi^2} exp\left(-\frac{\pi^2 D_L t}{\delta^2}\right) \quad (4)$$

where M_t/M_∞ is the fractional drug release, t is the release time, D_E and D_L are the diffusional coefficients, and δ is the diffusional distance. Equation (3) is the early-time approximation and Equation (4) is the late-time approximation equation.

3.3 Design and Manufacturing Process

3.3.1 Design models

Scaffolds were designed using Rhinoceros 5.0 (Mc Neel & Associates, Seattle, USA), a 3D modeling software with the grasshopper plugin. Three types of scaffolds were designed and are shown in Figure 7, grid, voronoi, and hexagons (20mm width x 20mm length). Rhinoceros used grasshopper plugin, a graphical algorithm editor for the fabrication of parametric forms without the scripting experience. Parameters for this module were specifically selected to have reproducible and well-structured scaffolds. The parameters were line thickness (0.40 mm - 0.60 mm), cell size (depending on the cell number), and cell number (25 - 35).

3.3.2 Manufacturing process

For the extrusion process of hydrogels, a modified RepRap Mendelmax 3D printer (Fundació CIM, Barcelona, Spain) with a work volume of 20 x 20 x 15cm was used. The extrusion process was modified to work with a piston extruder such as a 10 mL (14 mm of diameter) syringes (20

G, BD Ltd., New Jersey, USA) with a needle of internal diameter of 0.25 mm (SNS-D 051/025, Nordson).

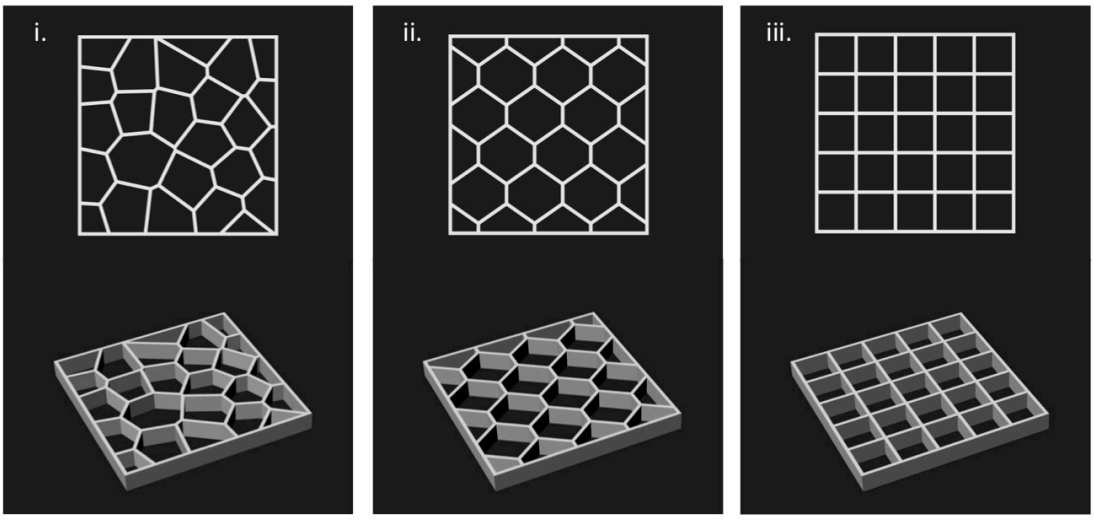

Figure 7. Scaffold designs (i) voronoi, (ii) hexagon, (iii) grid

The modified printer can be found in Figure 8, where the modified extruder designed for gels and viscous liquids is shown along with isometric views of the printer. For the generation of the G-code, the STL was introduced into open source software Cura 15.04.6 (Ultimaker, Geldermalsen, The Netherlands). Change in temperature was not required in this process. Qualitative analysis of the printed structures was performed using a SteREO Discovery.V8 equipped with a CCD camera AxioCam HRc (Carl Zeiss Micro imaging GmbH, Jena, Germany) and AxioVision 4.8 software.

3.3.3 Printed line deformation and Hydrogel Shrinkage

To measure line deformation in the scaffolds as the height of the design increases, the grid structure was printed with 0.15 mm, 0.75 mm, and 1.5 mm of height (1, 5, and 10 layers respectively). Afterwards, the line widths of the printed grid were measured in four separate locations of the structure with the SteREO and reported. This test was done for the second group of hydrogels in the experimental design (HG-1 to HG-6).

For the shrinkage of the hydrogel through the process (extrusion, crosslinking, and freeze-drying), the same methodology used to measure the line deformation was applied. The grid designs and the SteREO were used to measure shrinkage and its percentages were obtained.

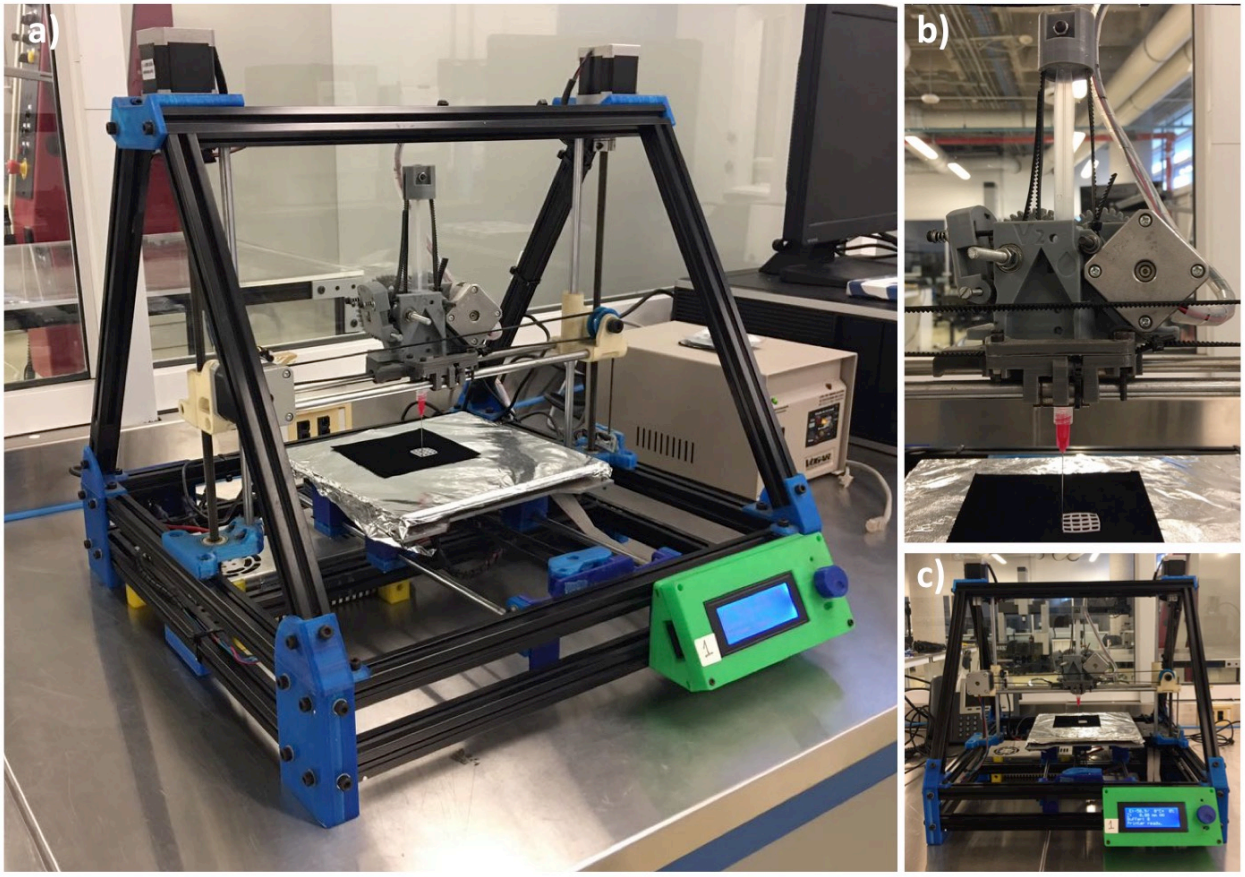

Figure 8. RepRap Mendelmax 3D printer with the modified extruder for the hydrogel printing
a) Isometric view b) Close-up view from the modified extruder c) Front view

Once the grid was printed, crosslinked and dried, a non-contact, three-dimensional, and based on focus-variation analysis was done with an InfinteFocus Alicona (Alicona, Graz, Austria). Although this equipment is used generally to obtain roughness from surfaces, using the lowest magnification, measurements of height and width were obtained from different locations of the grid structure once it was freeze-dried.

3.3.4 Die swell behavior

Also called the Barus effect, this was measured with a high speed DataPhysics OCA 15EC system (DataPhysics Instruments GmbH, Filderstadt, Germany). The needle used in the microextrusion

with a millimetric syringe was installed in a syringe pump programmed at 5 mL/h and the end of the needle was placed in front of the camera. Several images using the SCA20_U software (DataPhysics Instruments GmbH, Filderstadt, Germany) were taken while a drop of material was extruded. The width of the hydrogel solution drop was measured 0.08 mm from the end of the tip, which is the distance in the actual printing process from the end of the tip of the needle to the build surface of the 3D printer. After the formulation with the best resolution (and optimal viscosity) was chosen, a test to print a cubic structure 100% filled is done and printed grid designs with difference viscoelastic behavior are compared.

4. Chapter 4 – Results and Discussion

4.1 Study of the hydrogel ink

4.1.2 Viscoelastic properties

First, the rheological study of the pre-gel solutions with different pre-crosslinking percentages (Group 1) is presented in Figure 9. The solutions were synthesized with different concentrations of the cross-linker, calcium chloride. As the concentration of the premixed calcium chloride gets higher, the viscosity of the solution increases due to a higher percentage of crosslinked alginate monomers bonded with ionic bonds, as it is observed in Figure 9a. To have a better insight of its viscoelastic properties, an amplitude sweep was also measured.

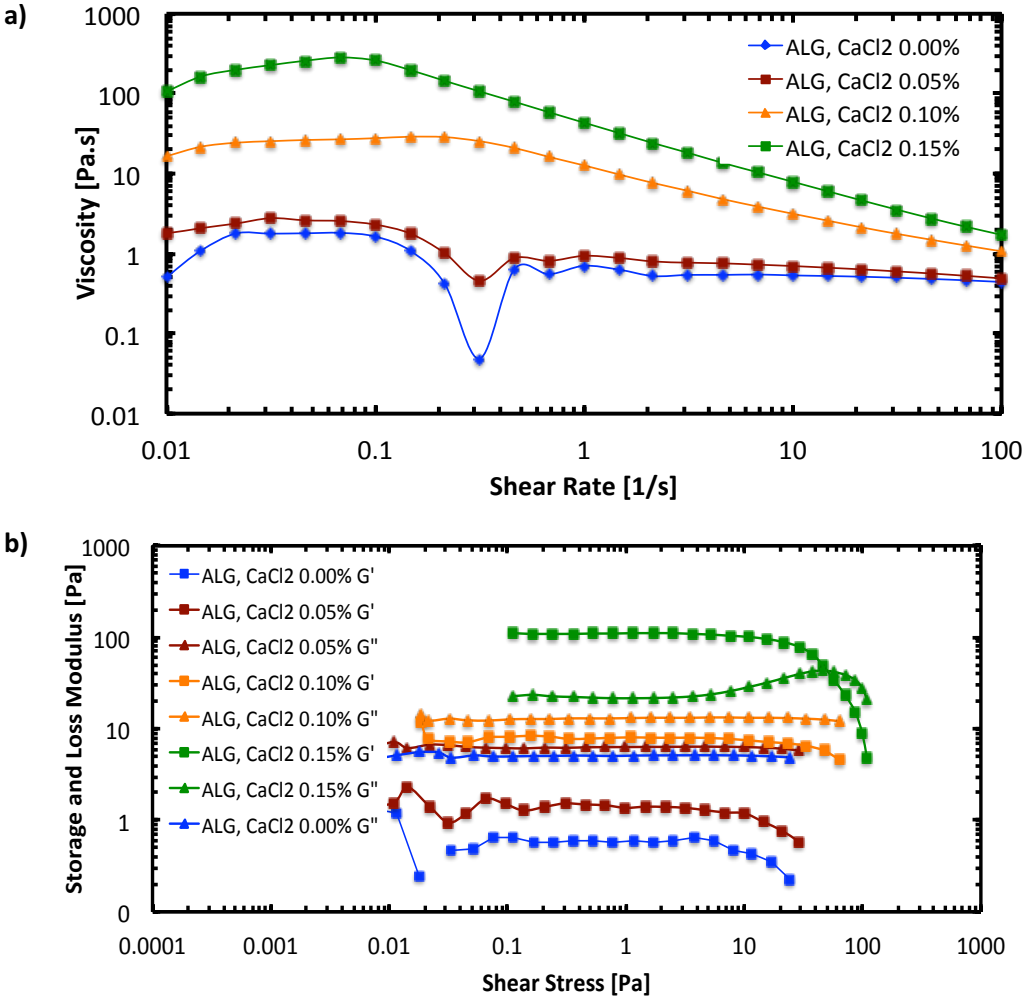

Figure 9. Rheology tests a) Flow curve for pre-crosslinked solutions b) Amplitude sweep for pre-crosslinked solutions

As it can be observed in Figure 9b, when the crosslinker reaches a concentration of 0.15 w/v% in the solution (1:13 ratio of $CaCl_2$ to alginate), the storage modulus is higher than the loss modulus (G' > G'') at low shear rates. This characteristic is essential to the hydrogel ink to avoid the collapse of the scaffold structure when it is being printed. Lower concentration than 0.15 w/v% of calcium chloride (keeping the ratio), the solution acts as a liquid even when no force is applied to the solution, so the structure will collapse after it is extruded. In an extrusion test, all hydrogels with 2 w/v% alginate and lower than 0.15 w/v% $CaCl_2$ were not feasible. The curve of HG-0.4 is not graphed because the viscosity was so high at low shear rates that it required too much force to extrude from the syringe used later for printing, and it was discarded from the study. Further tests were done with 0.20 w/v% $CaCl_2$ pre-crosslinking concentration.

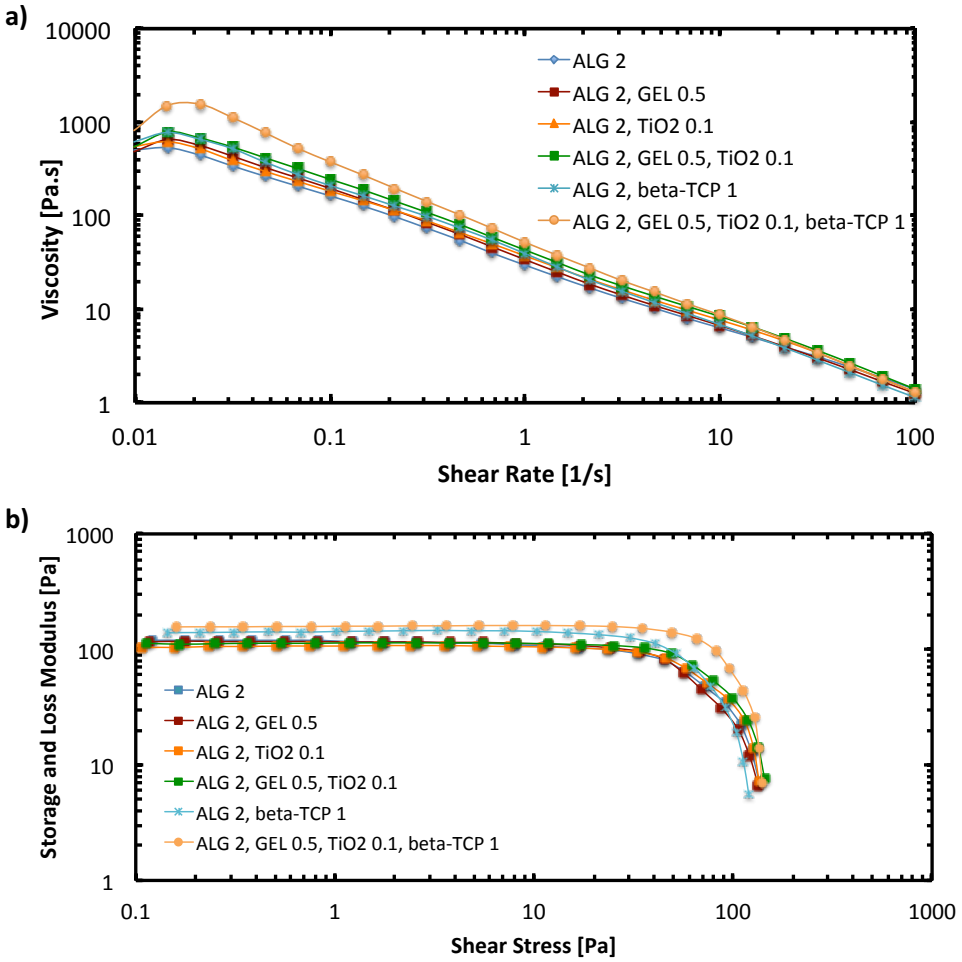

Figure 10. Rheology tests a) Flow curve of hydrogels with different compositions with 0.20% of pre-crosslinker b) Amplitude sweep (just storage modulus) of hydrogels with different compositions with 0.20% of pre-crosslinker

Regarding the varied factors in the composition, the addition of gelatin or TiO_2 nanoparticles, seem to not affect the viscosity of the solution nor their viscoelastic behavior, as it can be observed in Figure 10. Nevertheless, addition of β-TCP (1.0 w/v%) combined with gelatin and TiO_2 increases the viscosity of the pre-crosslinked hydrogel solution in the low shear rate range. This may translate into a better printability and less deformation of the gel after extrusion and will be discussed further later in this chapter.

Finally, the same tests were performed to the third group of hydrogel systems in the experimental design, hydrogels with and without microemulsions, to see the effect these microemulsions will have on the viscoelastic properties. As it can be observed in Figure 11a, stable microemulsions up to 20% of volume factor in the solution does not affect viscosity. Theoretically, as the dispersed phase of the solution is increased, its viscosity will also increase.

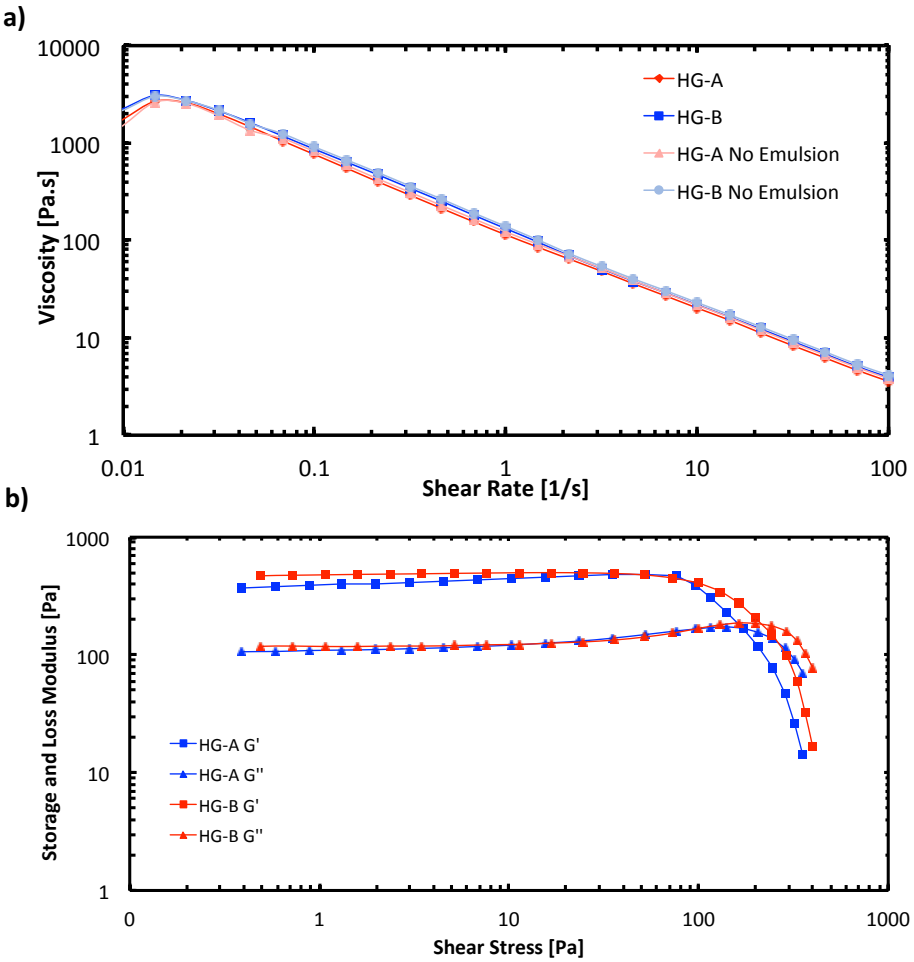

Figure 11. Rheology tests a) Flow curve for solutions with and without microemulsions b) Amplitude sweep for solutions HG-A and HG-B

In Appendix I a study of the viscoelasticity of different solutions with microemulsions with different volume factors is presented. For this work a volume factor of 20% was used (HG-A and HG-B). With this percentage, the viscosity of the system did not change. Viscosity of a solution with microemulsions will depend mainly on the viscosity of the continuous phase and the volume factor of the emulsions. In literature it has been presented that viscosity of emulsions will change significantly with volume factors greater than 0.45 [58].

4.1.2 Emulsion-laden pre-crosslinked hydrogel

To make sure the emulsions were stable after being mixed up with the pre-crosslinked hydrogel solution plus the PVA as emulsifier, optical microscope images were taken at the final synthesized microemulsion solutions. It is important to mention that bubbles were a problem when the viscosity of the pre-crosslinked hydrogels increased, trapping bubbles more easily as it was mixed. Therefore, it was important to differentiate bubbles from emulsions. In Figure 12, the emulsion of HG-1 versus HG-7 is presented. In HG-1, there could be observed some microemulsions, but much less than what was expected for a volume factor of 20%. In HG-7 more microemulsions were observed in the images. It must be noted that both solutions were mixed for the same time and using the same technique.

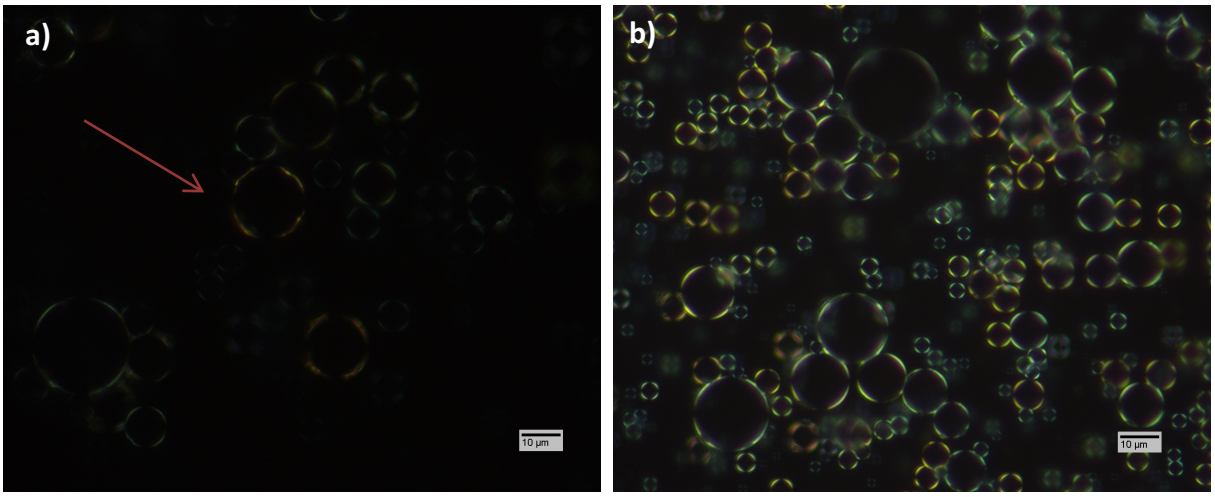

Figure 12. Optical microscope image of microemulsions a) HG-1 b) stable emulsion of HG-7

It was easier to create a stable emulsion with the solution with the higher viscosity, HG-7, using 2.0 w/v% PVA as emulsifier and DCM as solvent. This is one of the reasons, beside better printing resolution that will be discussed later in this chapter, that the same concentration of

alginate of HG-7 was chosen to load an active pharmaceutical ingredient in HG-A and HG-B. An independent study was done to screen for a solvent and emulsifier. The results are shown in Appendix II where a table of all the solvents considered for the test is shown. Furthermore, a series of images of the microemulsions for different emulsifiers and the solvents previously chosen are also shown. DCM was chosen as a solvent and PVA as emulsifier.

4.2 Study of the composite hydrogel

4.2.1 FTIR AND XRD CHARACTERIZATIONS

In Figure 13a it is compared the FTIR spectra of the different hydrogels. It was observed that the alginate chemical structure was maintained with the addition of other components. The bands at 3273 cm^{-1} represent the stretching vibrations of O-H in calcium alginate, while the peaks at 1590 cm^{-1} and 1410 cm^{-1} represent the stretching vibrations of C=O, and finally the strong peak observed at 1030 cm^{-1} is assigned to COC and C-C vibrations. Other bond vibrations, such as the one of Ti-O, could also be identified in the figure for the hydrogels where this component was added, such as the HG-3, HG-4, and HG-6 hydrogels. The sharp peaks representing the stretching of PO_4 in β-TCP are at 561 cm^{-1} and 607 cm^{-1}. In Appendix III, FTIR measurements for the materials used in the composite hydrogels were done.

Furthermore, in Figure 13b, FTIR identification was done to HG-A and HG-B comparing the reference (without API) to the loaded hydrogel. No significance difference was found between the reference and the loaded hydrogel. This means that loaded API, ibuprofen, has no molecular interaction with the polymers or bioceramics of the hydrogel, leading to faster dissolution profiles, which are discussed later in this chapter.

In Figure 14, the results of the XRD test with peak identification can be found. The XRD results showed the crystallized form of TiO_2 nanopowder. Alginate and gelatin showed no characteristic peaks, given that they form an amorphous polymer. The crystalline form of TiO_2 is anatase, with characteristic peaks at 21, 23, 48° (JCPDS 01-073-1764), can be found in the samples where the oxide was added (HG-3 and HG-6). Of the hydrogels containing β-TCP, HG-6 is shown in Figure 14a, showing characteristics peaks of calcium phosphate at 23, 31, 35, and 53° (JCPDS 01-073-4879). Some peaks that are not identified in the graph come from sodium chloride, which is a

by-product from the crosslinking process of alginate with calcium chloride. Most of the sodium chloride is removed with the washes done with deionized water after crosslinking, but some crystals may remain in the surface after the material is dried.

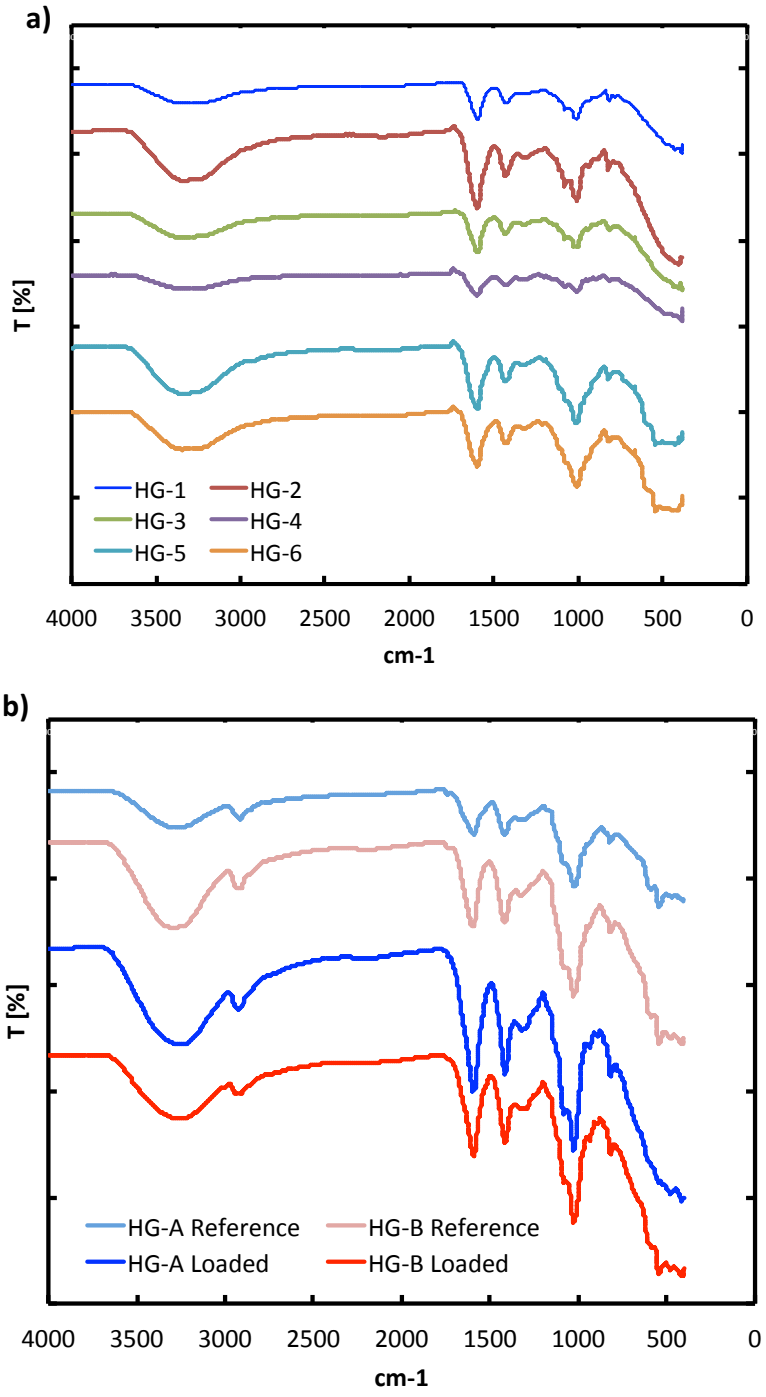

Figure 13. FT-IR Identification a) functional groups of the dried composite hydrogels (HG-1 to HG-6) b) HG-A and HG-B reference vs. loaded

In Figure 14, the results of the XRD test with peak identification can be found. The XRD results showed the crystallized form of TiO_2 nanopowder. Alginate and gelatin showed no characteristic peaks, given that they form an amorphous polymer. The crystalline form of TiO_2 is anatase, with characteristic peaks at 21, 23, 48° (JCPDS 01-073-1764), can be found in the samples where the oxide was added (HG-3 and HG-6). Of the hydrogels containing β-TCP, HG-6 is shown in Figure 14a, showing characteristics peaks of calcium phosphate at 23, 31, 35, and 53° (JCPDS 01-073-4879). Some peaks that are not identified in the graph come from sodium chloride, which is a by-product from the crosslinking process of alginate with calcium chloride. Most of the sodium chloride is removed with the washes done with deionized water after crosslinking, but some crystals may remain in the surface after the material is dried.

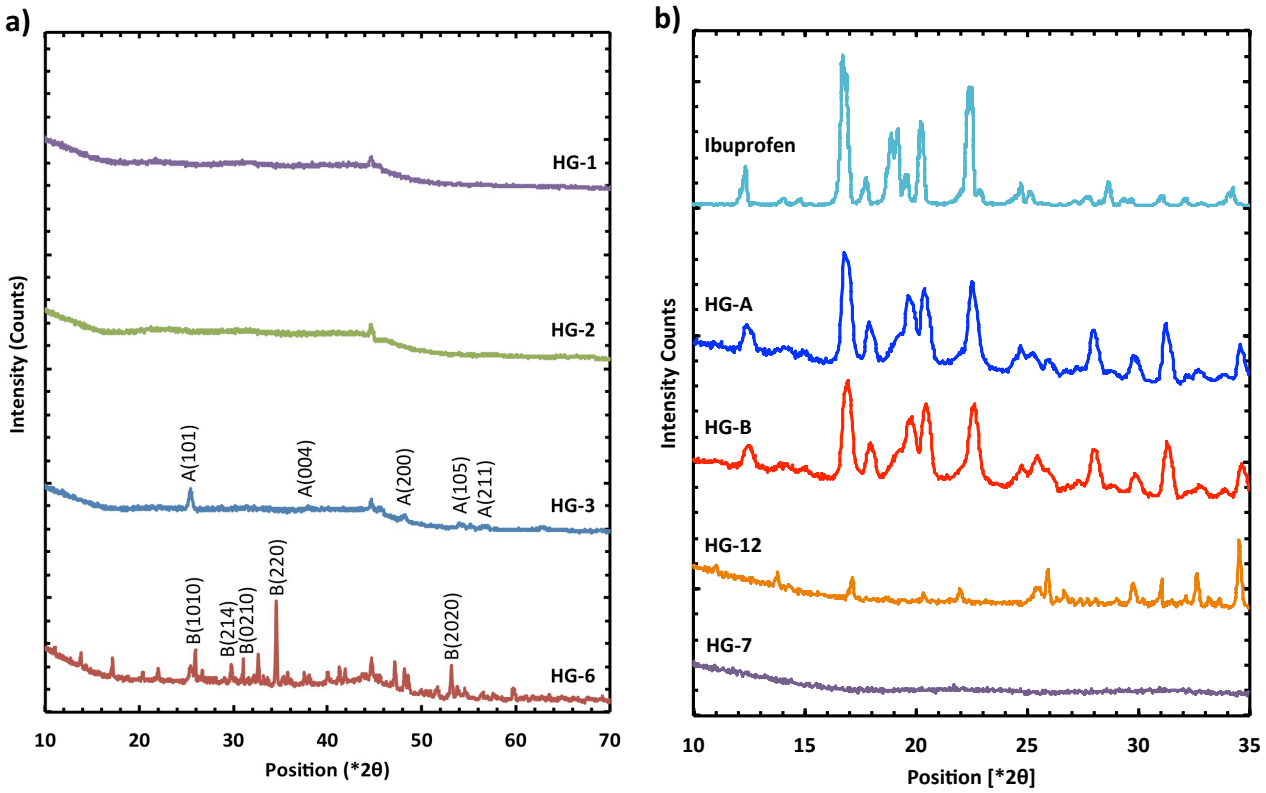

Figure 14. a) XRD plots of dry hydrogels with gelatin, TiO_2, and β-TCP as additives b) XRD plots of dry hydrogels loaded with ibuprofen and their references

In Figure 14b, the results of the hydrogels loaded with ibuprofen can be found. As the main purpose of the test was to assure the crystallization of ibuprofen, the results of both hydrogels are compared to the result of pure crystallized IBU. PVA, just like alginate and gelatin, showed

no characteristic peaks. On the other hand, when comparing the results with pure IBU, it can be found that most of the characteristic peaks match, confirming the crystal growth of the API inside the porous structure of the composite hydrogel. In Figure 14b a reference of a hydrogel containing just alginate (HG-7) with no peaks, and the composite hydrogel with the two biopolymers, TiO_2, and β-TCP (HG-12), are added to the graph. In the curve of HG-12, the peaks belonging to the anatase form of titanium dioxide and of the calcium phosphates are shown, to differentiate them from the crystals of ibuprofen.

4.2.2 TGA AND DSC

The main purpose of doing a thermogravimetric analysis and differential scanning calorimetry was to confirm the formation of crystals of the ibuprofen. For this, the two systems of group three were tested. In Figure 15 the results of both methods are show in a graph for HG-A and HG-B respectively. Analyzing the measurements of DSC first, the results exhibit a well-defined endotherm at approximately 75.5 °C in both cases, characteristic of the melting point of a pure ibuprofen crystal. The not so well-defined endotherm at 200 °C correspond to the melting point of PVA of the composite hydrogel. The lack of definition is due to the amorphous state of the polymer in the material. The endotherm of ibuprofen, combined with the XRD measurements, demonstrates that the encapsulated ibuprofen is in the crystalline state within the porous matrix of the hydrogel. In the next section, some of these crystals will be visible with SEM imaging.

Regarding the measurements of TGA, three major slopes can be identified. The first slope, that goes from 30 °C to 90 °C corresponds to all the moisture that was trapped inside the hydrogel matrix. Even though the materials were freeze-dried previously, it was found that the porous matrix is hygroscopic, and absorbs moisture readily. The loss of mass is less than 5% in this step. The second slope that goes from 130 °C to 200 °C corresponds to the loss of ibuprofen. This time, the loss of mass is around 35%. In the next sections, the actual loading and the theoretical loading of ibuprofen are obtained, and it will be observed that the numbers match.

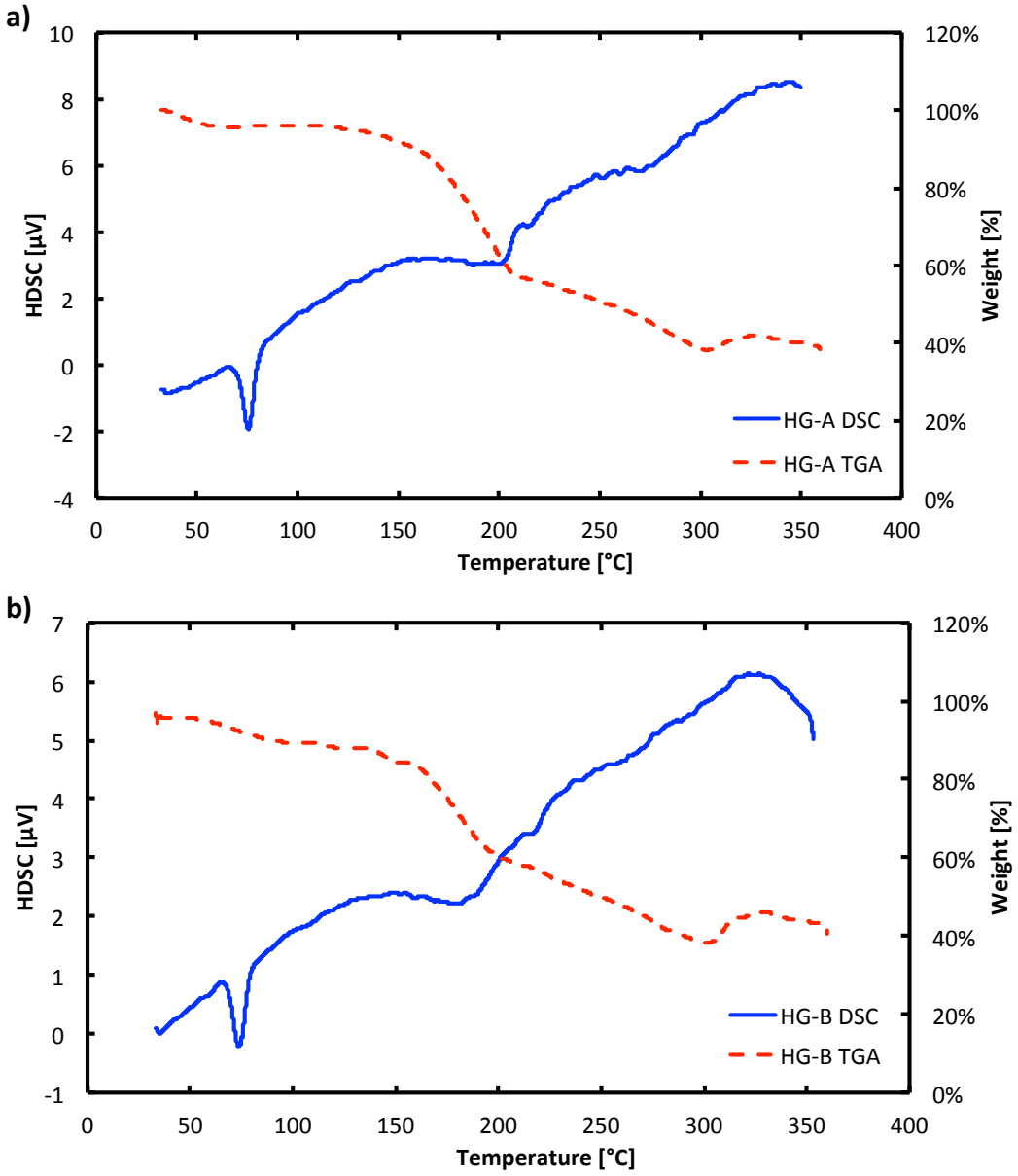

Figure 15. TGA and DSC of a) HG-A and b) HG-B

Finally, the third major slope goes from 200 °C to 300 °C. This mass loss corresponds to the partial decomposition of the polymers. Given that the three of them have similar decomposition temperatures, it is difficult to differentiate from one another. The mass loss is around 21% in both cases. That leaves a total mass loss of around 61%, leaving behind 39% that corresponds to the bioceramics, TiO_2 when it was added, and the remaining polymer. It is important to notice that the addition of 0.10% of TiO_2 nanoparticles did not have any significant effect on the thermogravimetric properties of the polymers.

4.2.3 Porosity, Structure, and Elemental Analysis

All the hydrogels in Figure 16a show high porosity, property looked after in tissue engineering for biological delivery. An average pore size that ranges from 110 µm to 200 µm is observed. Nevertheless, a trend can be observed in the average pore size of the samples in Figure 16b. When a second biopolymer, in this case gelatin in HG-2, or TiO_2 nanopowder in HG-3 is added to the solution, there is a reduction of the average pore size. This reduction can be related to the increased degree of entanglement of the alginate polymer chains and the change in the hydrogels' internal structure, both caused by the addition of a second component. Overall, its average pore size (160 µm ± 45 µm) is in the range of an adequate scaffold pore size to promote cell proliferation of bones and cartilages.

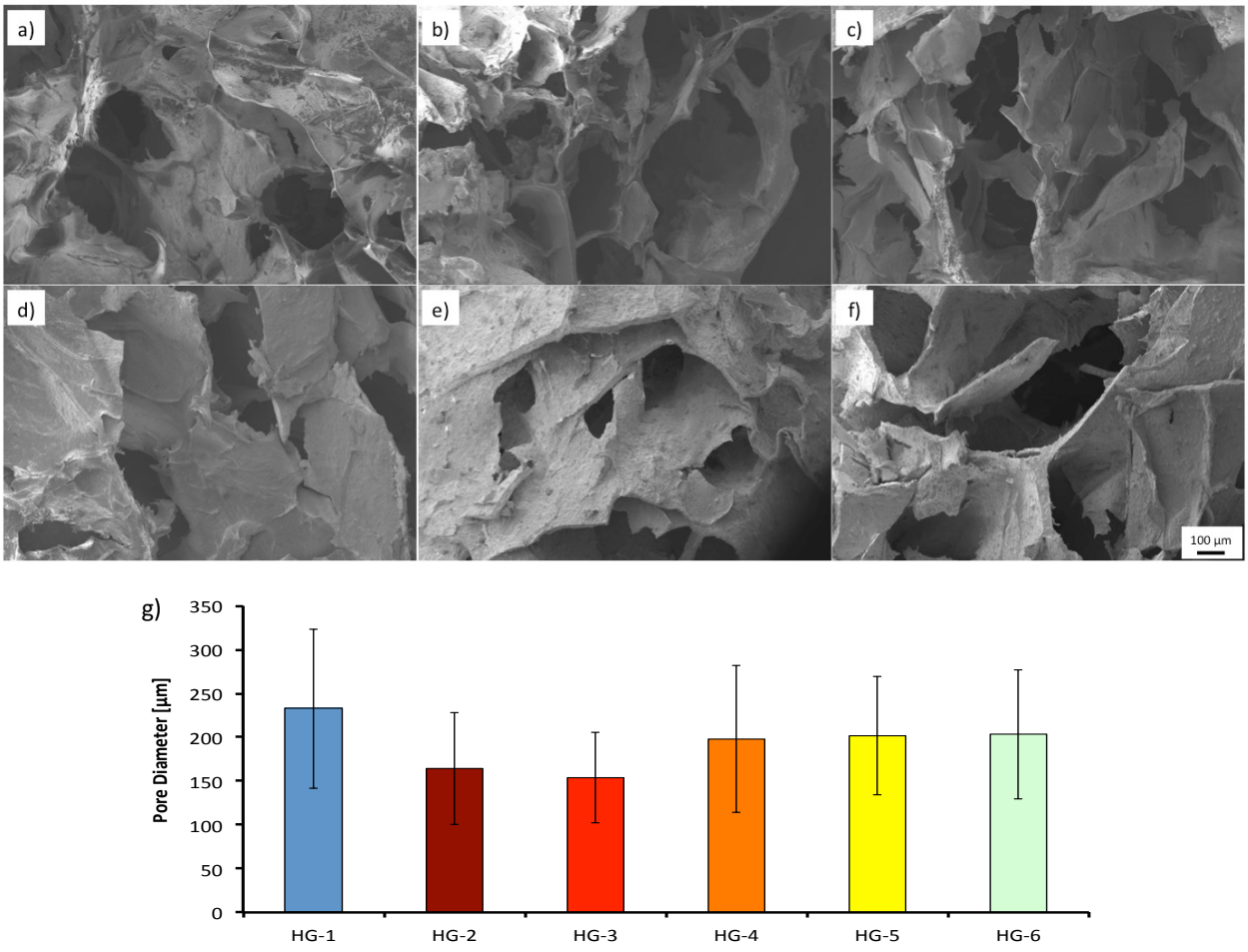

Figure 16. SEM imaging of the hydrogel systems of a) HG-1 b) HG-2 c) HG-3 d) HG-4 e) HG-5 f) HG-6 g) Average pore size of hydrogel systems HG-1 to HG-6

In Figure 17, both hydrogel systems are presented together with their reference containing no drug. No significant difference can be found between both systems, and they have an average pore size that ranges from 25 µm to 50 µm. Further work needs to be done to increase the average pore size of these hydrogels to reach the adequate range for cell proliferation. A recommended starting point could be the optimization of emulsifier (PVA) in the solution.

Crystals can be observed in the cross-section cut of the hydrogel. When the pre-crosslinked emulsion-laden solution was crosslinked with the CaCl2 solution, the microemulsions were trapped inside the hydrogel matrix. Once the solvent used for the microemulsion and the water from the hydrogel evaporated, these crystals grew in the available space, which were the pores. The size of the crystals is in the range of 7 µm to 18 µm. The size or amount of the crystals can be modified by changing the concentration of the API dissolved in the solvent, by modifying the mixing method, or even by changing the volume factor of the emulsion. As the amount of API dissolved reaches saturation, the crystals will be bigger. When the mixing method is changed, the size of the emulsion droplets will also change and as consequence, the crystal size will change as well.

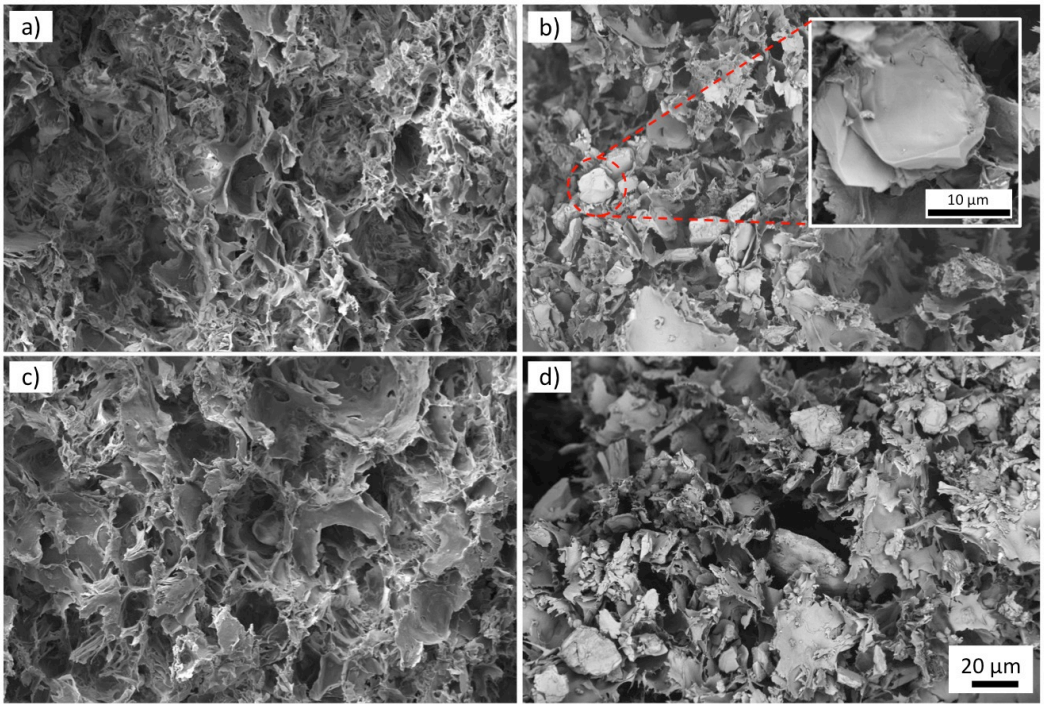

Figure 17. SEM imaging of hydrogels a) reference HG-A b) HG-A loaded with ibuprofen c) reference HG-B d) HG-B loaded with ibuprofen

The EDX generated a general elemental analysis to the images of HG-A and HG-B. Furthermore, point elemental analysis was also generated for the surface of the hydrogel, inside the pores, the bioceramic particles, and the ibuprofen crystals. In Table 6 the results of the general elemental analysis can be found. The major difference between both hydrogel systems is the presence of titanium in HG-B due to the TiO_2 nanoparticles. No agglomeration of nanoparticles or bioceramics was observed. This confirmed a good mixing during the synthesis of the pre-crosslinked inks.

Table 6. General elemental analysis results of HG-A and HG-B

Element	At. No.	HG-A		HG-B	
		Mass [%]	Atom [%]	Mass [%]	Atom [%]
Carbon	6	50.03	61.70	46.48	58.00
Oxygen	8	35.06	32.46	38.70	36.25
Calcium	20	11.87	4.39	10.75	4.02
Phosphorus	15	3.04	1.45	2.66	1.29
Titanium	22	-	-	1.42	0.44

In Appendix IV the complete report obtained from the EDX measurement is shown. This report includes the graph showing the element peaks, the image analyzed, and the table containing the exact resulting amounts of the elements (mass and atom) with their error. In addition to both hydrogel systems, there is a third EDX report where a single ibuprofen crystal of the HG-B system was analyzed.

4.2.4 Mechanical test

To determine the potential use of the alginate/gelatin composite hydrogel in tissue engineering applications, mechanical properties were measured with tensile tests of the dried hydrogels. McKee et al. measured different values of elastic modulus of soft tissue engineering that ranges all the way from 2 MPa for spinal cords, all the way up to 560 MPa in some tendons [59], but for oral soft tissues Goktas et al. showed that gingival tissue shows an elastic modulus of 19.75 ± 6.2 MPa [60]. Results of the tensile test of the different dry hydrogels can be found in Figure 18. The elastic modulus obtained from the different hydrogel composites range from 9 MPa to 20

MPa. The reference hydrogel HG-1, containing alginate alone, was too fragile even to measure, breaking up while handling the dumbbell shaped probe. Nevertheless, as gelatin (HG-2) or the TiO_2 nanoparticles (HG-3) are added, the elastic modulus is increased to 9 MPa and to 13 MPa respectively.

Furthermore, when both components (gelatin and nanoparticles in HG-4) are added, its elastic modulus is further increased to 20 MPa. This is believed to happen due to the increased entanglement of the crosslinked polymer chains when a second component is added, same behavior that caused the reduction in the average pore size discussed previously. When β -TCP is added to the hydrogel probe, the elastic modulus decreases. Instead of promoting entanglement of the alginate chains, β-TCP is causing a sooner fracture of the hydrogel probes.

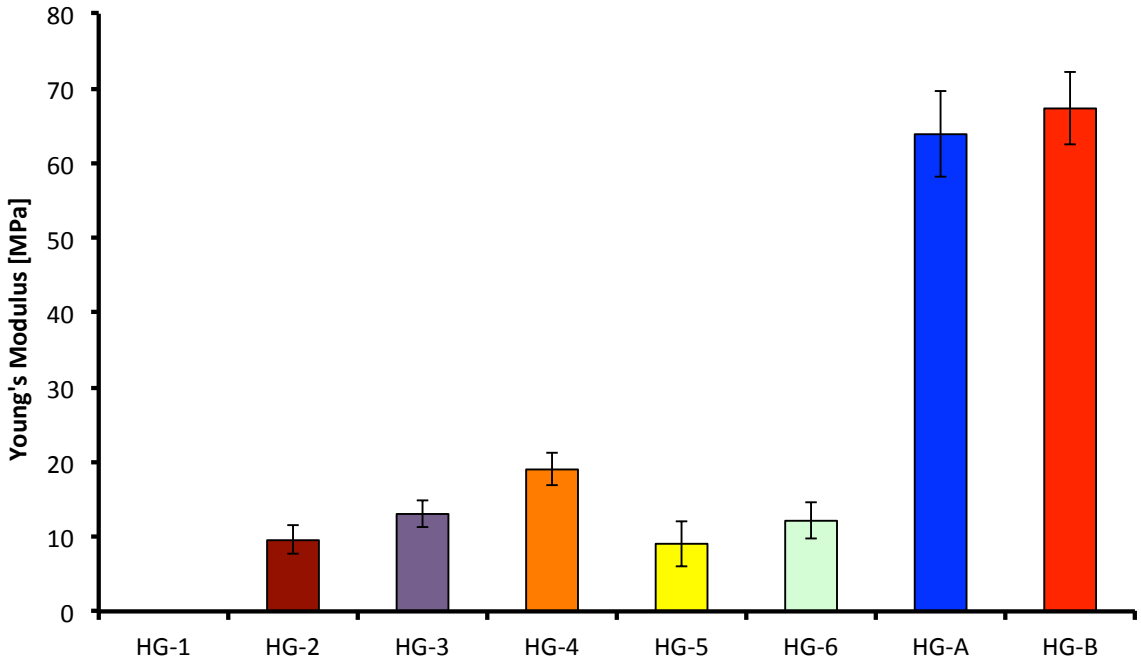

Figure 18. Young's modulus of the hydrogels HG-1 to HG-6, HG-A, and HG-B obtained from tensile tests in the universal machine

This is probably caused by the high percentage added of calcium phosphate, which is in the ratio of 1:2 of alginate in the solution. It is important to address that the tensile tests were done with dry hydrogels. Wet hydrogels will show a completely different value of elastic modulus. Because of the nature of the alginate crosslinked with an ionic bond with Ca^{+2}, the mechanical properties, as mentioned previously, are still a challenge. The third group of hydrogels systems

was also tested for mechanical properties using the tensile test. The biggest difference between the second and third groups is increased concentrations of alginate and gelatin and the use of a third polymer, PVA.

As it was expected, the elastic modulus increased. The Young's Modulus of HG-A and HG-B can be observed in Figure 18. The addition of a third polymer (PVA) and increasing the concentrations of alginate and gelatin resulted in more than three times the value of the elastic modulus of the hydrogels in the first group, 65.5 MPa. As it was observed in the porous structure of HG-A and HG-B, there is a more packed structure and an increased entanglement of the crosslinked polymer chains, resulting in a smaller pore and an increased strength. In Appendix V the actual curves from HG-2, HG-4, HG-A, and HG-B, obtained from the universal machine, can be founded. In that graph, it is easily noticeable how the change of composition can affect the complete mechanical behavior of the composite hydrogels.

4.2.5 DRUG LOADING

The loading percentage can be expressed as the amount of drug dissolved in the dispersed phase over the final weight of the dried hydrogel and is obtained with the following equation.

$$\boldsymbol{Loading}\% = \frac{\boldsymbol{W_{loaded} - W_{reference}}}{\boldsymbol{W_{loaded}}}\ \boldsymbol{x\ 100} \qquad (5)$$

Where W_{loaded} is the dried weight of the hydrogel with ibuprofen and $W_{reference}$ is the dried weight of hydrogel without any drug. This percentage was compared to the theoretical percentage based on the compositions used to synthesize the hydrogel

$$\boldsymbol{Theoretical\ loading}\% = \frac{\boldsymbol{C_{IBU} V \phi}}{\boldsymbol{(C_{HG}) V (1-\phi) + C_{IBU} V \phi}} \qquad (6)$$

where $C_{IBU}V\phi$ is mass of embedded ibuprofen in the hydrogel with volume V, C_{HG} is the sum of the concentration of the biopolymers, emulsifiers, and the additives (alginate, gelatin, PVA, β-TCP, and TiO_2), and $V(1-\phi)$ represents the volume of the continuous phase in the hydrogel.

In Table 7 it can be found the results of the experimental loading and theoretical loading. The experimental values are slightly lower than the expected values; this may be due to the loss of some microemulsions during the crosslinking process or the washing steps after crosslinking, or even loss of small API crystals during handling of the dry hydrogel.

Table 7. Experimental loading versus theoretical loading of HG-A and HG-B systems

Hydrogel	API	Loading [%]	Theoretical Loading [%]
HG-A	Ibuprofen	32.5%	35.2%
HG-B	Ibuprofen	33.1%	34.8%

It is important to note that this drug loading percentage was achieved with just 0.20 of volume fraction in the microemulsion and with 20% of ibuprofen dissolved in the solvent. This is less than half of the saturation. If it is needed, adjusting these two variables, volume fraction and amount of drug in the solvent, could modify the material loading. Nevertheless, further studies are necessary to prove its use in microextrusion and assess its physicochemical properties. These loading percentages agree with the results from the thermogravimetric analysis, where the same mass of ibuprofen was lost after increasing the temperature of the sample, causing the ibuprofen to decompose and evaporate.

4.2.6 Bioactivity

The results of the bioactivity test are shown in Figure 19. As it was mentioned in the methodologies Chapter, for this test SEM images were taken to samples after they were introduced in simulated body fluid solution (SBF) and examined after certain days to see if there was nucleation of calcium phosphate in the surface of the material.

For the HG-A, the agglomerates of calcium phosphate are in the range of 1.5 µm to 3.0 µm, which are the same size as the particles of β-TCP (Figure 20). This means that there was no significant nucleation in the first seven days when the samples were inside the SBF. After 14 days, the agglomerates increase size up to an average of 5.0 µm and then up to around 10.0 µm in the 21st day.

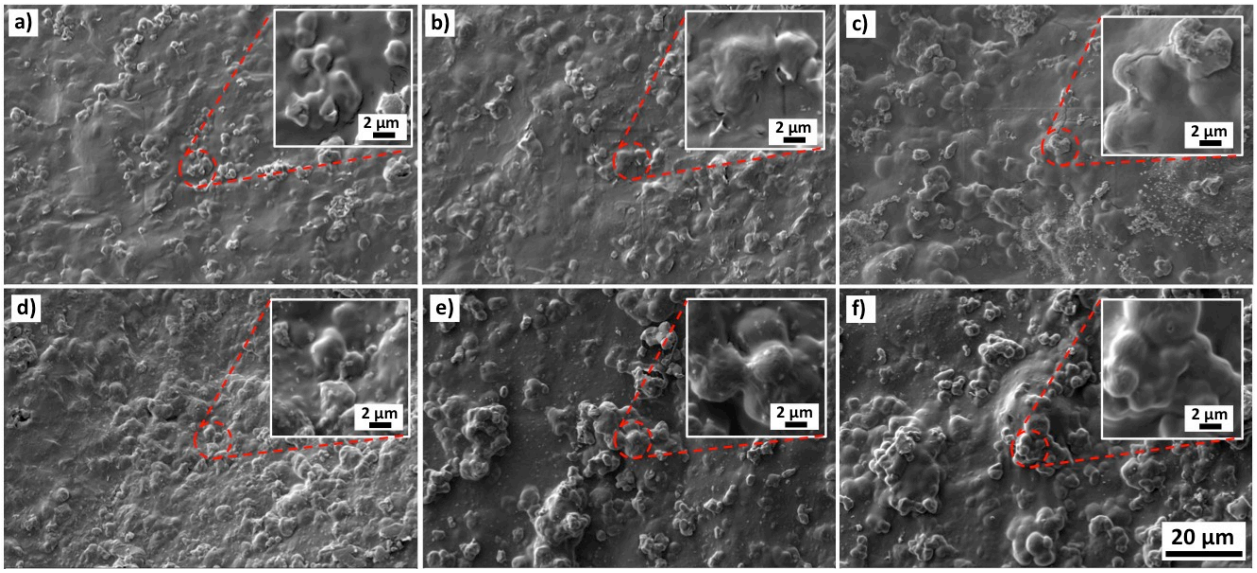

Figure 19. Bioactivity test, nucleation of hydroxyapatite in HG-A and HG-B systems a) HG-A 7 days in SBF b) HG-A 14 days in SBF c) HG-A 21 days in SBF d) HG-B 7 days in SBF e) HG-B 14 days in SBF f) HG-B 21 days in SBF

This means that significant nucleation of calcium phosphate happens on the surface of the material after a week. For the HG-B, the nucleation process happened faster. After just seven days, the agglomerates already reached a size of 4.5 µm. After 14 and 21 days, the average size of the agglomerates is 15 µm and there is no significant difference between both results. It is important to note that the tests were not dynamic and the SBF was not changed during the time of the test, which could lack to represent completely how the organism works. If the test is to be repeated in future works, dynamic assays are recommended.

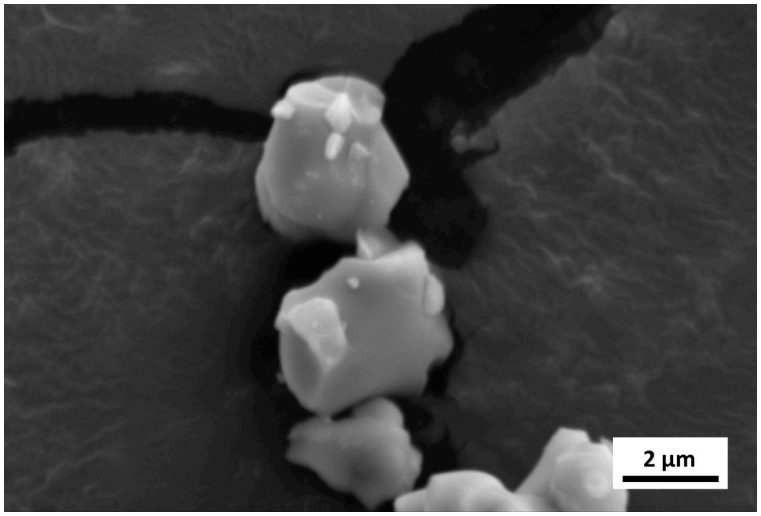

Figure 20. Single particles of β-TCP

As it has been mentioned before, the only difference between HG-A and HG-B is the presence of TiO_2 nanoparticles in the second one. This leads to think that the presence of TiO_2 is promoting the nucleation of calcium phosphate. EDX was done to the agglomerates after 21 days. In Table 8 the results of the EDX are shown. There it can be observed that the Ca/P ratio is greater than 1.5 in both systems. This means that the nucleation of calcium phosphate is not calcium deficient.

Table 8. General EDX of hydrogels samples in bioactivity test after 21 days in SBF

Element	At. No.	HG-A after 21 days		HG-B after 21 days	
		Mass [%]	Atom [%]	Mass [%]	Atom [%]
Oxygen	8	39.14	46.57	41.21	50.81
Calcium	20	28.83	13.69	26.37	12.22
Carbon	6	20.51	32.50	18.29	29.61
Phosphorus	15	10.77	6.62	8.96	5.27
Sodium	11	0.48	0.39	0.48	0.39
Magnesium	12	0.24	0.22	0.20	0.15
Titanium	22	-	-	4.49	1.55
Ca/P (atomic ratio)		2.06		2.32	

In Appendix VI the complete report of the EDX of two elemental analysis (point analysis) is included. The first point is located on one of the agglomerates, while the second point is located on the surface of the polymer avoiding any agglomerate. This comparison is made to confirm the presence of more calcium and phosphate in the agglomerates than in the surface of the polymer. The results showed that the agglomerates indeed contain more of those elements.

4.2.7 Drug dissolution curves

After putting approximately 18.0 mg of the composite hydrogel (HG-A and HG-B) in phosphate buffer saline (PBS) solution, the absorbance was measured every certain amount of time in the UV-Vis. Both systems have similar dissolution profile and are presented in Figure 21. The first 45 minutes there is a fast dissolution of ibuprofen, with more than 60% of the total concentration already dissolved in the PBS solution. Afterwards the dissolution starts to slow down until the

last 2% is dissolved just after 300 minutes. It took a little bit more than 7 hours to reach a steady state. The drug release was hindered due to the crosslinking nature of the alginate. In this case, the nanoparticles of TiO_2 had no effect in the dissolution profile of the ibuprofen crystals.

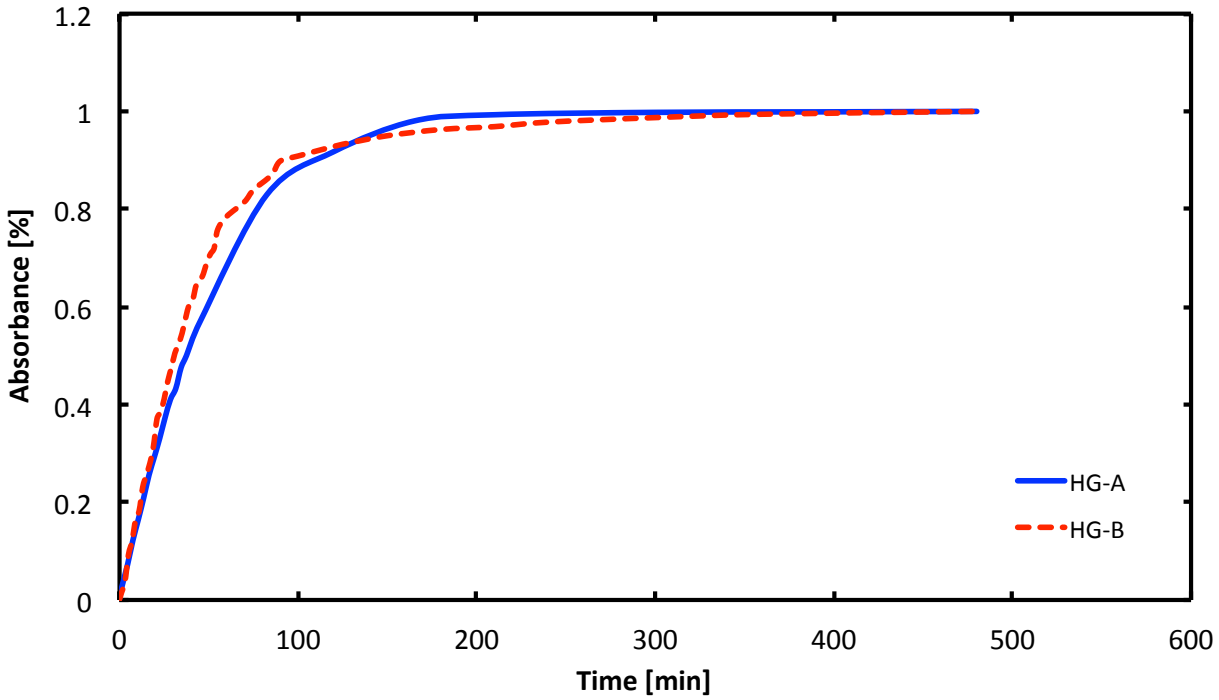

Figure 21. Dissolution profiles of ibuprofen of HG-A and HG-B

It is observed in Table 9 that the calculated values of *n* correspond to Non-Fickian diffusion mechanism in both hydrogel systems (0.5 to 1.0). This usually happens when the diffusion rate and the relaxation rate of the matrix are comparable. The release of ibuprofen depends on two simultaneous processes, water migration into the polymer matrix and ibuprofen diffusion through the hydrogel. Furthermore, data obtained from the release studies were fitted to the early-time and late-time approximation equations of the mathematical model explained in Chapter 2. The corresponding diffusion coefficients were calculated and presented in the table. The values of the initial diffusion coefficient (D_E) are greater than the values of the late diffusion coefficients (D_L) in both hydrogel systems. This is easily observed in the release curves of Figure 21 where there is an initial burst of the drug release happening in the first 45 minutes, whereas in the following hours the release is much slower, proving that the values of the coefficients make sense.

Table 9. Results of diffusion coefficients of hydrogel systems HG-A and HG-B

Hydrogel	API	Diffusion exponent n	Gel constant k	D_E [cm^2/s] x 10^{-5}	R^2	D_L [cm^2/s] X 10^{-5}	R^2
HG-A	Ibuprofen	0.6481	0.0373	12.2718	0.96	0.2205	0.99
HG-B	Ibuprofen	0.7002	0.0356	16.5130	0.94	0.2131	0.99

A calibration curve was done with known concentrations of released ibuprofen in the PBS (Figure 22). With this calibration, it was determined if the amount of ibuprofen dissolved in the solution was lower or equal to the loading of the material. With Equation (1) the curve was obtained, *Abs = 0.0024 * conc + 5E-06* with an R^2 of 0.999. Using this curve, it was found that the amount dissolved from HG-A was around 6.3 mg of ibuprofen and from HG-B 6.1 mg, which corresponds to approximately 35% and 34% respectively from the 18 mg of the sample used for the test. This, again, matches the loading obtained in previous sections, meaning that all the ibuprofen was released from the porous matrix of the hydrogel and dissolved in the PBS.

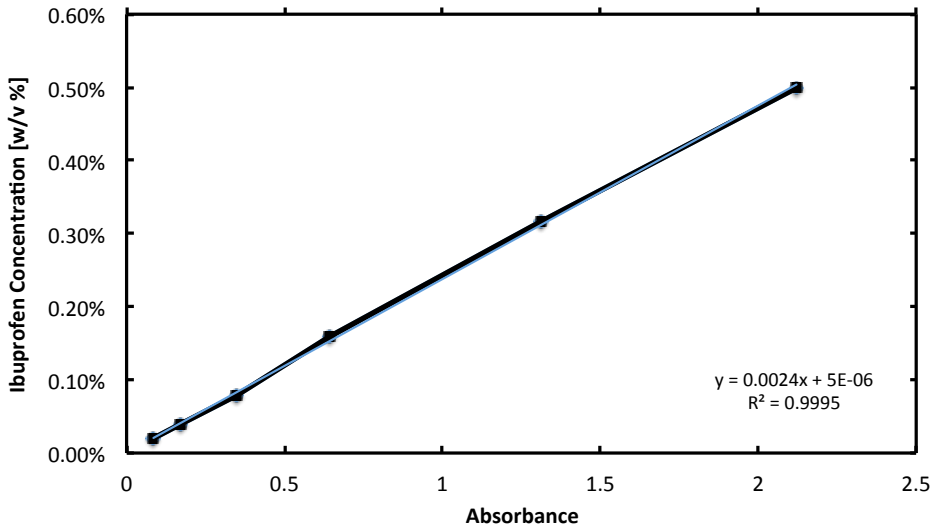

Figure 22. Calibration curve of ibuprofen in PBS

4.3 Design and Manufacturing Process

4.3.1 Die Swell Behavior

The images taken in the high-speed video camera show the swelling of polymer as it exits the die. This phenomenon was studied for some of the solutions of the second group (HG-1 to HG-6) and all resulted in the same magnitude of swelling, 0.56 mm ± 0.04 mm of diameter. In Figure 23, it can be observed the sequenced photos of HG-6 taken while a drop of the pre-crosslinked solution exits the precision tip. In Figure 23a, the width of the hydrogel solution drop was measured 0.08 mm from the end of the tip and resulted in 0.58 mm.

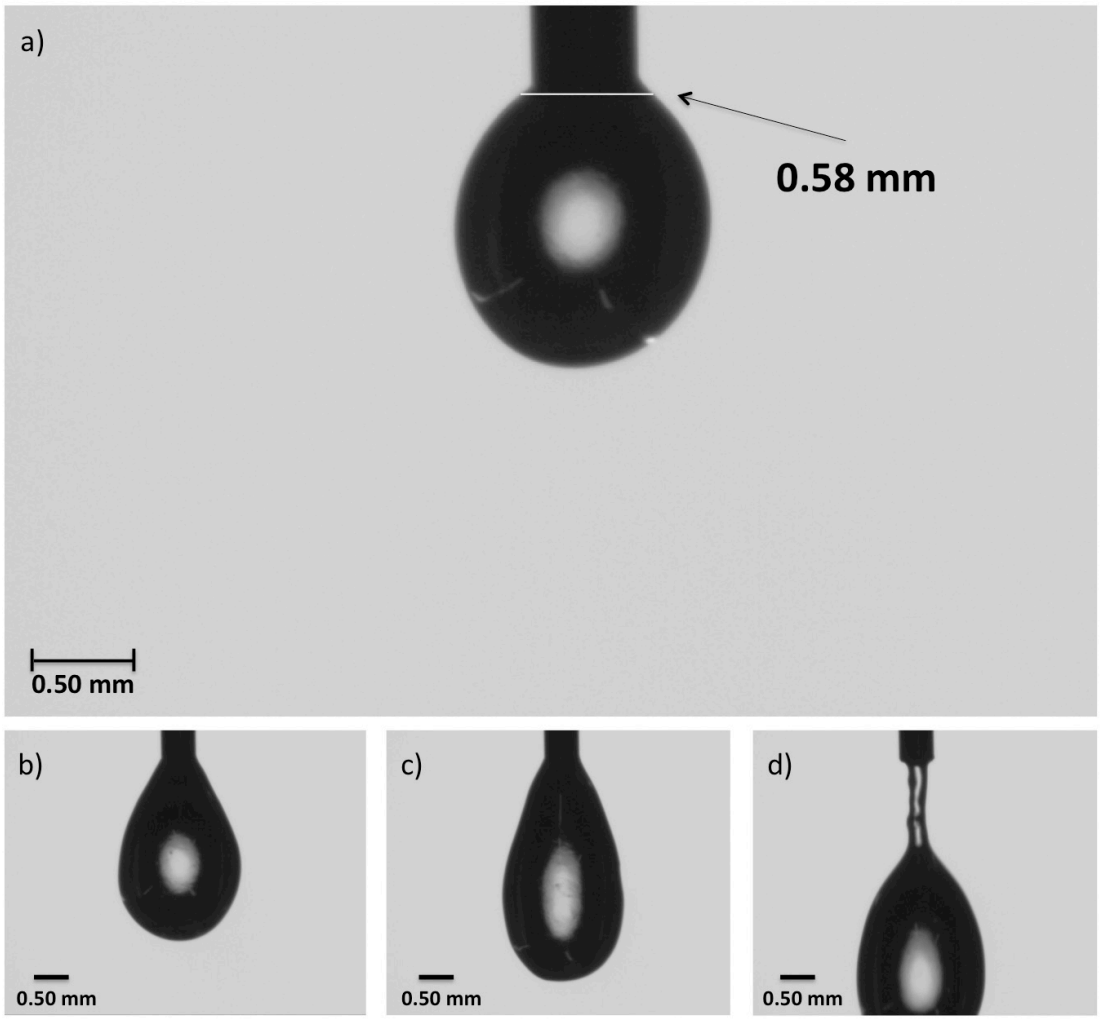

Figure 23. Die swell test image sequence with HG-6 in a Nordson precision tip of inner diameter of 0.25 mm a) the width of the drop was taken at 0.08 mm of the tip b) growth of drop c) just before separation from the tip d) the drop falls off the tip

The distance of 0.08 mm is the same distance between the extrusion tip and the build surface of the modified printer. That means that with a Nordson tip with 0.25 mm of inner diameter and the systems of hydrogels used in this work, the lower limit for a resolution that can be achieved is about 0.60 mm. This result translates into an extruded line width of 132% the size of the inner diameter of the tip and must be considered when designing the structure to be printed. In Figure 23b to Figure 23d, the rest of the sequence while the drop is extruded is shown.

4.3.2 Extrusion Test and Printing

Parameters for the scaffolds production were optimized. Scaffolds were fabricated with a layer height of 0.15 mm, a shell thickness of 0.25 mm, and a continuous flow of 100%. For the extrusion process, a speed of 4.5 mm/s was used with a fill density of 100%. To obtain these parameters, different x/y speeds in the machine were used pairing them up with the viscosity of the pre-crosslinked hydrogel. In Table 10 the screening of the 3D manufacturing process parameters is shown, where the adequate post-production process was established and the best inner diameter for the extruder and print speed. Given the rapid crosslinking nature of the alginate with $CaCl_2$, for the structure to maintain its given design, it must be printed completely first and then introduced in the $CaCl_2$ solution. An important note to mention is that this process is slow compared to other additive manufacturing techniques, where the printing speed can reach above 100 mm/s.

Furthermore, in Figure 24 a graphical scheme explaining the effect of the x/y print speed on the printing resolution is shown. When the x/y speed was too fast, the extrusion of the material through the needle was not fast or continuous enough, so an interrupted dash-line was deposited in the build platform of the machine. This happens because the pressure of the mechanic extruder is not enough to produce a continuous volume flow. When the x/y speed was to slow, the opposite happened. More than the expected gel was extruded, causing a thicker line than the programmed in the machine. That is why extrusion and x/y speed was important to calibrate altogether with the material viscosity.

Table 10. Screening of 3D microextrusion process parameters for alginate composite hydrogel in modified 3D printer

#	Crosslinking Method	Print Speed [mm/s]	Extruder Diameter [mm]	Screening	Observations
1	Crosslinking after printing design	-	-	✓	Viscosity must be optimized for designs with good resolution
2	Crosslinking layer by layer during print	-	-	✗	Independent layers in the structure without accomplishing final design
3	Bioplotting (print alginate in crosslinking solution)	-	-	✗	Printed line crosslinked immediately not allowing a correct construction of the design
4	Inverse bioplotting (print crosslinking agent in alginate)	-	-	✗	Not recommended for intended application
5	Crosslinking after printing design	15.0	0.50	✗	Fast printing, line is not printed forming dots instead
6	Crosslinking after printing design	10.0	0.50	✗	Fast printing, line is not printed all the times
7	Crosslinking after printing design	5.0	0.50	✓	Line is printed in the platform. Resolution can be improved
8	Crosslinking after printing design	2.0	0.50	✗	Design takes too long to print (>4 hours)
9	Crosslinking after printing design	5.0	0.10	✗	Not enough material is extruded. Needle partially blocked
10	Crosslinking after printing design	5.0	0.25	✓	Increased resolution of printed line
11	Crosslinking after printing design	5.0	0.75	✗	Line printed with poor resolution

Furthermore, the effect of viscosity alone is also shown on the graphical scheme. When the viscosity was too high, the pressure of the machine was not enough to extrude the pre-crosslinked hydrogel through the needle, and nothing would be deposited in the build platform. If the viscosity was too low, the extruded gel would not maintain its deigned structure in the build platform and it would spill like any other liquid wetting the base.

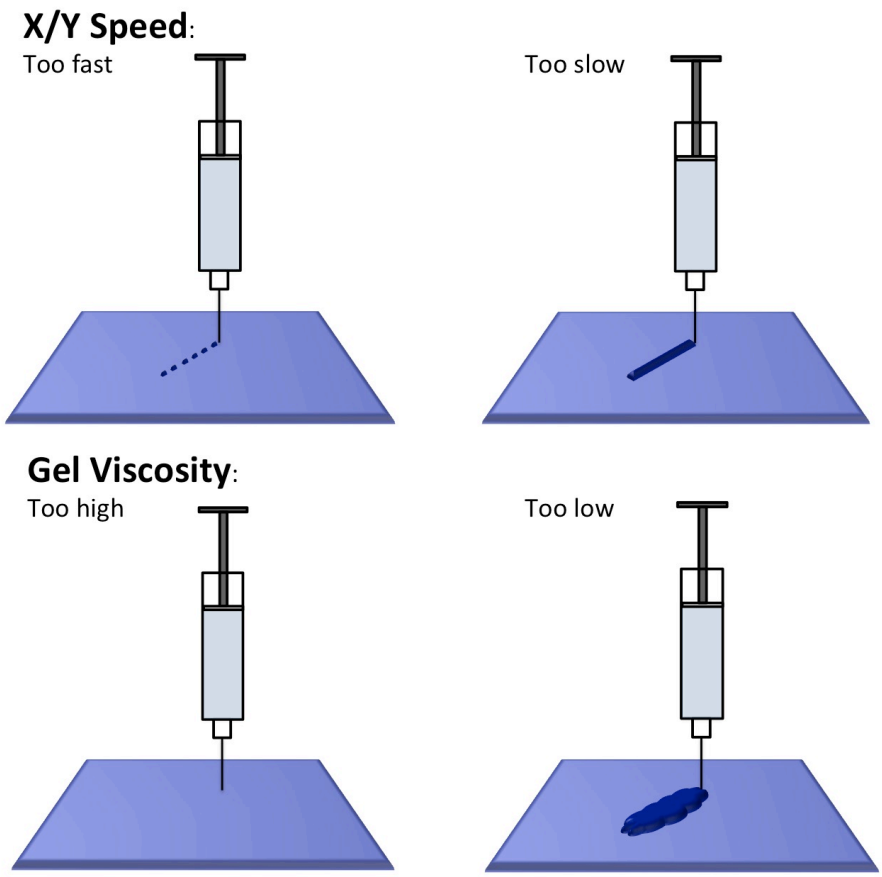

Figure 24. Graphical scheme of the printing resolution depending on the parameters: x/y speed of the machine and viscosity

In Figure 25 a graphical scheme of an ideal printing resolution is shown and compared to an actual printed line of pre-crosslinked hydrogel in the build platform of the 3D printer. Another important parameter to accomplish a steady and uninterrupted line is the distance from the tip of the needle to the build platform. If the tip of the needle is too far away from the platform, the resolution of the line will look like an interrupted line (like when the x/y speed is too fast) and with big bulks. If the needle is too close to the platform, the extrusion will be blocked by the platform and there would not be continuous extrusion of the gel. As it was mentioned in the previous section of die swelling, 0.08 mm was found to be an ideal distance. In Appendix VII the complete lists of parameters used to print the designs are shown. A copy of the modified route to generate the G-code in the software Cura is also shown.

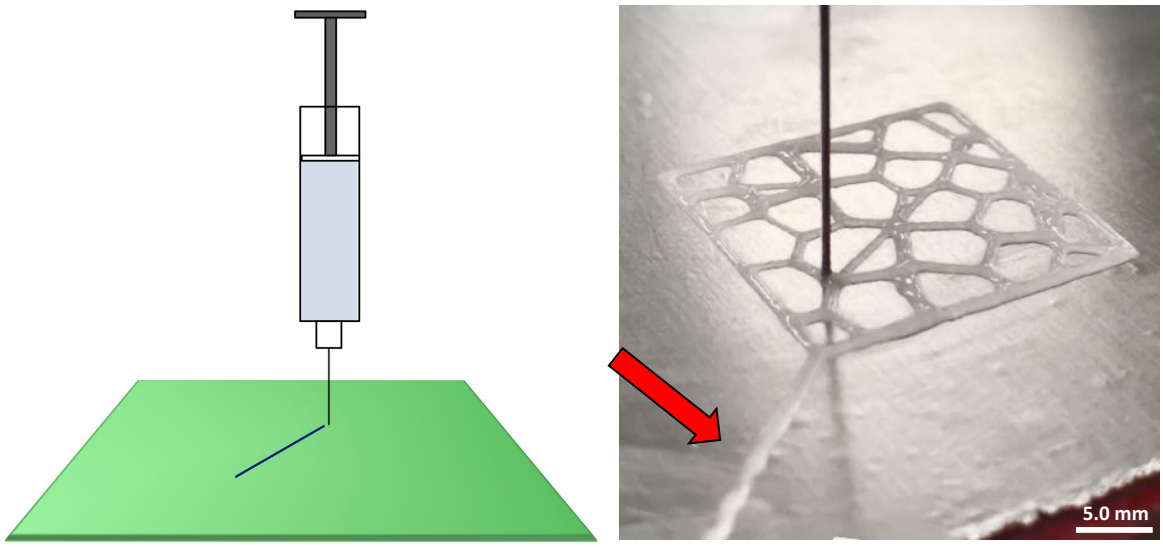

Figure 25. Graphical scheme of the ideal printing resolution compared to actual printed line in the build platform

For the extrusion test, the modified RepRap Mendelmax 3D printer shown in Figure 8 was used. The G-code was generated with the software Cura and the designs shown in Figure 7 were printed. After printing the design in the build platform, the structure was submerged in a 6 w/v % solution of sodium chloride for a complete crosslinking of the alginate. In Figure 26a, Figure 26b, and Figure 26c it can be observed the three different printed designs (grid, hexagon, and voronoi respectively). The designs were printed with the HG-6 system.

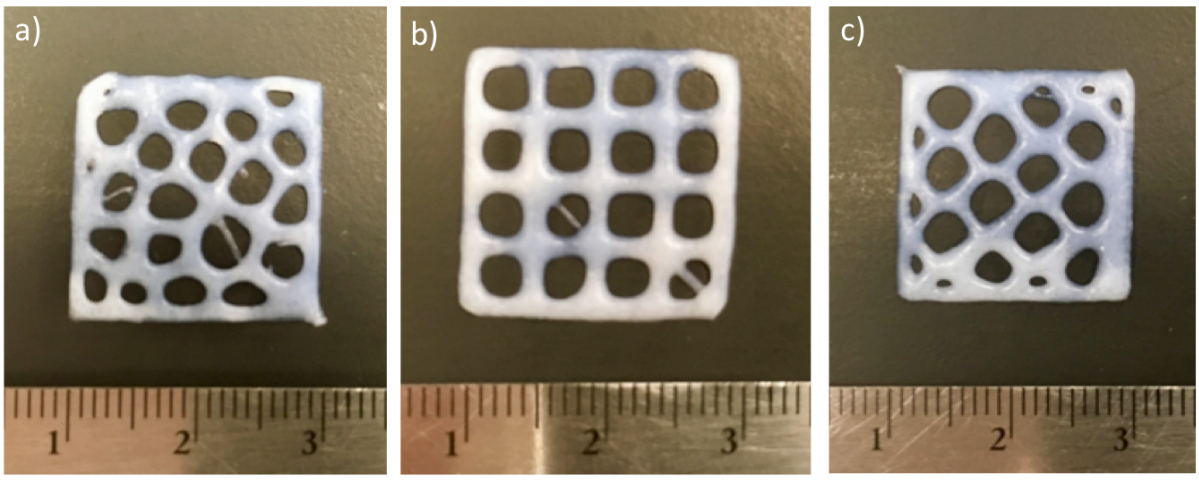

Figure 26. Printed hydrogel designs a) voronoi design b) hexagon design c) grid design

It must be noted that according to the rheological tests performed on the pre-crosslinked solutions, after they are deposited in the platform, they can deform when force is applied to them. This is the main reason for the lack of resolution in the printed designs. In other words, as more layers are printed on top of the other, the layers at the bottom receive the weight from the top layers causing deformation.

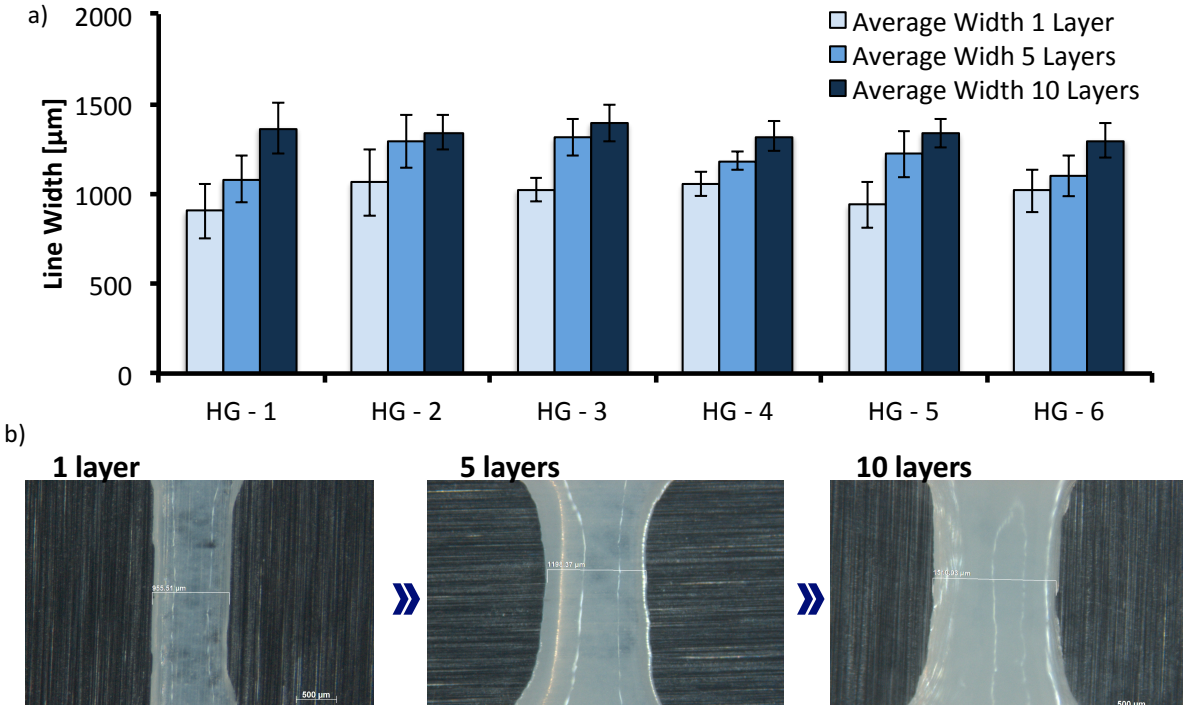

Figure 27. Line resolution test a) Average line width of the printed HG systems for the grid design with one, five, and ten layers b) HG-6 graphical resolution

Quantitative results were obtained of the layers deformation with the grid design (one, five, and ten layers; 0.15 mm, 0.75 mm, and 1.5 mm of height respectively). The results showed no statistical difference of the performance between the six different hydrogel systems (HG-1 to HG-6), as it can be observed in the graph of Figure 27. The behavior of the systems is consistent with the results of the viscoelasticity of the hydrogels as there is also no statistical difference between them with the addition of different factors in their composition.

However, there was an increase in the line width of the design with one layer (0.90 mm average line width), compared to the design with five layers (1.15 mm average line width), and subsequently in the design with ten layers (1.30 mm average line width); following the same

behavior mentioned previously with the weight of the top layers acting upon and deforming the bottom layers.

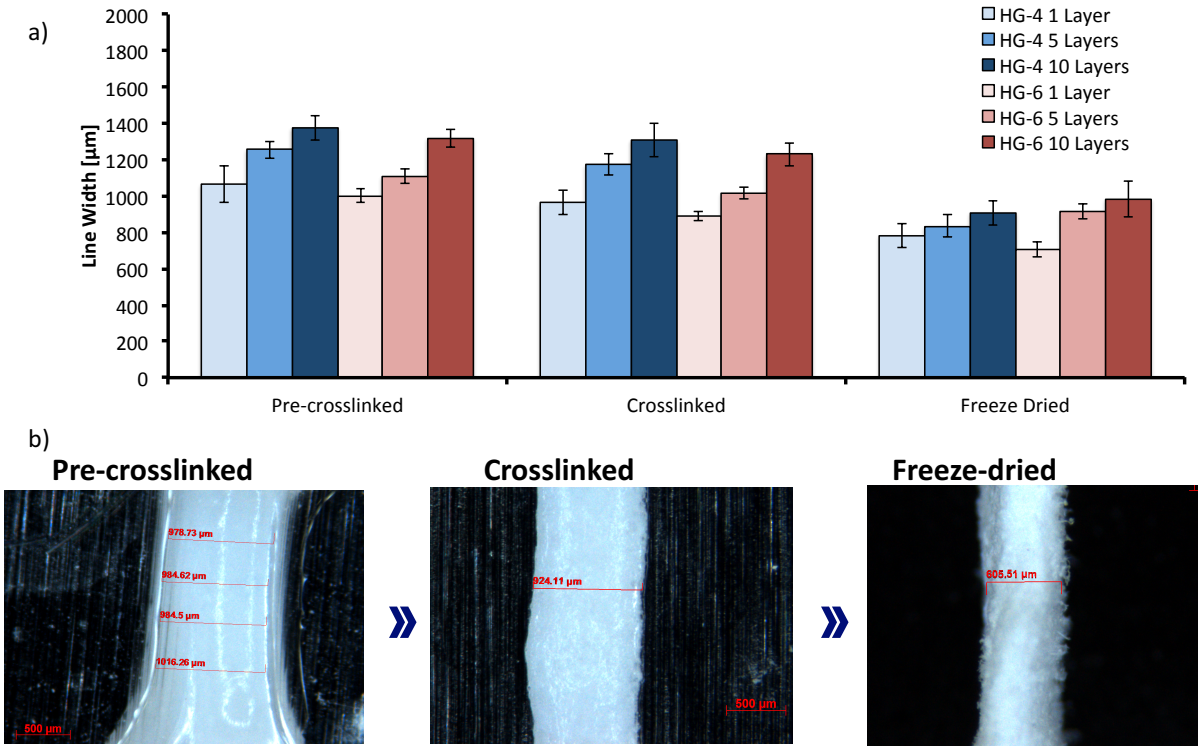

Figure 28. Line test a) average line width of the hydrogel in the different processes, after printing (pre-crosslinked gel), after crosslinking, and after freeze-drying b) graphical resolution of the three processes

The processes that come after printing the design can also affect the final measurements of the sample. These are crosslinking and freeze-drying. The line widths of the printed grid design in the two hydrogel systems (HG-4 and HG-6) were measured after printing (pre-crosslinked hydrogel), after crosslinking in the calcium chloride solution, and finally after freeze-drying. As it can be observed in the graph of Figure 28, there was an average line width reduction of 7.8% after crosslinking, and an average total reduction of 27.5% after freeze-drying.

The reduction in size after crosslinking is caused by the ionic bonding between the excess of Ca^{+2} used and the alginate chains, which come closer of each other after the chemical reaction. Further reduction in the freeze-drying process is caused by the fact that free volume is reduced when the water molecules are removed from the structure and given the low strength of the ionic bonding of the alginate, shrinkage between the crosslinked biopolymer chains happen.

To print a 3D complex structure, the gel must have the right viscosity. As it was mentioned before, if it is not viscous enough, the structure will collapse under the weight of the own material. If the gel is too viscous, the extruder will probably get block and no material will be printed. In Figure 29, the grid design was printed with different hydrogel systems. The first one is HG-0.3, where a low viscosity was obtained, all the way to HG-A, which is a more viscous gel without reaching the upper limit where the extruder is blocked.

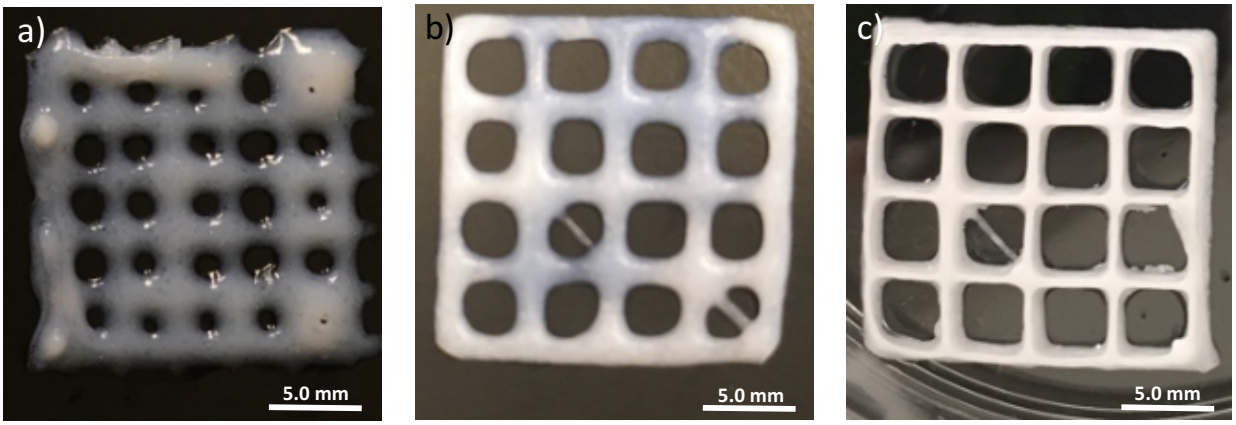

Figure 29. Resolution of the crosslinked grid design as the viscosity of the pre-crosslinked hydrogel increases a) HG-0.3 b) HG-6 c) HG-A

The structure in image Figure 29c was measured on the Alicona optical microscope to generate a 3D image showing the exact height and width of the grid line in various locations through the design. As it is observed in Figure 30, the average height of the structure lines is 2.25 mm. This average was obtained from 15 different measurements in separate locations. Furthermore, the structure was design to have 20 layers (each one of 0.15 mm) that is equivalent to 3 millimeters. Given that the structure was measured in the Alicona after it was freeze-dried, it had already shrunk. In the previous section it has been stated that the shrinkage after crosslinked and freeze-dried was about 27.5%. In this case, the shrinkage was 25%, which is also inside the error of the measurements. This is the first signal of how important is to take in consideration the shrinkage since the structure is first designed. Another interesting measurement observed in the Alicona 3D imaging results is how the width of the line gets bigger in the base. This phenomenon was explained in the previous section, and it is caused by the viscoelastic behavior of the material as it is printed.

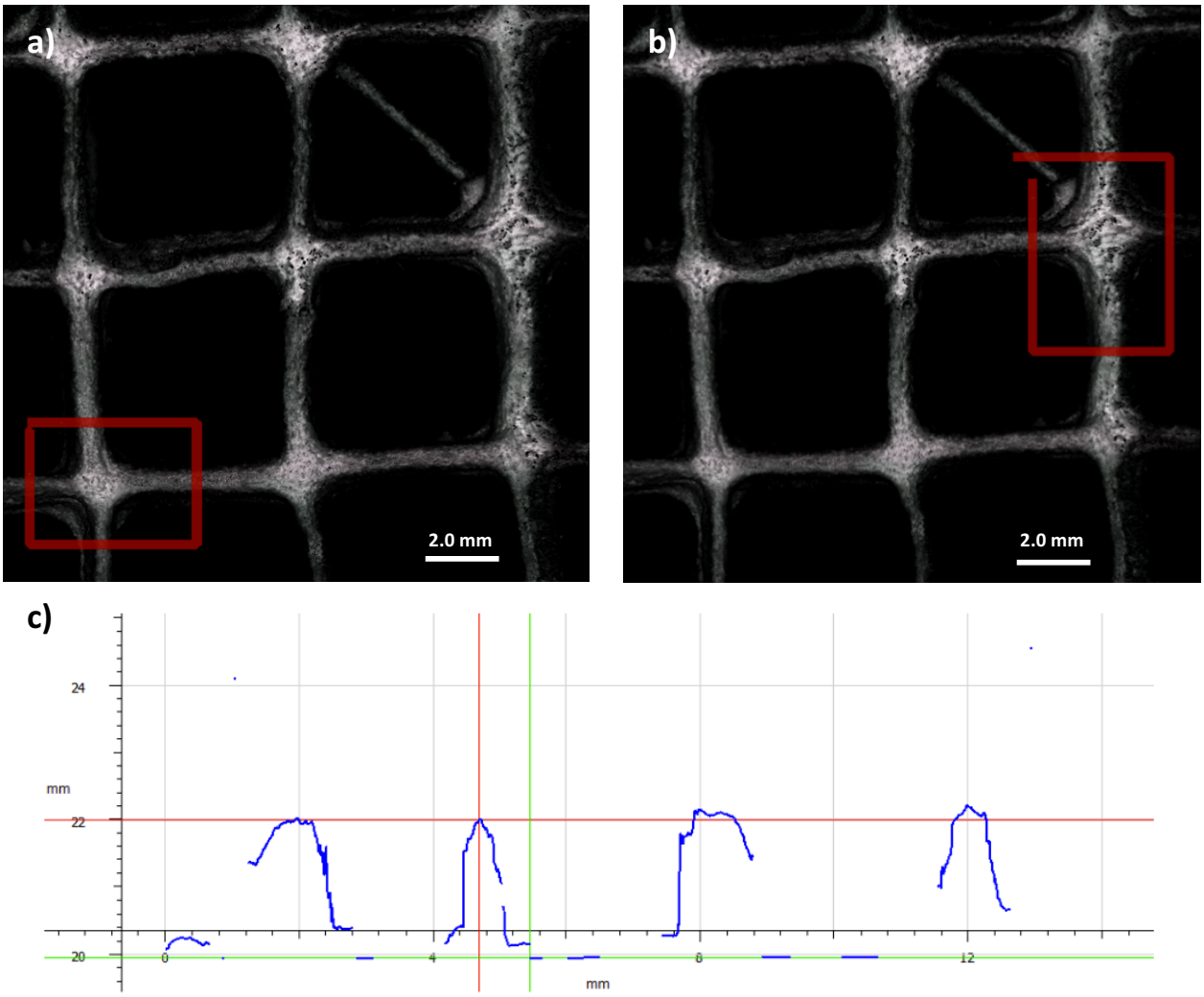

Figure 30. 3D imaging of grid design of HG-A in the Alicona microscope a) first location of measurements taken b) second location c) graph of 3D mapping of image

The next step was to study if a 100% filled structure was also printable with the G-code route programmed in Cura, using the available 3D printer, and with the viscosity of the pre-crosslinked hydrogel. In Figure 31 the sequence of a 100% filled cubic structure is shown. In Figure 31a, only the first two layers were printed. Subsequently, the images show the same structure with 10, 30, and 50 layers respectively. If observed carefully, the extruder follows a diagonal pattern filling the cube. The software Cura created that route when the image was loaded to the machine. If the corners are observed, the 90° angle of the edges becomes more round as the layers increase, as it was expected due to the material viscoelastic behavior.

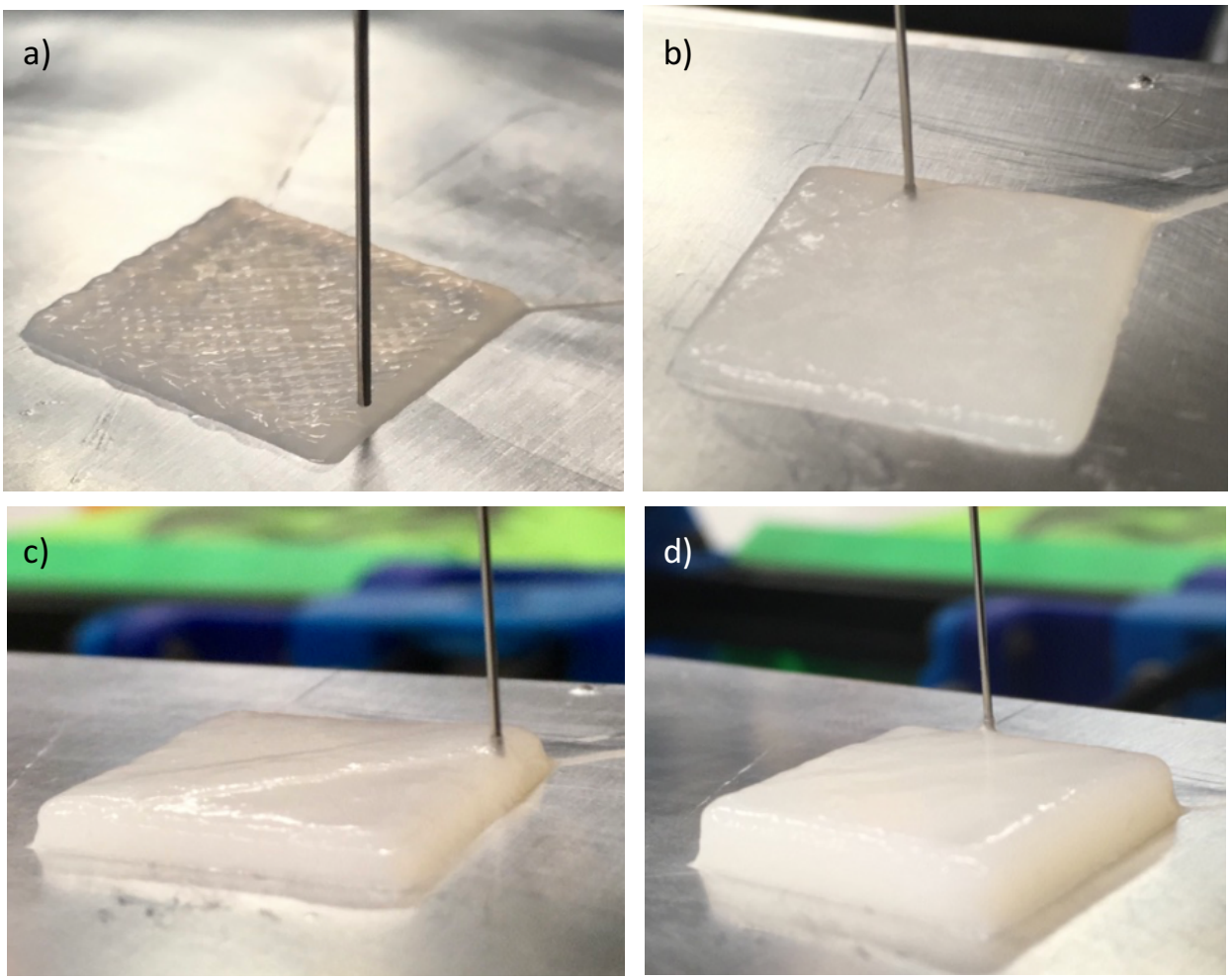

Figure 31. Printing process of a 100% filled cubic structure a) two layers b) ten layers c) 30 layers d) 50 layers

Based on the results and discussions of all the previous sections in this chapter, overall conclusions of the specific objectives stated in the first chapter are made and presented in Chapter 5. Furthermore, recommendations for future work are given and general outlook of this research in the future.

5. Chapter 5 – Overall Conclusions and Outlook

In this work, alginate/gelatin composite hydrogel pre-crosslinked solutions were prepared, and their 3D-printability was studied. After studying the physicochemical effects of adding two factors into the formulation, β-TCP and TiO_2, these hydrogels were loaded with an active pharmaceutical ingredient (API). The hydrogels were loaded by making solvent/water microemulsions in the pre-crosslinked solution. The API loaded was the hydrophobic anti-inflammatory ibuprofen and it was dissolved in the solvent. After printing the hydrogel in a modified 3D printer, crystallization of the API was also studied, along with their dissolution profiles, bioactivity, and thermal behavior.

First, the effect of pre-crosslinking percentage was investigated, where formulations with greater storage modulus (G'>G") at low shear conditions were identified and proved better for 3D-printing than formulations with greater loss modulus (G''>G'). Using calcium chloride as a pre-crosslinking agent with a ratio of 1:10 of $CaCl_2$ with respect to alginate made printing feasible. The addition of hydrogel additives like TiO_2 and β-TCP had no significant effect on the viscoelastic properties of the material in the concentrations used in this work. The addition of microemulsions to the solution with a volume factor of 20% also resulted in no significant changes in the viscoelastic behavior of the material.

Once the hydrogel was dried, crystallinity of the additives and the API was determined. TiO_2 was presented in its anatase form, and the hydrogels containing β-TCP presented the calcium phosphate peaks in the diffractometer. Ibuprofen crystallized in its pure form. This was later confirmed with the thermal analysis, where the DSC results showed a clear endotherm at 75.5 °C. It was also determined that the material concentrations used in HG-1 to HG-6 resulted in a pore size range going from 110 µm to 200 µm, which is adequate for tissue regeneration. Furthermore, when the loaded hydrogels HG-A and HG-B, with greater alginate and gelatin concentrations and the addition of polyvinyl alcohol as emulsifier, were measured, presented an average pore size range of 40 µm. Further work is needed to increase this pore size and fin the optimized amount of PVA to be added to the solution. In the same imaging measurement, crystals were observed to grow inside the pores of the hydrogel matrix without any chemical

bond to the material. The size of the crystals was smaller than the pores, given that the amount of ibuprofen dissolved in the solvent was lower than 0.5 of the saturation.

Furthermore, tensile tests showed that the hydrogels stand in the lower range of the ideal elastic modulus as observed in some of the oral soft tissues. The highest elastic modulus between HG-1 to HG-6 was accomplished with the alginate/gelatin composite hydrogel containing TiO_2 (HG-4), 20 MPa. It was observed that even though the addition of gelatin or nanoparticles did not affect the pre-crosslinked solution viscoelastic properties, it did affect its mechanical properties after crosslinking of the alginate. As it was expected, HG-A and HG-B showed higher elastic modulus than the first group, up to 65 MPa, due to the increased concentration of the polymers in the formulations and the more packed structure observed in the porosity imaging.

Bioactivity for HG-A and HG-B was studied, presenting more nucleation of calcium phosphate in HG-B, assumed to be due to the presence of nanoparticles of TiO_2. The drug loading accomplished in both hydrogel systems (HG-A and HG-B) was around 35% matching the theoretical value. This assured the stability of the previous synthesized microemulsion, resulting in not phase separation before complete crosslinking. The release curves of the API showed >98% dissolved drug in the PBS solution after just 300 minutes.

Finally, in the extrusion test and printing, with the parameters described in the experimental design, it was proved that distinct designs with multiple layers of 0.15 mm could be printed. Designs with a line-structure will lose resolution as the height is increased due to deformation of the bottom layers of the design due to the increasing weight of the top layers. However, there is a reduction of the width and height of the structure after it is crosslinked (7.8%) and freeze-dried (27.5%) compared to the initial printed design. Addition of gelatin, TiO_2, β-TCP, or microemulsions to the pre-crosslinked alginate solution does not affect significantly the printability. As the viscosity of the solution increased, the resolution of the printed grid design improved. Overall, the modification of the extruder to print gel materials in the RepRap Mendelmax was a success.

The study proved new insight of possibilities of alginate/gelatin added with TiO_2 nanoparticles and β-TCP composite hydrogel 3D printing for tissue regeneration, where further assays are being made to prove cytotoxicity, and cell proliferation. The controllable loading method of a hydrophobic API by microemulsion also proved new possibilities in the tissue-engineering field using hydrogel scaffolds. Although an anti-inflammatory was used in this work, it can be extended to related antibiotics, useful in this field of study. Additionally, by changing the concentration of the drug in the solvent altogether with the volume factor in the emulsion, can change the drug crystal size inside the hydrogel porous matrix and therefore the sustained release profile. This is an interesting behavior of crystal nucleation recommended for future work.

Including further studies of the material, an assay of cell adhesion and cytotoxicity is necessary to continue the development of the hydrogel. This is work being done at the moment but is not included in this report. Furthermore, some modifications to the 3D printer to improve the printing resolution are recommended. These recommendations include the addition of controllable temperature in the build platform, working in the program of the route to print the design, and a more automated way to calibrate the “z-axis” of the printer. Nevertheless, this low cost open-source machine is a proof-of-work that can continue with other types of hydrogels and should be used in future works to study gel-like materials, characterizing and optimizing these materials with the aid of the methodology developed in this report.

6. References

[1] K. Y. Lee and D. J. Mooney, “Hydrogels for Tissue Engineering,” *Chem. Rev.*, vol. 101, no. 7, 2001.

[2] J. S. Colombo, A. N. Moore, J. D. Hartgerink, and R. N. D’Souza, “Scaffolds to Control Inflammation and Facilitate Dental Pulp Regeneration,” *J Endod*, vol. 40, no. 4 0, pp. 1–17, 2014.

[3] S. S. Jensen and H. Terheyden, “Bone augmentation procedures in localized defects in the alveolar ridge: clinical results with different bone grafts and bone-substitute materials.,” *Int. J. Oral Maxillofac. Implants*, vol. 24 Suppl, pp. 218–36, 2009.

[4] E. M. Ahmed, “Hydrogel: Preparation, characterization, and applications: A review,” *J. Adv. Res.*, vol. 6, no. 2, pp. 105–121, 2015.

[5] T. R. Hoare and D. S. Kohane, “Hydrogels in drug delivery: Progress and challenges,” *Polymer (Guildf).*, vol. 49, no. 8, pp. 1993–2007, 2008.

[6] I. El-Sherbiny and M. Yacoub, “Hydrogel scaffolds for tissue engineering: Progress and challenges,” *Glob. Cardiol. Sci. Pract.*, vol. 2013, no. 3, pp. 316–42, 2013.

[7] J. Fisher and A. Reddi, “Functional tissue engineering of bone: signals and scaffolds,” *Top. Tissue Eng.*, p. ch5, 2003.

[8] A. Tangprasert, C. Tansakul, N. Thuaksubun, and J. Meesane, “Mimicked extracellular matrix of calcified soft tissue based on chitosan/gelatin/compounded calcium phosphate hydrogel to design ex vivo model for heterotopic ossification,” *Mater. Des.*, vol. 134, pp. 486–493, 2017.

[9] B. V Slaughter and O. Z. Fisher, “Hydrogels in regenrative medicine,” *Adv. Mater.*, vol. 21, no. 0, pp. 3307–3329, 2009.

[10] R. R. Jose, M. J. Rodriguez, T. A. Dixon, F. Omenetto, and D. L. Kaplan, “Evolution of

Bioinks and Additive Manufacturing Technologies for 3D Bioprinting," *ACS Biomater. Sci. Eng.*, p. acsbiomaterials.6b00088, 2016.

[11] A. D. Augst, H. J. Kong, and D. J. Mooney, "Alginate hydrogels as biomaterials," *Macromol. Biosci.*, vol. 6, no. 8, pp. 623–633, 2006.

[12] K. Yue, G. Trujillo-de Santiago, M. M. Alvarez, A. Tamayol, N. Annabi, and A. Khademhosseini, "Synthesis, properties, and biomedical applications of gelatin methacryloyl (GelMA) hydrogels," *Biomaterials*, vol. 73, pp. 254–271, 2015.

[13] F. Camponeschi, A. Atrei, G. Rocchigiani, L. Mencuccini, M. Uva, and R. Barbucci, "New Formulations of Polysaccharide-Based Hydrogels for Drug Release and Tissue Engineering," *Gels*, vol. 1, no. 1, pp. 3–23, 2015.

[14] E. Caló and V. V. Khutoryanskiy, "Biomedical applications of hydrogels: A review of patents and commercial products," *Eur. Polym. J.*, vol. 65, pp. 252–267, 2015.

[15] S. J. Buwalda, K. W. M. Boere, P. J. Dijkstra, J. Feijen, T. Vermonden, and W. E. Hennink, "Hydrogels in a historical perspective: From simple networks to smart materials," *J. Control. Release*, vol. 190, pp. 254–273, 2014.

[16] X. Shen, J. L. Shamshina, P. Berton, G. Gurau, and R. D. Rogers, "Hydrogels Based on Cellulose and Chitin: Fabrication, Properties, and Applications," *Green Chem.*, no. Mc, pp. 53–75, 2015.

[17] E. Josef, M. Zilberman, and H. Bianco-Peled, "Composite alginate hydrogels: An innovative approach for the controlled release of hydrophobic drugs," *Acta Biomater.*, vol. 6, no. 12, pp. 4642–4649, 2010.

[18] H. B. Eral, M. O'Mahony, R. Shaw, B. L. Trout, A. S. Myerson, and P. S. Doyle, "Composite hydrogels laden with crystalline active pharmaceutical ingredients of controlled size and loading," *Chem. Mater.*, vol. 26, no. 21, pp. 6213–6220, 2014.

[19] S. Sowmya, P. T. S. Kumar, K. P. Chennazhi, S. V. Nair, H. Tamura, and R. Jayakumar,

"Biocompatible ??-chitin hydrogel/nanobioactive glass ceramic nanocomposite scaffolds for periodontal bone regeneration," *Trends Biomater. Artif. Organs*, vol. 25, no. 1, pp. 1–11, 2011.

[20] Y. Y. Chen, H. C. Wu, J. S. Sun, G. C. Dong, and T. W. Wang, "Injectable and thermoresponsive self-assembled nanocomposite hydrogel for long-term anticancer drug delivery," *Langmuir*, vol. 29, no. 11, pp. 3721–3729, 2013.

[21] C. Hu, H. Feng, and C. Zhu, "Preparation and characterization of rifampicin-PLGA microspheres/sodium alginate in situ gel combination delivery system," *Colloids Surfaces B Biointerfaces*, vol. 95, pp. 162–169, 2012.

[22] E. Rajalakshmanan, T. H. Lin, S. C. Wu, J. K. Chang, G. J. Wang, and M. L. Ho, "A Novel hyaluronan thermoresponsive hydrogel for hADSCs transplantation in cartilage tissue engineering," 2011.

[23] K. D. Roehm and S. V Madihally, "Bioprinted chitosan-gelatin thermosensitive hydrogels using an inexpensive 3D printer," *Biofabrication*, 2017.

[24] R. E. Webber and K. R. Shull, "Strain Dependence of the Viscoelastic Properties of Alginate Hydrogels," pp. 6153–6160, 2004.

[25] R. P. Narayanan, G. Melman, N. J. Letourneau, N. L. Mendelson, and A. Melman, "Photodegradable Iron(III) Cross-Linked Alginate Gels," no. Iii, 2012.

[26] R. Mahou, F. Borcard, V. Crivelli, E. Montanari, S. Passemard, F. Noverraz, S. Gerber-Lemaire, L. Bühler, and C. Wandrey, "Tuning the Properties of Hydrogel Microspheres by Adding Chemical Cross-linking Functionality to Sodium Alginate," *Chem. Mater.*, vol. 27, no. 12, pp. 4380–4389, 2015.

[27] X. Lou and T. V. Chirila, "Swelling behavior and mechanical properties of chemically cross-linked Journal of Biomaterials," no. August 2015, 1999.

[28] B. Balakrishnan, N. Joshi, A. Jayakrishnan, and R. Banerjee, "Self-crosslinked oxidized

alginate / gelatin hydrogel as injectable , adhesive biomimetic scaffolds for cartilage regeneration," *Acta Biomater.*, vol. 10, no. 8, pp. 3650–3663, 2014.

[29] T. Zehnder, B. Sarker, A. R. Boccaccini, and R. Detsch, "Evaluation of an alginate-gelatine crosslinked hydrogel for bioplotting.," *Biofabrication*, vol. 7, no. 2, p. 25001, 2015.

[30] E. Rosellini, C. Cristallini, N. Barbani, G. Vozzi, and P. Giusti, "Preparation and characterization of alginate / gelatin blend films for cardiac tissue engineering," 2008.

[31] F. You, X. Wu, and X. Chen, "3D printing of porous alginate/gelatin hydrogel scaffolds and their mechanical property characterization," *Int. J. Polym. Mater. Polym. Biomater.*, vol. 66, no. 6, pp. 299–306, 2017.

[32] A. Z. Aroguz, K. Baysal, Z. Adiguzel, and B. M. Baysal, "Alginate / Polyoxyethylene and Alginate / Gelatin Hydrogels : Preparation , Characterization , and Application in Tissue ...," no. April 2015, 2014.

[33] B. Sarker, R. Singh, R. Silva, J. A. Roether, J. Kaschta, R. Detsch, D. W. Schubert, I. Cicha, and A. R. Boccaccini, "Evaluation of fibroblasts adhesion and proliferation on alginate-gelatin crosslinked hydrogel," *PLoS One*, vol. 9, no. 9, pp. 1–12, 2014.

[34] F. Despang, A. Börner, R. Dittrich, G. Tomandl, W. Pompe, and M. Gelinsky, "Alginate/calcium phosphate scaffolds with oriented, tube-like pores," *Materwiss. Werksttech.*, vol. 36, no. 12, pp. 761–767, 2005.

[35] D. Alves Cardoso, J. J. J. P. Van Den Beucken, L. L. H. Both, J. Bender, J. A. Jansen, and S. C. G. Leeuwenburgh, "Gelation and biocompatibility of injectable alginate-calcium phosphate gels for bone regeneration," *J. Biomed. Mater. Res. - Part A*, vol. 102, no. 3, pp. 808–817, 2014.

[36] B. P. Santana, F. Nedel, E. Piva, R. V. De Carvalho, F. F. Demarco, N. Lenin, and V. Carreño, "Preparation , Modification , and Characterization of Alginate Hydrogel with Nano- / Microfibers : A New Perspective for Tissue Engineering," *Hindawi Publ. Corp. Biomed Res.*

Int., vol. 2013, no. 307602, pp. 1–6, 2013.

[37] L. Chen, R. Shen, S. Komasa, Y. Xue, B. Jin, Y. Hou, J. Okazaki, and J. Gao, "Drug-loadable calcium alginate hydrogel system for use in oral bone tissue repair," *Int. J. Mol. Sci.*, vol. 18, no. 5, 2017.

[38] A. Z. M. Badruddoza, P. D. Godfrin, A. S. Myerson, B. L. Trout, and P. S. Doyle, "Core–Shell Composite Hydrogels for Controlled Nanocrystal Formation and Release of Hydrophobic Active Pharmaceutical Ingredients," *Adv. Healthc. Mater.*, vol. 5, no. 15, pp. 1960–1968, 2016.

[39] M. Lovett, K. Lee, A. Edwards, and D. L. Kaplan, "Vascularization strategies for tissue engineering.," *Tissue Eng. Part B. Rev.*, vol. 15, no. 3, pp. 353–70, 2009.

[40] J. Zhu and R. E. Marchant, "Design properties of hydrogel tissue-engineering scaffolds," *Expert Rev Med Devices*, vol. 8, no. 5, pp. 607–626, 2012.

[41] K. J. Rambhia and P. X. Ma, "Controlled drug release for tissue engineering," *J. Control. Release*, vol. 219, pp. 119–128, 2015.

[42] H. B. Eral, V. López-Mejías, M. O'Mahony, B. L. Trout, A. S. Myerson, and P. S. Doyle, "Biocompatible alginate microgel particles as heteronucleants and encapsulating vehicles for hydrophilic and hydrophobic drugs," *Cryst. Growth Des.*, vol. 14, no. 4, pp. 2073–2082, 2014.

[43] C. C. Lin and A. T. Metters, "Hydrogels in controlled release formulations: Network design and mathematical modeling," *Adv. Drug Deliv. Rev.*, vol. 58, no. 12–13, pp. 1379–1408, 2006.

[44] S. C. Lee, I. K. Kwon, and K. Park, "Hydrogels for delivery of bioactive agents: A historical perspective," *Adv. Drug Deliv. Rev.*, vol. 65, no. 1, pp. 17–20, 2013.

[45] J. K. Oh, D. I. Lee, and J. M. Park, "Biopolymer-based microgels/nanogels for drug delivery applications," *Prog. Polym. Sci.*, vol. 34, no. 12, pp. 1261–1282, 2009.

[46] S. Cardea, L. Baldino, M. Scognamiglio, and E. Reverchon, “3D PLLA/Ibuprofen composite scaffolds obtained by a supercritical fluids assisted process,” *J. Mater. Sci. Mater. Med.*, vol. 25, no. 4, pp. 989–998, 2014.

[47] A. A. Mostafa, M. M. H. El-Sayed, A. A. Mahmoud, and A. M. Gamal-Eldeen, “Bioactive/Natural Polymeric Scaffolds Loaded with Ciprofloxacin for Treatment of Osteomyelitis,” *AAPS PharmSciTech*, vol. 18, no. 4, pp. 1056–1069, 2017.

[48] H. Bikas, P. Stavropoulos, and G. Chryssolouris, “Additive manufacturing methods and modeling approaches: A critical review,” *Int. J. Adv. Manuf. Technol.*, vol. 83, no. 1–4, pp. 389–405, 2016.

[49] W. Shi, R. He, and Y. Liu, “3D printing scaffolds with hydrogel materials for biomedical applications,” *2015*, vol. 1, no. 3, p. 6, 2015.

[50] I. T. Ozbolat and M. Hospodiuk, “Current advances and future perspectives in extrusion-based bioprinting,” *Biomaterials*, vol. 76, pp. 321–343, 2016.

[51] J. M. Lee and W. Y. Yeong, “Design and Printing Strategies in 3D Bioprinting of Cell-Hydrogels: A Review,” *Adv. Healthc. Mater.*, vol. 5, no. 22, pp. 2856–2865, 2016.

[52] Y. He, F. Yang, H. Zhao, Q. Gao, B. Xia, and J. Fu, “Research on the printability of hydrogels in 3D bioprinting,” *Sci. Rep.*, vol. 6, p. 29977, 2016.

[53] X. Li, R. Cui, L. Sun, K. E. Aifantis, Y. Fan, Q. Feng, F. Cui, and F. Watari, “Review Article 3D-Printed Biopolymers for Tissue Engineering Application,” vol. 2014, 2014.

[54] M. Fantini, M. Curto, and F. De Crescenzio, “A method to design biomimetic scaffolds for bone tissue engineering based on Voronoi lattices,” *Virtual Phys. Prototyp.*, vol. 11, no. 2, pp. 77–90, 2016.

[55] T. Kokubo and H. Takadama, “How useful is SBF in predicting in vivo bone bioactivity?,” *Biomaterials*, vol. 27, no. 15, pp. 2907–2915, 2006.

[56] B. Singh, D. K. Sharma, and A. Gupta, “Controlled release of thiram fungicide from starch-based hydrogels,” *J. Environ. Sci. Heal. - Part B Pestic. Food Contam. Agric. Wastes*, vol. 42, no. 6, pp. 677–695, 2007.

[57] L. Serra, J. Doménech, and N. A. Peppas, “Drug transport mechanisms and release kinetics from molecularly designed poly(acrylic acid-g-ethylene glycol) hydrogels,” *Biomaterials*, vol. 27, no. 31, pp. 5440–5451, 2006.

[58] T. F. Tadros, “Emulsion Formation,Stability, and Rheology,” *Emuls. Form. Stab.*, pp. 1–76, 2013.

[59] C. T. McKee, J. A. Last, P. Russell, and C. J. Murphy, “Indentation Versus Tensile Measurements of Young’s Modulus for Soft Biological Tissues,” *Tissue Eng. Part B Rev.*, vol. 17, no. 3, pp. 155–164, 2011.

[60] S. Goktas, J. J. Dmytryk, and P. S. McFetridge, “Biomechanical Behavior of Oral Soft Tissues,” *J. Periodontol.*, vol. 82, no. 8, pp. 1178–1186, 2011.

Appendix I – Viscoelasticity vs. emulsion volume factor

Study of the viscoelastic behavior of different pre-gel solutions with different volume factors. This study was done independently in the Myerson Lab, at MIT. The resulting graphs are shown next, where it can be observed that when the volume factor of the emulsion was increased, there was no effect on the material viscosity.

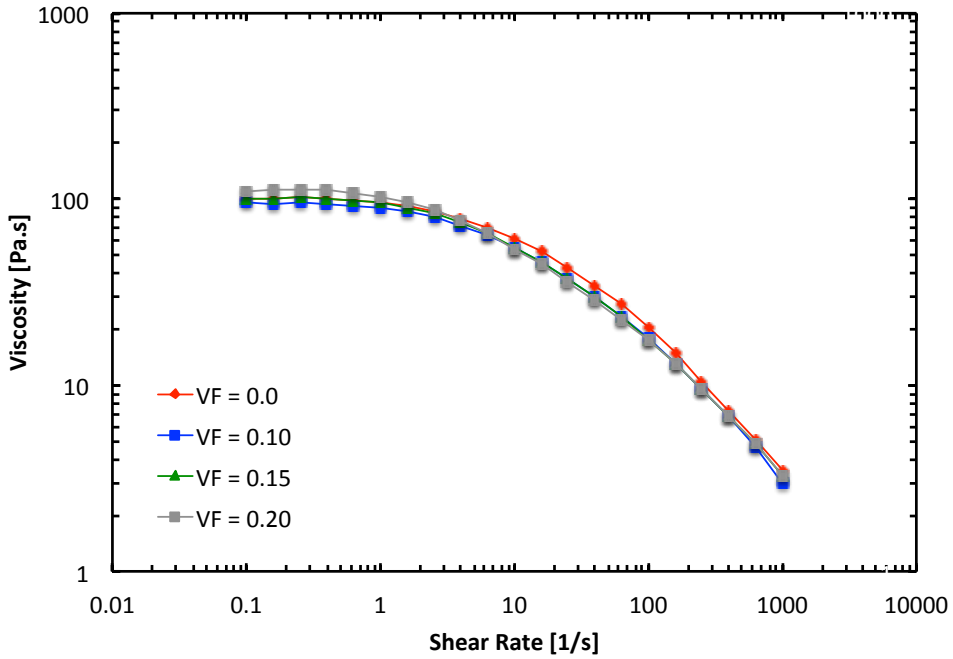

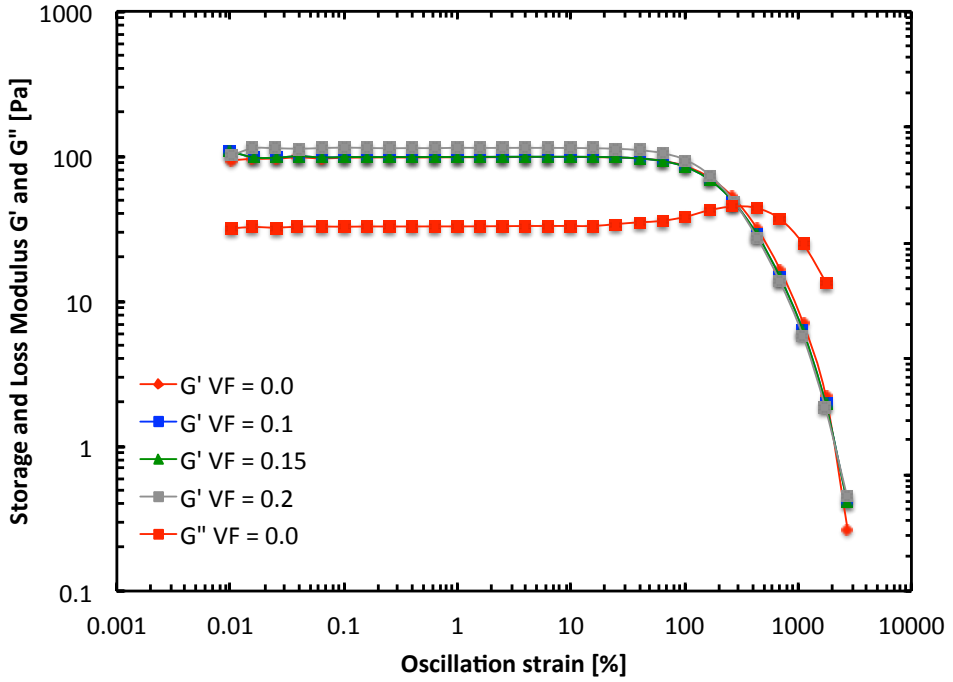

Appendix II – Screening of emulsifier and solvent for microemulsions

First a table was prepared naming the available solvents to dissolve ibuprofen. Following certain characteristics of the solvents, some of them were eliminated. These characteristics include: miscibility, solubility in water, boiling point, ibuprofen solubility and vapor pressure. Another important property was its category as a class type solvent in pharmaceutical industry.

Solvent	I	Class Type Solvent	Solubility in Water [g/100 mL]	Boiling Point [C]	Ibuprofen Solubility	Vapor Pressure @ 20C [mm Hg]
acetic acid	x					
acetone	x					
acetonitrile	x					
benzene		Class 1	0.184	80.1		
n-butanol		Class 3	6.800	117.7		
butyl acetate		Class 3	0.840	126.0	30.4	10.0
carbon tetrachloride		Class 1	0.100	170.1		
chloroform		Class 2	0.800	61.2	55.0	160.0
cyclohexane		Class 2	0.005	80.7	15.8	78.0
1,2-dichloroetahne		Class 1	0.870	83.5		
dichloromethane		Class 2	1.300	39.6	47.93	350.0
dimethyl formamide	x					
dimethyl sulfoxide	x					
dioxane	x					
ethanol	x					
ethyl acetate		Class 3	8.000	77.1		
diethyl ether		Class 3	6.900	35.0		
heptane		Class 3	0.000	98.4	4.07	40.0
hexane		Class 2	0.001	69.0	5.38	124.0
methanol	x					
methyl-t-butyl ether		Class 3	4.200	55.0		
2-butanone		Class 3	22.000	79.6		
pentane		Class 3	0.004	36.0		533.0
n-propanol	x					
isopropanol	x					
diisopropyl ether		N/A	0.200	69.0		
tetrahydrofuran	x					
toluene		Class 2	0.005	111.0		
trichloroethylene		Class 2	0.128	87.2		58.0
anisole		Class 3	0.104	155.0	28.0	3.5
xylene		Class 2	0.017	140.0		

Four solvents where chosen and used with three different emulsifiers. Depending on emulsion stability, the best combination was chosen. Sodium dodecyl sulfate (SDS) was discarded given its toxicity with human cells. Kolliphor® P188 was discarded given its lack of stable emulsions with the amount used in the solutions (2.00 w/v%).

Emulsifier > ***Solvent v***	**Sodium dodecyl sulfate (SDS)**	**Kolliphor® P188**	**Polyvinyl Alcohol (PVA)**
Chloroform	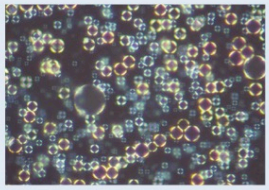	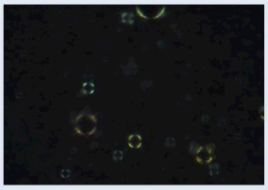	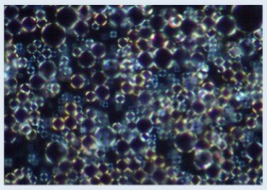
Anisole	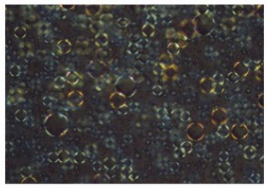	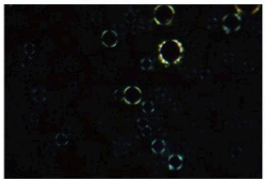	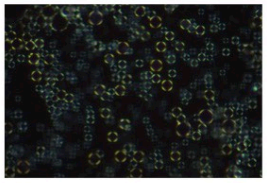
Butyl Acetate		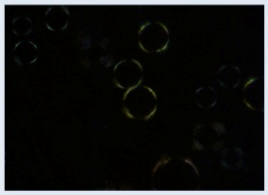	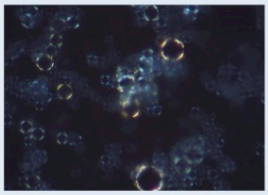
Dichloromethane			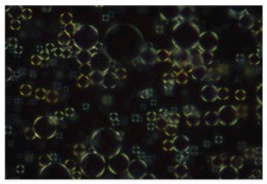

Appendix III – FT-IR measurements of materials used to synthesize the composite hydrogel

FT-IR measurements of alginate, gelatin, beta-TCP, and TiO_2. Characteristics peaks of each material were circled and are the peaks explained in Chapter 4.

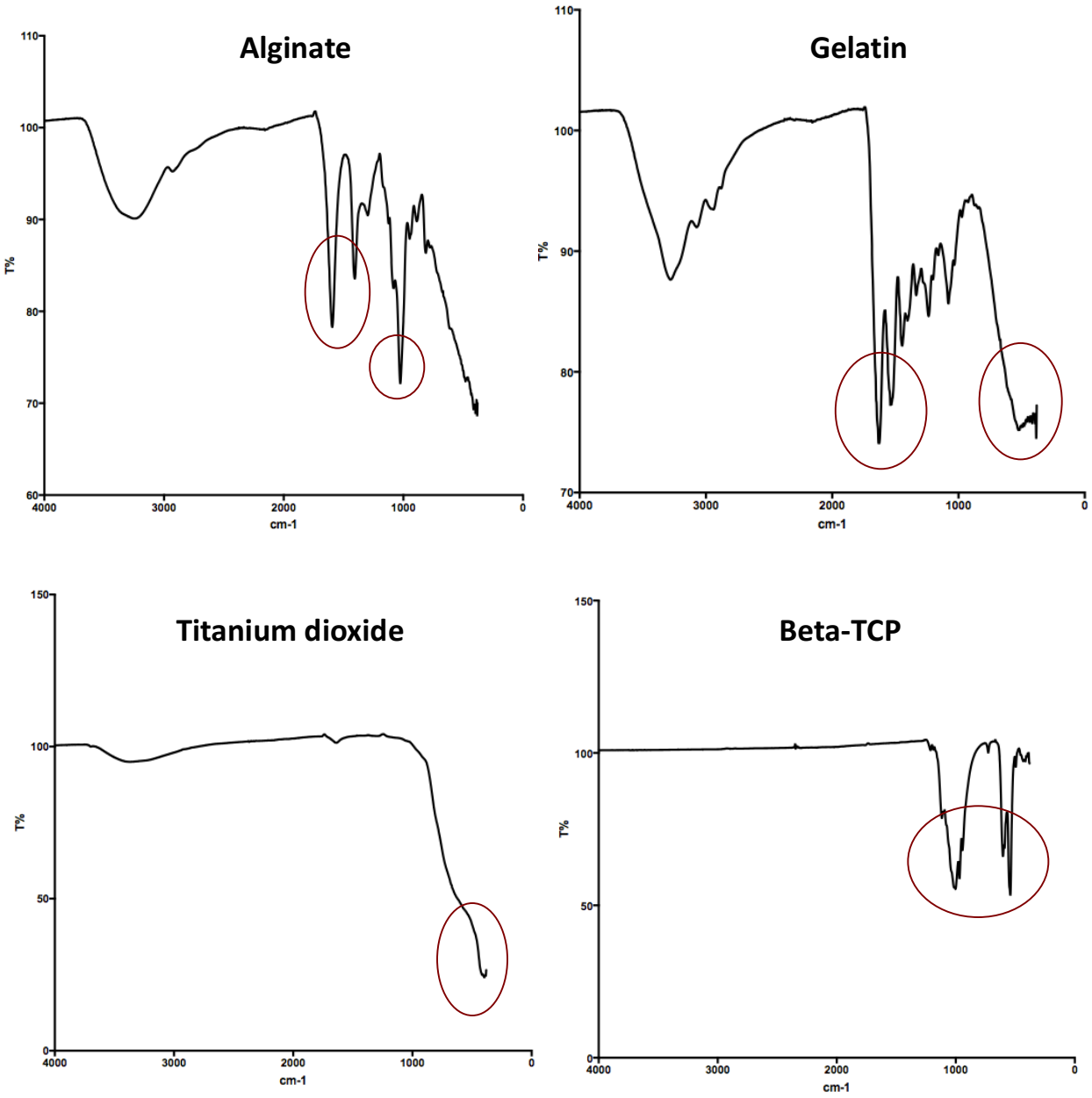

Appendix IV – EDX reports of elemental analysis of HG-A and HG-B systems

In this report, the graph of the intensity of each element is showed, its table containing the exact amount calculated for each element (mass and atom), and the image where the analysis was taken from. The first one is of the hydrogel system HG-A.

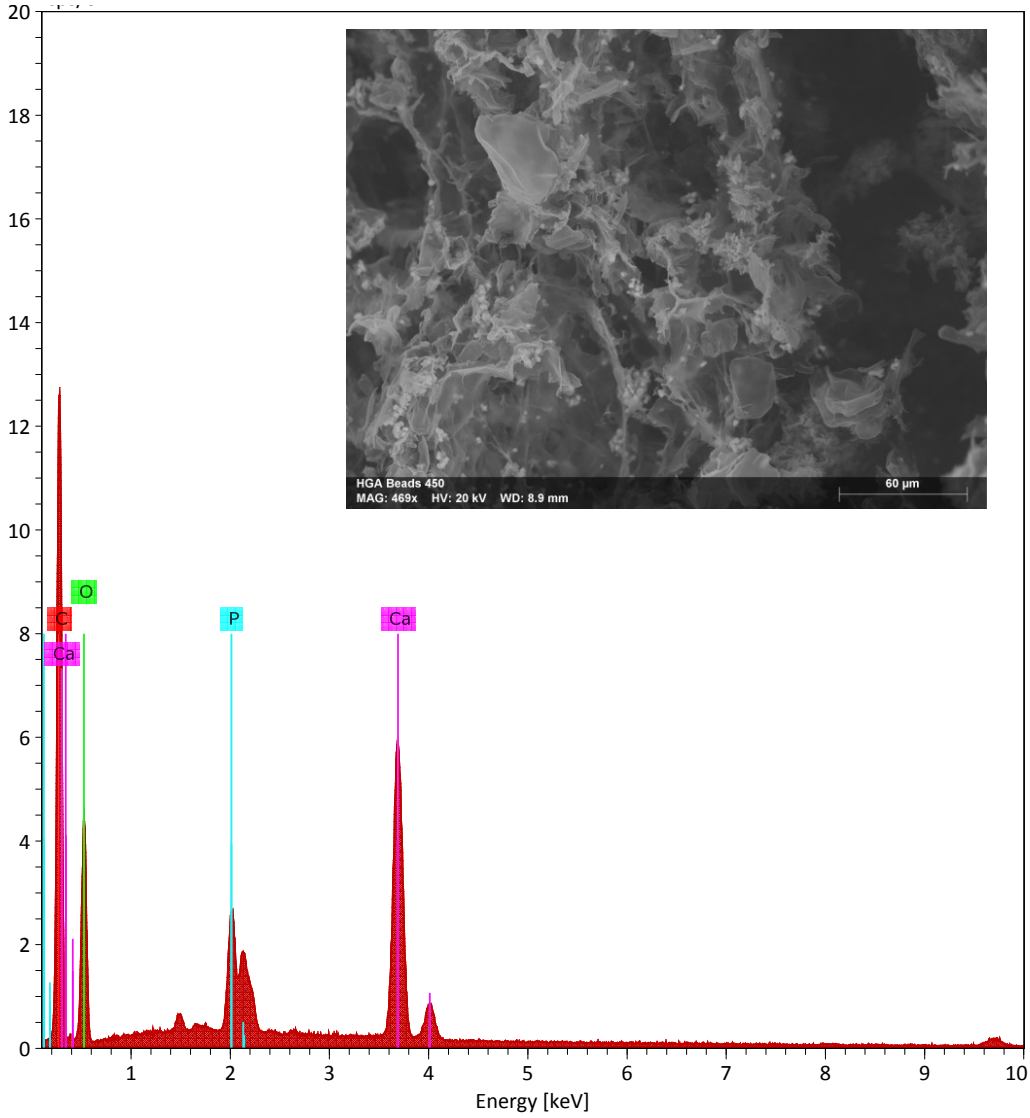

HGA Beads 246

Element	At. No.	Line s.	Netto	Mass [%]	Mass Norm. [%]	Atom [%]	abs. error [%] (1 sigma)	abs. error [%] (2 sigma)	rel. error [%] (1 sigma)
Carbon	6	K-Serie	83297	40.10	50.03	61.70	4.59	9.18	11.45
Oxygen	8	K-Serie	32902	28.10	35.06	32.46	3.45	6.91	12.29
Calcium	20	K-Serie	95440	9.51	11.87	4.39	0.30	0.61	3.20
Phosphorus	15	K-Serie	31022	2.43	3.04	1.45	0.12	0.24	4.97
			Sum	**80.15**	**100.00**	**100.00**			

This report shows the hydrogel system HG-B.

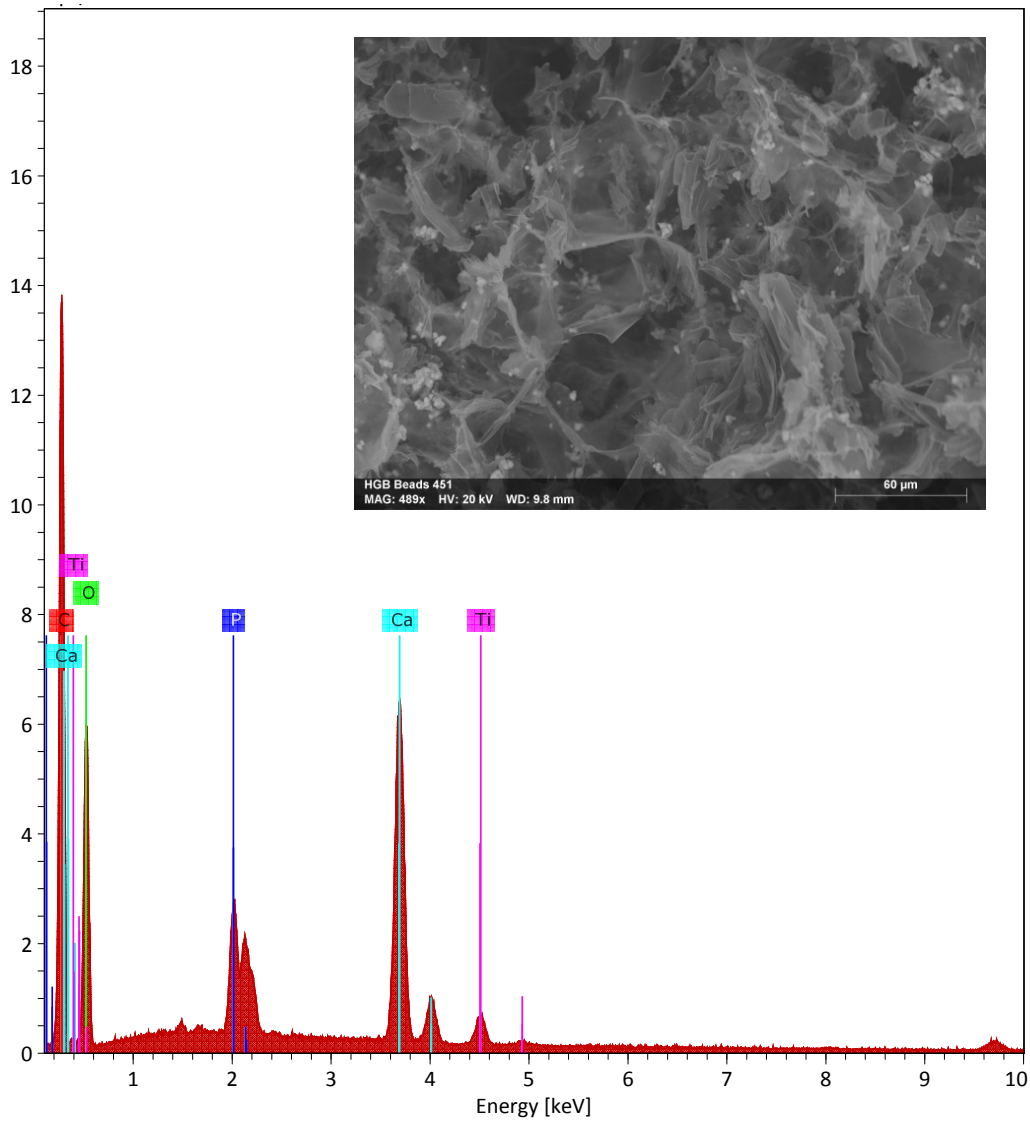

HGB Beads 248

Element	At. No.	Line s.	Netto	Mass [%]	Mass Norm. [%]	Atom [%]	abs. error [%] (1 sigma)	abs. error [%] (2 sigma)	rel. error [%] (1 sigma)
Carbon	6	K-Serie	80153	39.73	46.48	58.00	4.56	9.12	11.48
Oxygen	8	K-Serie	39532	33.08	38.70	36.25	4.00	8.00	12.09
Calcium	20	K-Serie	90820	9.19	10.75	4.02	0.29	0.59	3.21
Phosphorus	15	K-Serie	28595	2.27	2.66	1.29	0.11	0.23	5.05
Titanium	22	K-Serie	8364	1.21	1.42	0.44	0.06	0.12	5.10
			Sum	**85.48**	**100.00**	**100.00**			

Finally, just an area inside a selected crystal of ibuprofen was selected to do punctual elemental analysis. This crystal was selected from the HG-B system; one of the causes there is a small percentage of titanium in the crystal surface.

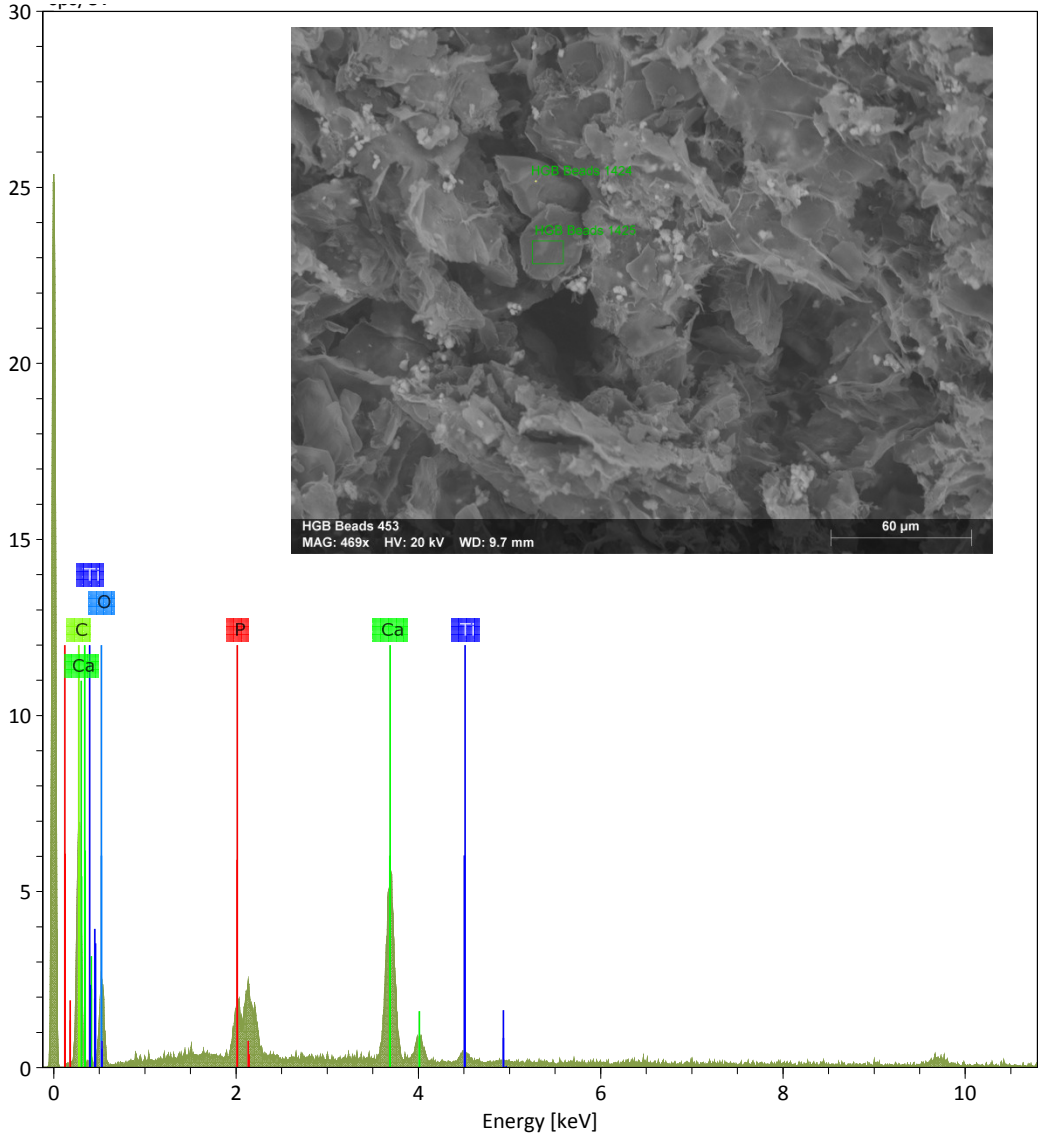

HGB Beads 1425

Element	At. No.	Line s.	Netto	Mass [%]	Mass Norm. [%]	Atom [%]	abs. error [%] (1 sigma)	abs. error [%] (2 sigma)	rel. error [%] (1 sigma)
Carbon	6	K-Serie	5382	23.37	43.94	57.25	3.64	7.27	15.56
Oxygen	8	K-Serie	2026	18.91	35.56	34.78	3.60	7.19	19.02
Calcium	20	K-Serie	9627	9.69	18.22	7.12	0.33	0.66	3.41
Titanium	22	K-Serie	622	0.89	1.67	0.55	0.07	0.14	8.05
Phosphorus	15	K-Serie	408	0.32	0.61	0.31	0.05	0.10	14.91
			Sum	**53.18**	**100.00**	**100.00**			

Appendix V – Mechanical test results of HG-2, HG-4, and HG-A

The resulting curves of a tensile test of three different dry hydrogel systems are showed in the next graph. For the hydrogel composition please refer to Table 5.

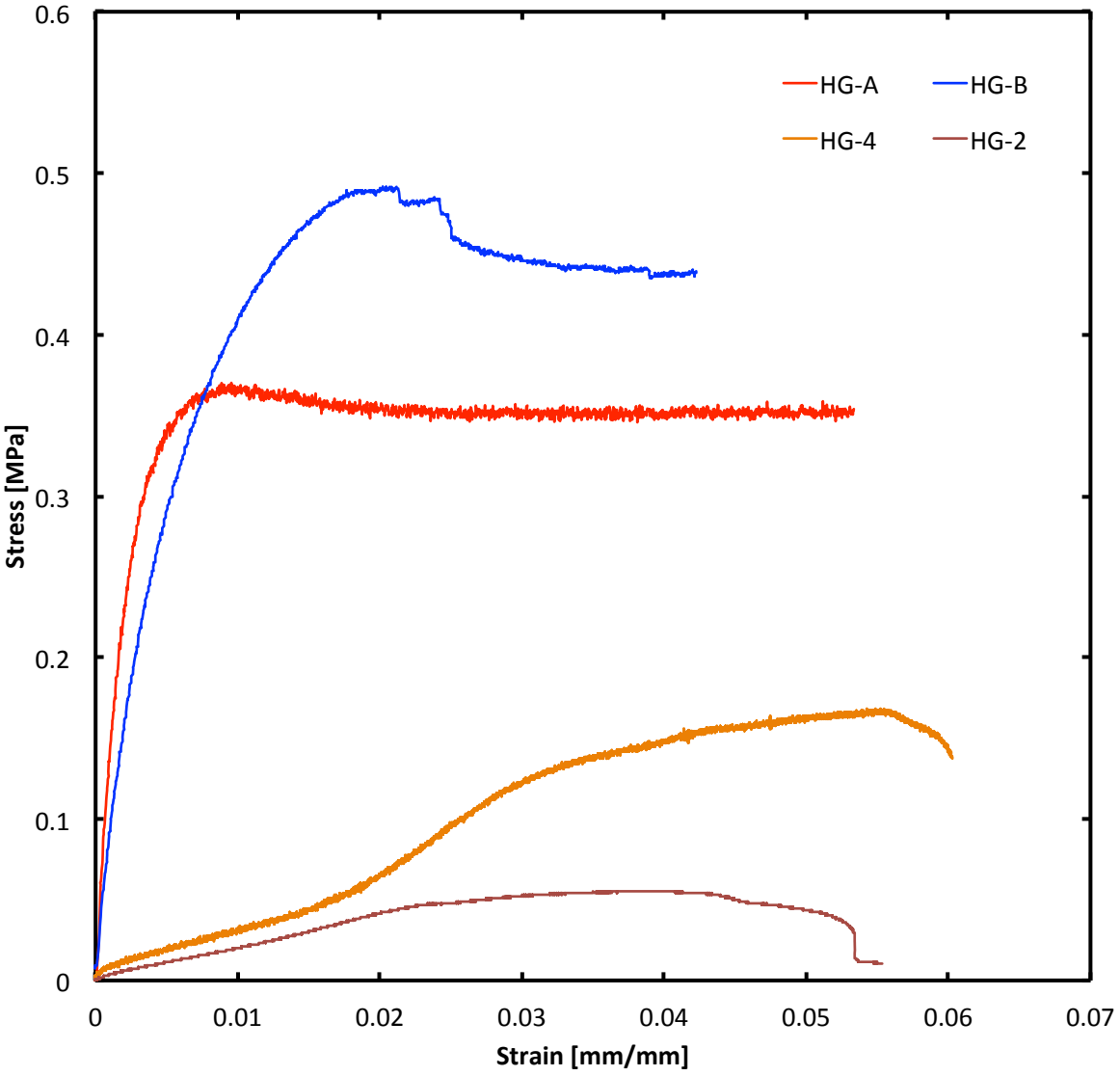

Appendix VI – EDX report of point elemental analysis of bioactivity test

In this first report, the point to do elemental analysis was located on one of the agglomerates found in the SEM image of the samples of bioactivity. The report includes the graph with the element peaks, the image that was analyzed, and the table with the numerical values.

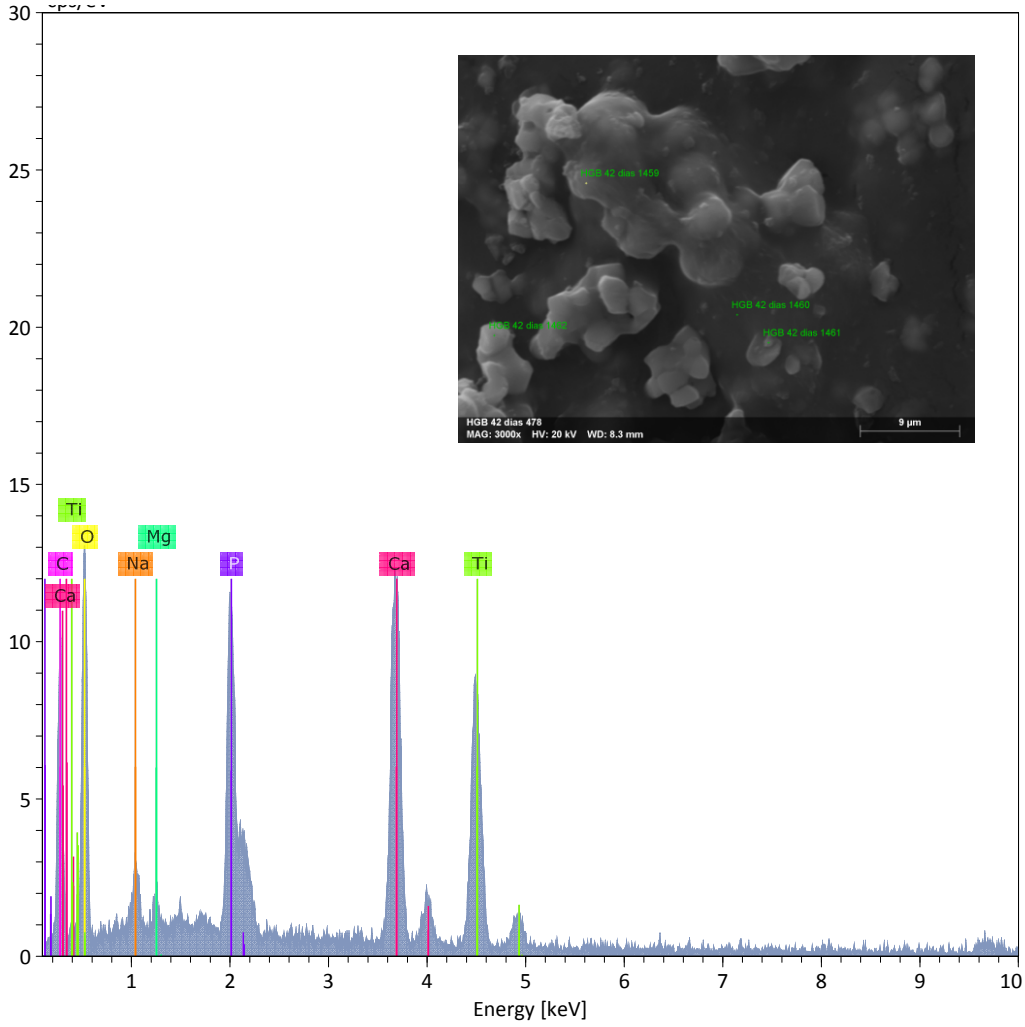

HGB 42 dias 1461

Element	At. No.	Line s.	Netto	Mass [%]	Mass Norm. [%]	Atom [%]	abs. error [%] (1 sigma)	abs. error [%] (2 sigma)	rel. error [%] (1 sigma)
Oxygen	8	K-Serie	3697	45.59	44.46	49.12	7.58	15.16	16.63
Carbon	6	K-Serie	2495	25.84	25.21	37.09	4.68	9.36	18.10
Titanium	22	K-Serie	5727	12.64	12.33	4.55	0.42	0.85	3.36
Calcium	20	K-Serie	7546	11.55	11.26	4.97	0.40	0.79	3.43
Phosphorus	15	K-Serie	4270	4.62	4.51	2.57	0.23	0.46	4.92
Sodium	11	K-Serie	654	1.73	1.68	1.29	0.18	0.35	10.27
Magnesium	12	K-Serie	326	0.56	0.55	0.40	0.08	0.16	13.79
			Sum	**102.53**	**100.00**	**100.00**			

In the second part of the test, the point to do the elemental analysis was located on the surface of the material avoiding any of the agglomerates that can be observed in the image. The mass percentage of calcium and phosphate drop significantly, while other elements increase, thus assuring the presence of calcium phosphate of the agglomerates.

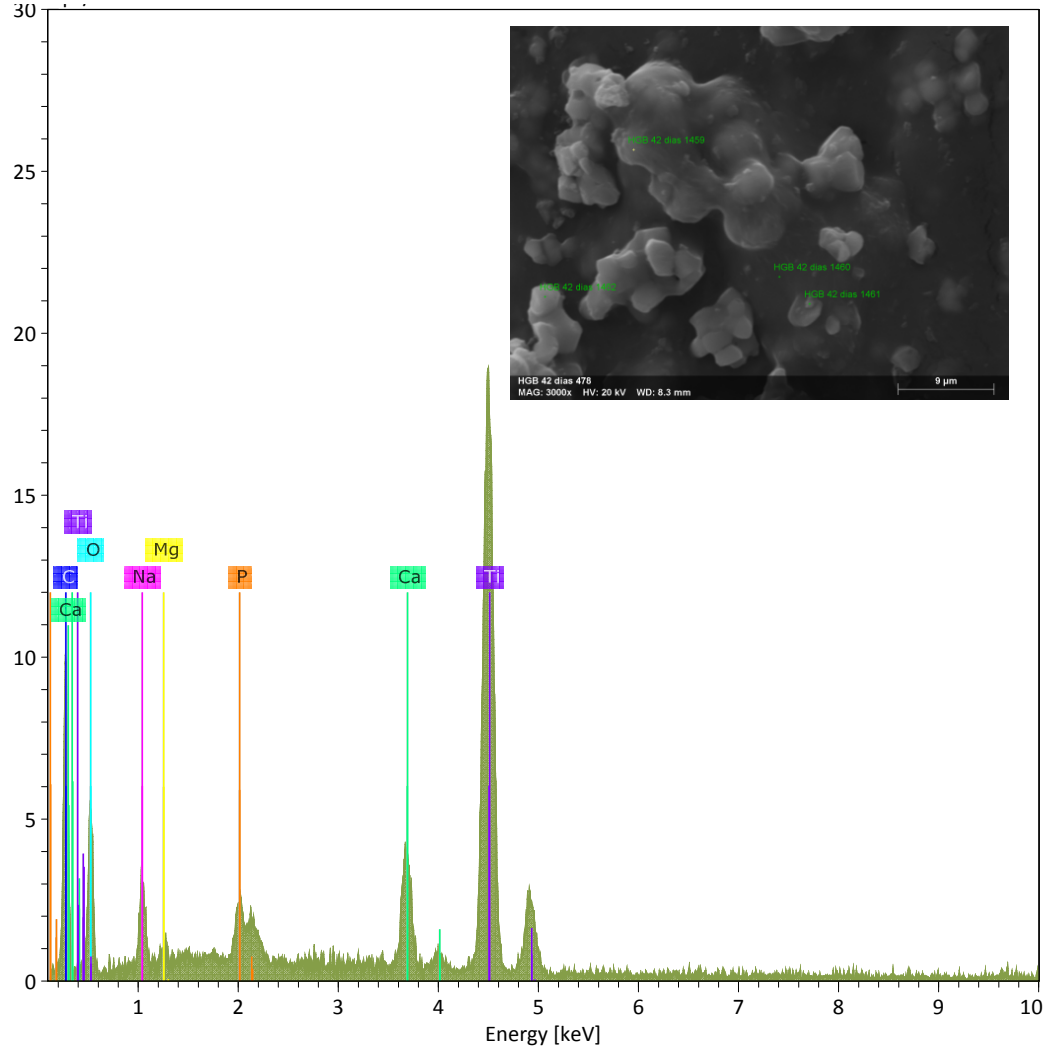

HGB 42 dias 1460

Element	At. No.	Line s.	Netto	Mass [%]	Mass Norm. [%]	Atom [%]	abs. error [%] (1 sigma)	abs. error [%] (2 sigma)	rel. error [%] (1 sigma)
Titanium	22	K-Serie	15945	28.96	33.74	13.64	0.87	1.74	3.00
Oxygen	8	K-Serie	1911	27.32	31.83	38.50	5.26	10.51	19.24
Carbon	6	K-Serie	2993	22.82	26.58	42.83	3.98	7.95	17.42
Calcium	20	K-Serie	2862	3.40	3.96	1.91	0.15	0.30	4.38
Sodium	11	K-Serie	1108	2.41	2.81	2.36	0.22	0.44	9.07
Phosphorus	15	K-Serie	655	0.55	0.64	0.40	0.06	0.12	10.84
Magnesium	12	K-Serie	248	0.39	0.45	0.36	0.06	0.13	16.56
			Sum	**85.84**	**100.00**	**100.00**			

Appendix VII – Complete list of parameters of the software Cura

Screenshots of the parameters used in the software Cura are shown. Parameters such as the filament diameter and nozzle size had to be adapted for syringe used in the process.

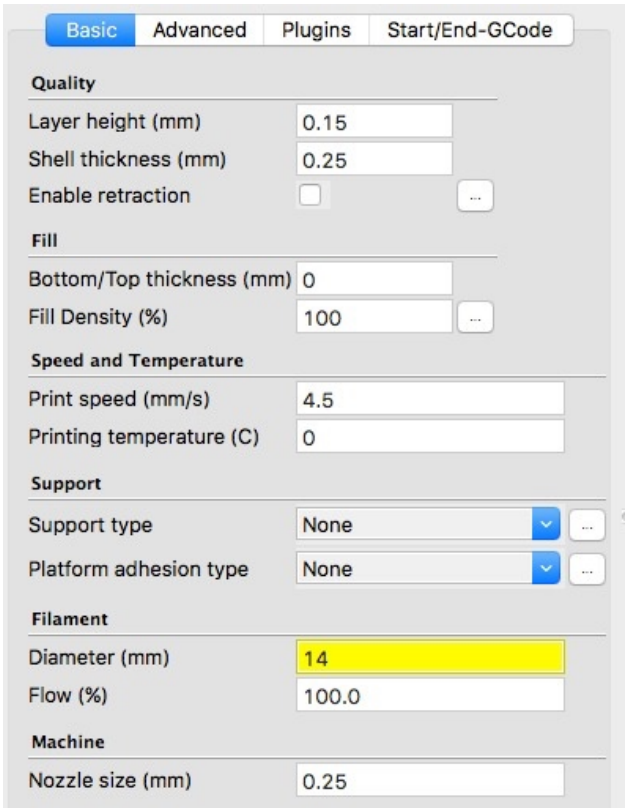

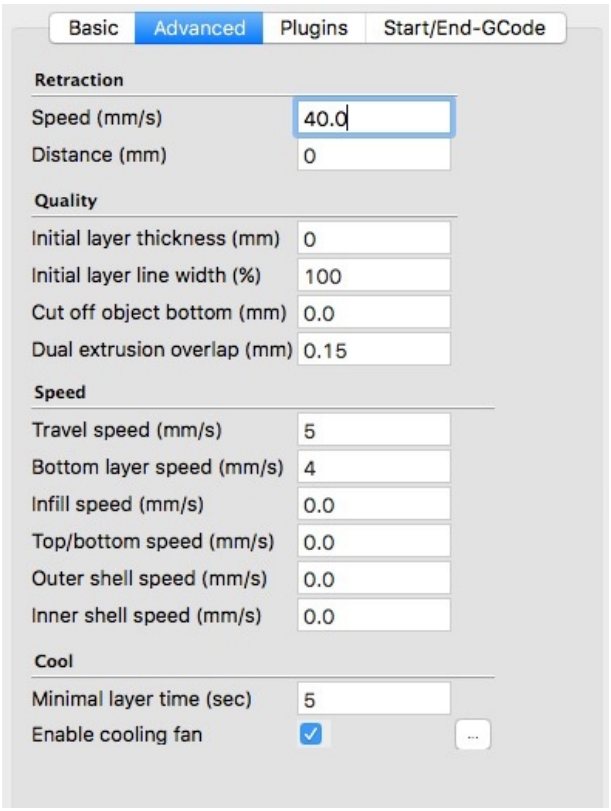

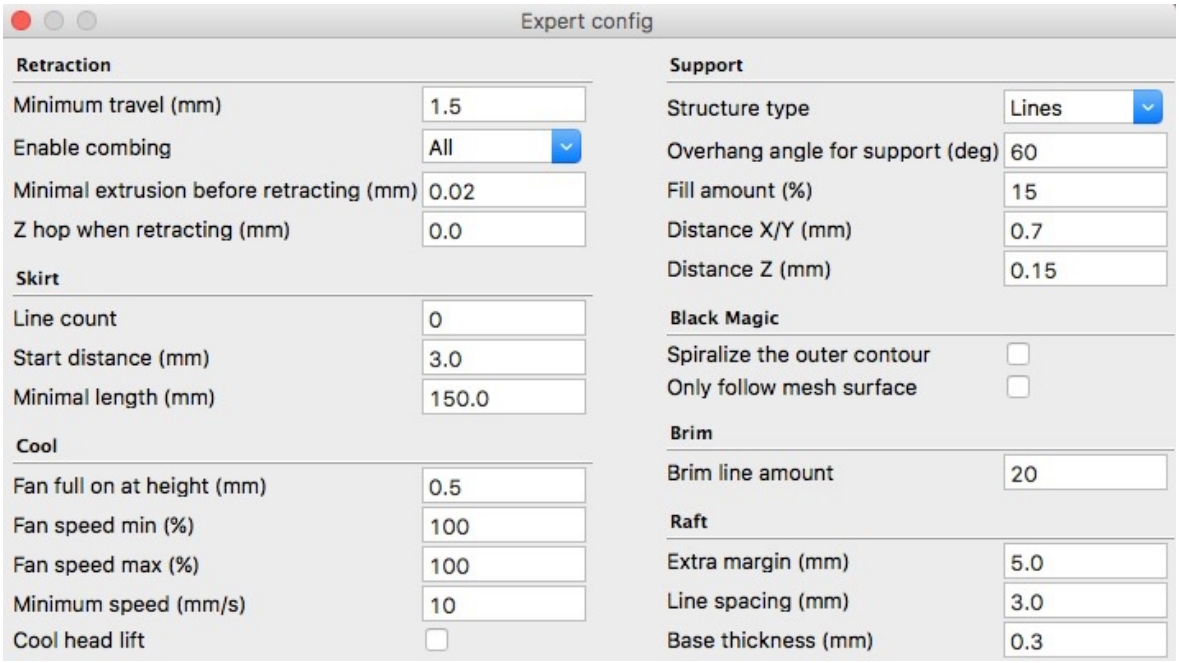

The start route to generate the G-code was also modified to optimize the extrusion of pre-crosslinked hydrogel. A screenshot of this route is shown.

Appendix VIII – Images of printed designs

The SteREO was used to take images to the printed designs of the hexagon, grid, and voronoi. The lines of the design were measured. The first image is a close-up of an intersection of the hexagon design. Is important to observe how the vertices lose resolution as the gel is printed over the build platform.

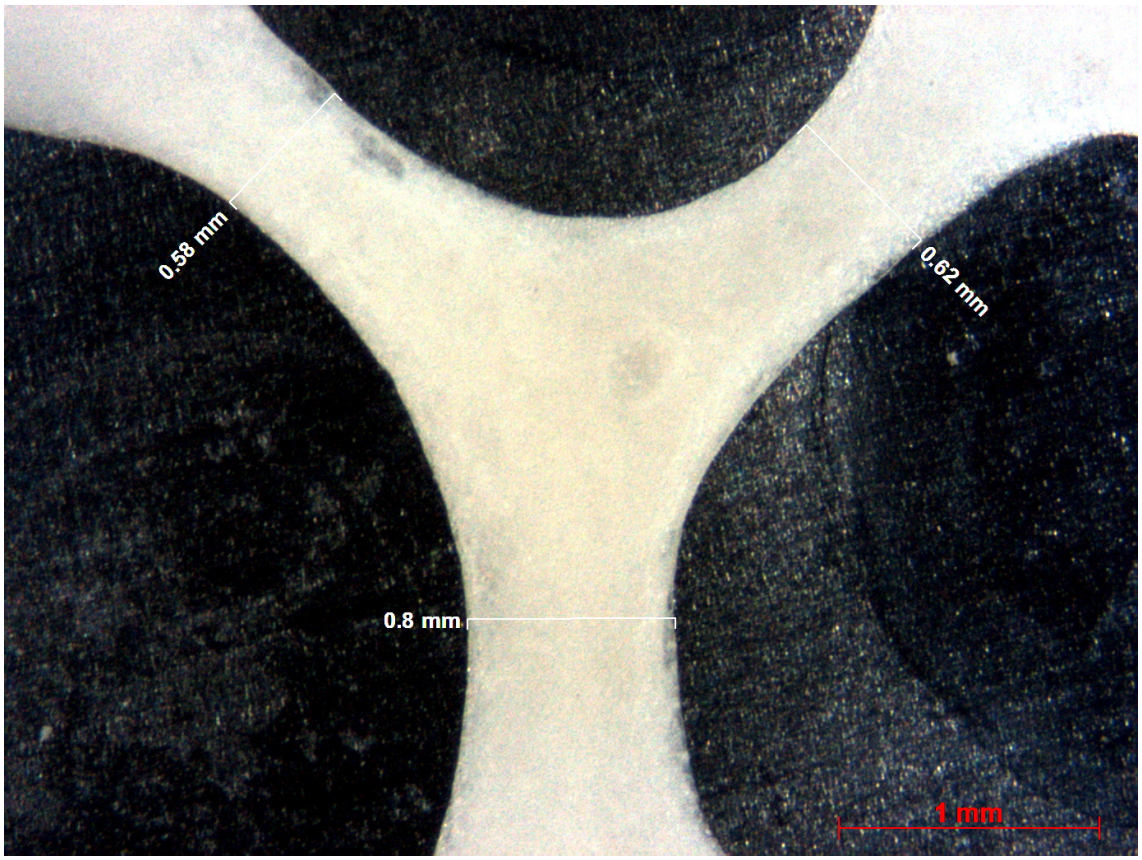

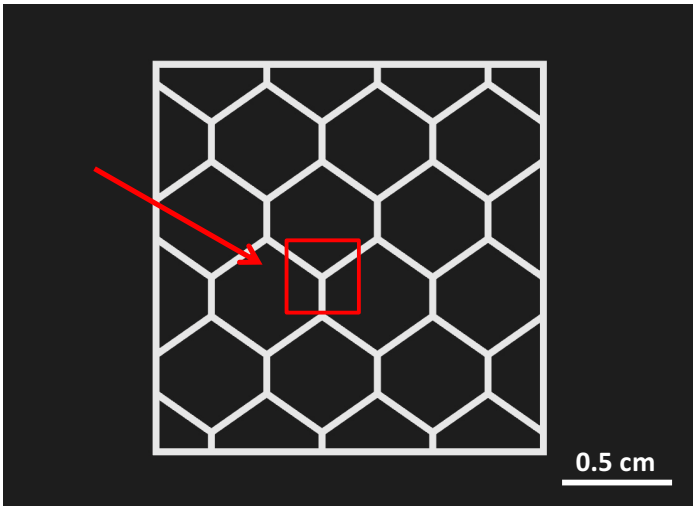

Close-up images of the design voronoi and its measurements.

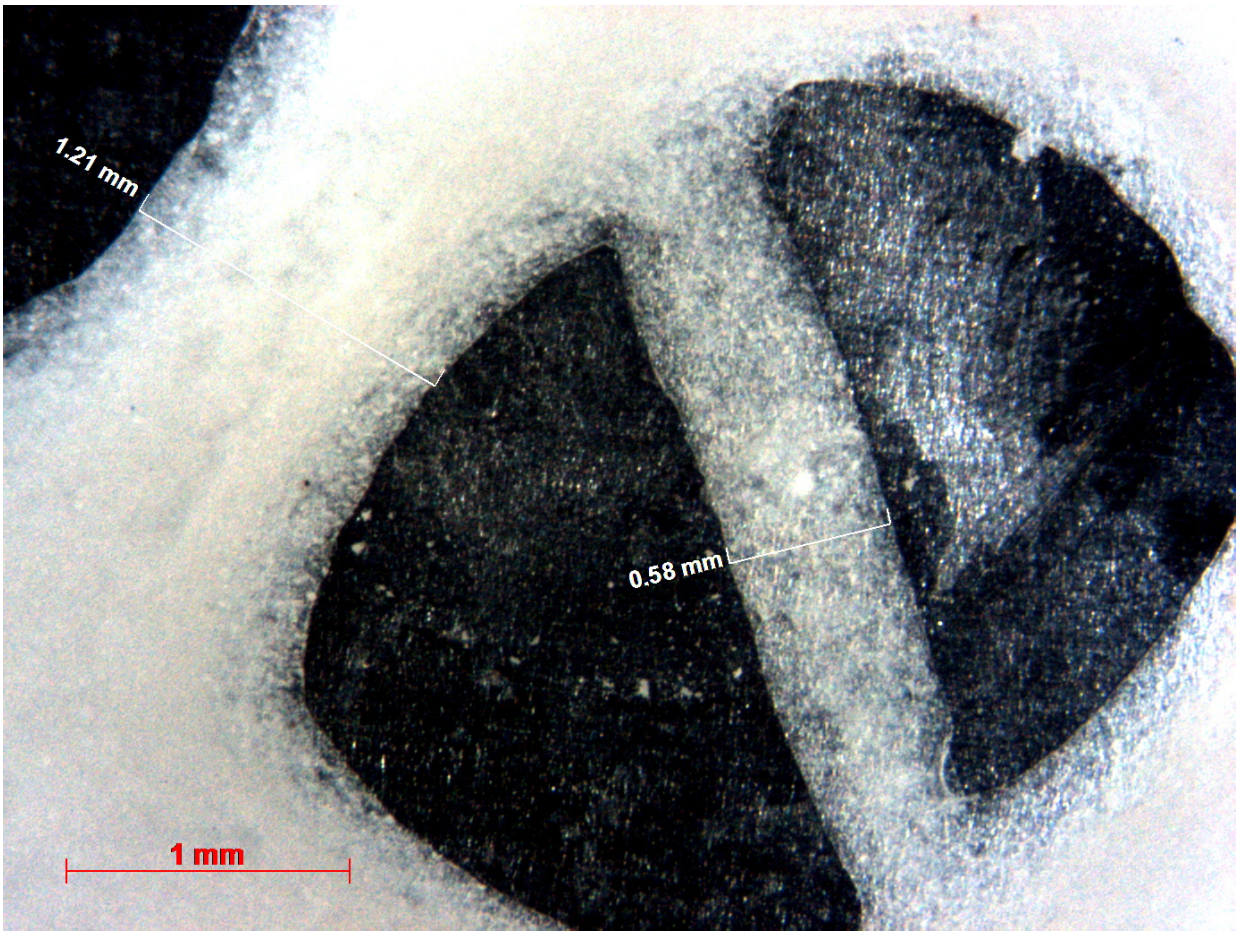

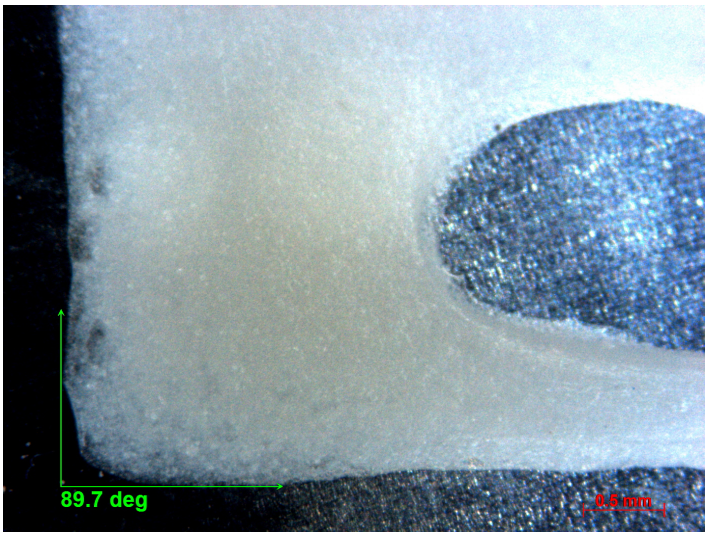

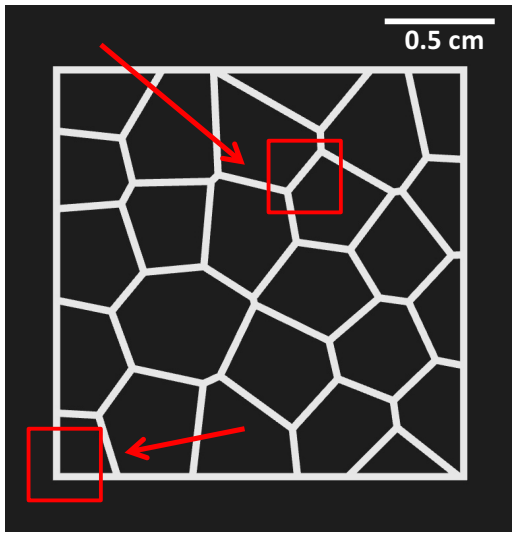

Appendix IX – Water absorption of hydrogels

A brief study of water absorption of some hydrogels (HG-8 to HG-12) was made. Just after 5 minutes of introducing the dry hydrogel in distilled water, they absorbed more than 80.0% of its weight of water. After 30 minutes it has reached equilibrium with more than 90.0% of water absorption. Further studies with repeatability tests need to be done to make a better analysis of re-absorption of the hydrogels after they are dried.

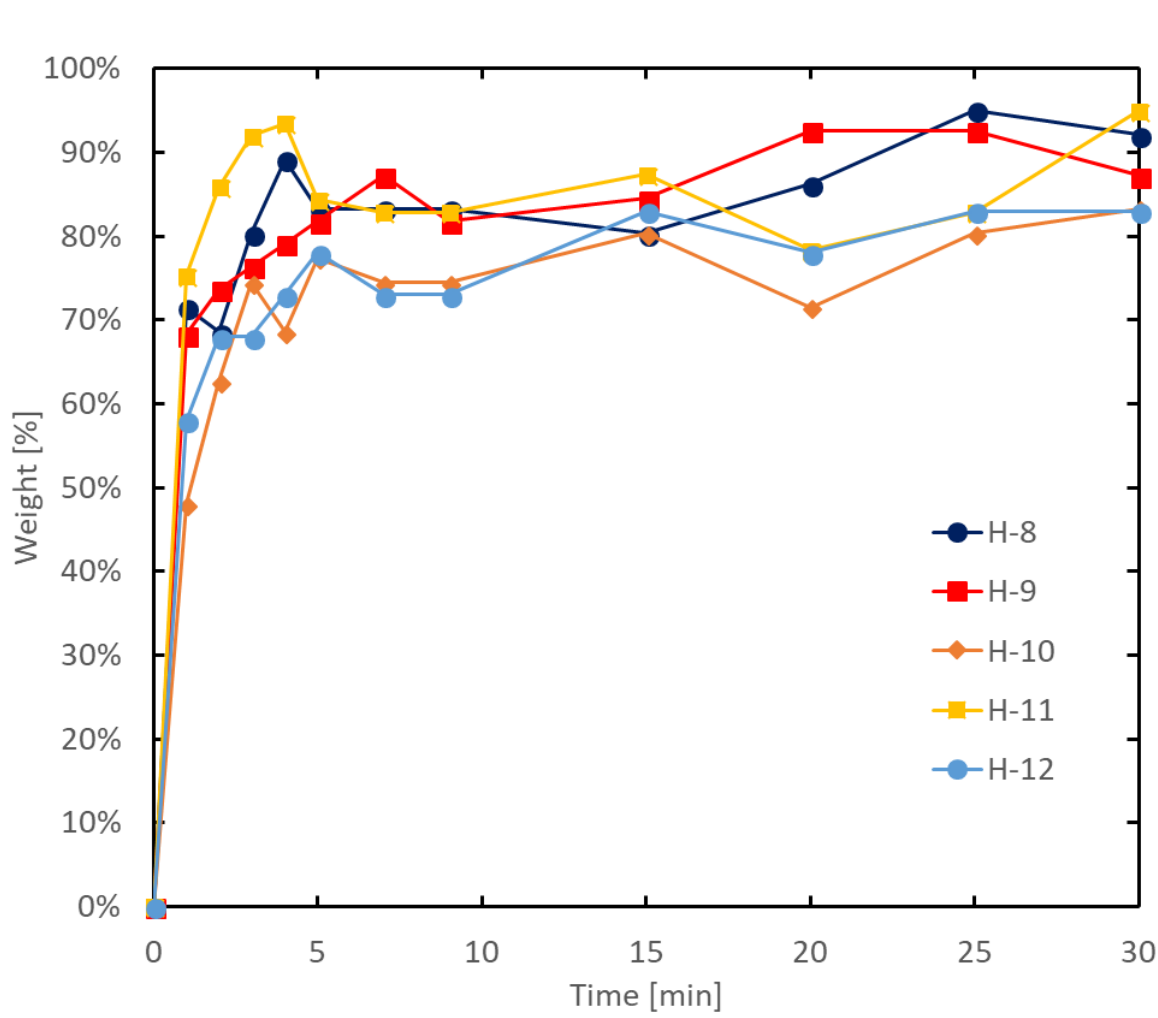

This assay was made by student Leonardo Daniel Cedillo Santos.